Université de Strasbourg

UNIVERSITÉ DE STRASBOURG

École doctorale
Sciences chimiques | ED 222
Université de Strasbourg

ÉCOLE DOCTORALE DES SCIENCES CHIMIQUES

UMR 7006

THÈSE présentée par :

Luís BARBOSA PIRES

soutenue le : **14 Décembre 2023**

pour obtenir le grade de : **Docteur de l'université de Strasbourg**

Discipline/ Spécialité : Physique

Entropic costs for Brownian protocols

Coûts entropiques pour protocoles Browniens

THÈSE dirigée par :
M. GENET Cyriaque Dr., CESQ-ISIS, Université de Strasbourg, CNRS

RAPPORTEURS :
Mme. KLAPP Sabine Prof., Institute of Theoretical Physics, Technische Universität Berlin
M. LOUYER Yann Dr., LOMA, Université de Bordeaux, CNRS

UTRES MEMBRES DU JURY :
M. RONDIN Loïc Dr., Laboratoire LuMIn, CNRS, ENS-Paris-Saclay, CentraleSupélec, Université Paris-Saclay
M. HERVIEUX Paul-Antoine Prof., IPCMS, Université de Strasbourg, CNRS

Acknowledgements

Completing this thesis was an intense journey marked by many highs and lows, yet bolstered by immense trust and support from various sources. My internal drive to learn and evolve as a researcher, coupled with the invaluable listening and support from many around me, steered this process.

Firstly, I would like to express my gratitude to my reviewers Sabine Klapp and Yann Louyer, to the jury president Paul-Antoine Hervieux, and to Loïc Rondin for joining the jury. I deeply value the time you dedicated to reviewing my manuscript, your valuable comments and insights, and all the kindness in encouraging the next steps of my work.

Alone, we achieve little. Since my first interaction with my supervisor, Cyriaque, I was determined to embark on the journey to cross the ocean to Strasbourg. His enthusiasm and attentive listening assured me that we could work together very productively. I am immensely grateful for this listening, welcoming, and support, especially during the times when they were most needed. Thank you very much! I also thanks to Thomas for welcoming me into the lab and allowing me to learn more about great leadership, and to Éloïse, a vital part in maintaining an excellent work environment. For all the availability and attention, I thank the administrative support provided by Marie-Claude and the rest of the administrative ISIS team. Equally important was the funding provided by QMat and the support from Alena.

I am very honoured to have been part of this team of talented scientists who have passed through the Laboratory of Nanostructures while I was here. Here, the atmosphere is one of cooperation, care, and support for each other. The list of young researchers I have lived with here is long, but I cherish the moments shared with each of them. With some colleagues, we intensely lived through discussions and experimental challenges. I thank Rémi, Arthur, and Antoine for their partnership and eagerness to discover and produce knowledge.

Here in Strasbourg, I had the great privilege of having friends so close that they ultimately felt like family. Far from home and the warmth of Brazil, I found in these friendships the energy to strengthen me and keep moving forward. The partnership with Kelton throughout the years here in Strasbourg, especially at the moment of

completing the thesis, made this time as enjoyable as possible. The bike rides with Bruno and the playful times with Íris helped me to stay connected with the present. The friendship with Yvilla, always attentive in listening and with good advice, along with Carol's positivity, have brightened and lightened my life here.

I am very proud to have met incredible and competent people along my academic journey who still remain a part of my life. Daniel and Rodrigo's support over the years has been very important in expanding my horizons of ideas and projects. It's comforting to know that I'm on the right track, feeling the welcome of my previous colleagues at UFRJ. Concluding this chapter in Strasbourg with Paulo in the audience - someone from whom I have learned immensely throughout my academic growth - was a much appreciated gift.

Finally, a special thanks to my parents Josias and Concinha and my siblings Huna and Áureo. Não importa para onde eu vá, eles estão sempre comigo. Sentindo essa presença, sinto-me mais forte.

Contents

Contents **5**

1 Introduction **7**
1.1 Engineering the energetic landscapes of Brownian particles 7
1.2 Acceleration and optimization of Brownian systems 13
1.3 Content of this thesis 16
1.4 List of publications 17

2 Time dependent temperature in an optical trap **19**
2.1 Introduction 19
2.1.1 Characteristic times 19
2.1.2 From stochastic variables to mobility distributions 21
2.2 Optically trapped Brownian particles 21
2.2.1 Experimental platform 21
2.2.2 Observables 26
2.3 Bath engineering 30
2.3.1 Acousto-optic modulator (AOM) 31
2.3.2 Bath engineering exploiting radiation pressure 34
2.4 From discontinuous changes to finite-time processes 41
2.4.1 Dynamical description 41
2.4.2 Isochocric discontinous transformations: STEP-like $T(t)$ protocol 43
2.4.3 Thermal engineered swift equilibration 45
2.5 Conclusion 47

3 Thermodynamics of a Brownian particle **49**
3.1 From stationary to dynamical state 49
3.1.1 Time scales 50
3.1.2 Connecting states and time dependent processes 51
3.2 Isotherm and isochoric processes 53

3.2.1 Thermodynamic First law . . . 53
3.2.2 Dissipated energy . . . 55
3.2.3 Thermodynamic Second law . . . 59
3.3 Non-equilibrium state functions . . . 60
3.3.1 Non-equilibrium free energy . . . 60
3.3.2 Non-equilibrium system entropy . . . 62
3.4 Thermodynamics consistence . . . 65
3.4.1 From the first to the second law . . . 65
3.4.2 Ken Sekimoto's approach to non-equilibrium system entropy . . . 69
3.5 Functional approach . . . 71
3.6 Conclusion . . . 73

4 Isochoric transformation **77**
4.1 Optimal isochoric finite time transformations . . . 77
4.1.1 Optimal protocol derivation . . . 78
4.1.2 Time-entropy bound . . . 81
4.2 Thermodynamic analyses of isochoric transformations . . . 82
4.2.1 STEP-like $T(t)$ protocol . . . 82
4.2.2 Thermodynamics of an optimal change . . . 88
4.3 Conclusion . . . 94

5 Conclusion and perspectives **97**

6 Résmé de la thèse **103**
6.1 Température dépendante du temps dans un piège optique . . . 103
6.2 Thermodynamics of a Brownian particle . . . 105
6.3 Isochoric transformation . . . 107

Bibliography **109**

Chapter 1

Introduction

This thesis delves into the dynamics of Brownian motion [1, 2], a phenomenon typical of intermediate length and time scales where the dynamical influence of molecules can be observed with naked eye [3]. The phenomenon corresponds to the apparently erratic movement of particles suspended in a fluid (liquid or gas) caused by the random collisions of these particles with the atoms or molecules of the fluid.

In this Introduction, some recent methods and problematics in the field of Brownian motion will be presented. The aim is to emphasize how such a "simple" phenomenon yields such rich landscape for research, enabling to re-investigate with new tools fundamental aspects of non-equilibrium thermodynamics. This renewal of approaches gives new entities in understanding stochastic systems from a mechanical and thermodynamic points of view, with even relevant potential technological applications ahead.

1.1 Engineering the energetic landscapes of Brownian particles

The harmonic oscillator is a paradigmatic model for both classical and quantum physical systems, whose dynamics can be further complexified when driven by an external stochastic field. This is one of the main models used in the investigation of the dynamics of microscopic systems in the area known as stochastic thermodynamics [4, 5, 6]. To illustrate the behavior of this paradigmatic system, we will present a few representative experiments in the field of levitodynamics [7], with nano or micro particles trapped in air [8] or vacuum [9]. The dynamics of single particles trapped under such conditions are described by the evolution of their instantaneous position and velocity, that in turn define their instantaneous potential and kinetic energies.

Due to its isolation from external influences, this system can serve as precision sensors. One example how precise it can be is the measurement of a trapped sil-

ica nanospheres mass, performed by different groups, down to the range of femto to picograms [10, 11]. Another example is the control and rapid measurement of charging and discharging events at the level of single elementary charge [12, 13].

Concerted effort to reduce the center-of-mass temperature of these vacuum, trapped particles has been made recently, exploiting two main techniques: autonomous feedback mediated through cavities [14], in which the light scattered by the particle is reflected by the cavity and, based on self-regulating mechanisms, lead to counter act on the particle. The other technique corresponds to measurement-based feedback schemes, using both electrical [15] or optical means [16, 17], as exemplified in Figure 1.1. The core of these methods is to dynamically adjust a counter reacting force on the nanoparticle, based on real-time measurements of its instantaneous position.

In the case described in Figure 1.1, the temperature of the center of mass of a silica nanoparticle, measured from its position spectrum, is cooled from the ambient temperature $T = 269$ K to a temperature of $T = 50$ mK, as shown in panel c). In this work, the cooling technique employed is called *parametric feedback cooling*, sketched in panel a). From the measurement of the position of the nanosphere, a signal is processed so that the trapping laser intensity increases when the particle moves away from the equilibrium position while the intensity decreases when the particle approaches. This signal, which has twice the resonance frequency 2Ω and phase $\Delta\phi$ adjusted accordingly, has the effect of reducing the amplitude of the nanoparticle's movement. In this scheme, the counteracting force to the nanoparticle's movement is the gradient force, always directed towards the center of the trap. Since the resonance frequency Ω for each of the directions is different, as shown in panel b), this technique allows the center of mass to be cooled in all three spatial directions simultaneously by the action of a single laser.

For those kind of systems, in which the center of mass of the particle gets cooler, a significant milestone reached in 2020 is the quantum ground state [18], followed by other groups [19, 20]. Although such a cooling process can be described mechanically from an additional damping in the equation of motion, its thermodynamic description is far from being trivial. For such systems, the temperature change, either autonomous or induced, is based on information processing and feedback. We note that the introduction of a feedback loop to modify the system dynamics for both isothermal processes [21, 22, 23], or non-isothermal ones [24, 25], has been already connected with thermodynamics. One example of such a connection is given through the concept of a Maxwell's demon [26], where it is necessary to take into account the thermodynamic cost of the measurement process itself [27].

Recent progress has been made in the field of thermodynamics of information [28], for example in relation with finite time features associated with measurement pro-

cesses [29, 30].This has open new means in addressing the actual thermodynamic cost

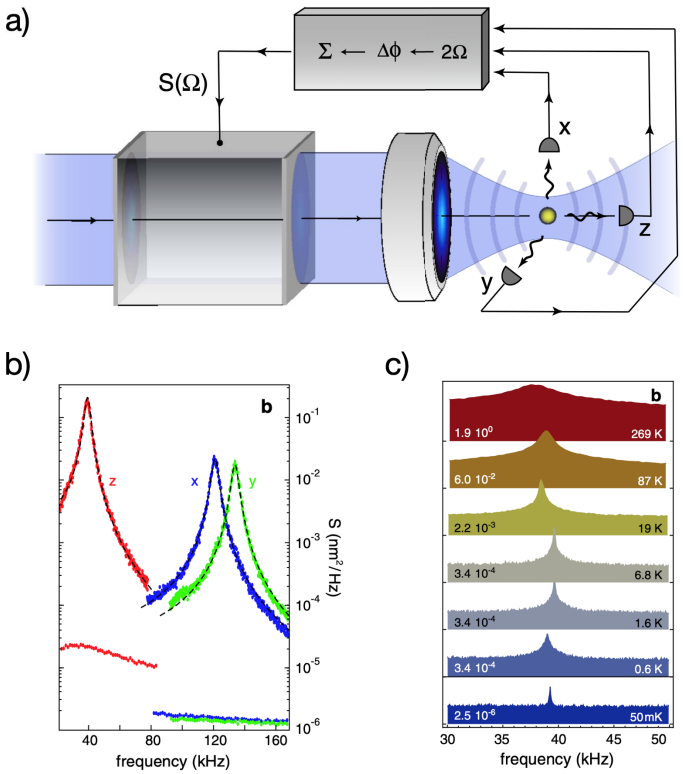

Figure 1.1: a) Mechanism of parametric feedback cooling. The center of mass position of a nanosphere is measured using three detectors. A signal with twice the resonance frequency 2Ω (for the 3 independent directions) of the oscillator is obtained by multiplying the instantaneous position with its derivative, $x(t)v(t)$. There, Ω is the natural mechanical resonance frequency of the nanosphere in the harmonic optical trap. This signal is continuously subjected to a phase-shift to ensure the damping of the center of mass position oscillations. This signal is then used to control the intensity of the trapping laser. b) Spectral density of the center of mass motion along the 3 independent directions. A difference in resonance frequency Ω for each of the directions can be observed: while the focus on the axial direction is more extended, leading to smaller stiffness compare with the transverse plane, polarization breaks the symmetry on this plane, leading to different stiffness on the x and y directions. c) Spectral density of the motion evaluated for different temperatures along the axial direction, proportional to the area of the spectrum, and the corresponding pressure, in mBar. Reproduced from ref. [17]

of information processing, with the problem of the minimum energy that must be dissipated to *erase* one bit of information limited by the Landauer's bound [31, 32]. Clearly, the non-equilibrium nature of changing the center of mass temperature by the action of feedback is rich. We will here however discuss simpler temperature controls.

Instead of cooling the center of mass of the trapped nanosphere, experimental efforts have also been directed towards heating the Brownian particle, either by directly heating the fluid [34], also involving feedback techniques [35], or by adding stochastic forces, such as an external electric field [33]. In panel a) of Figure 1.2, a polystyrene

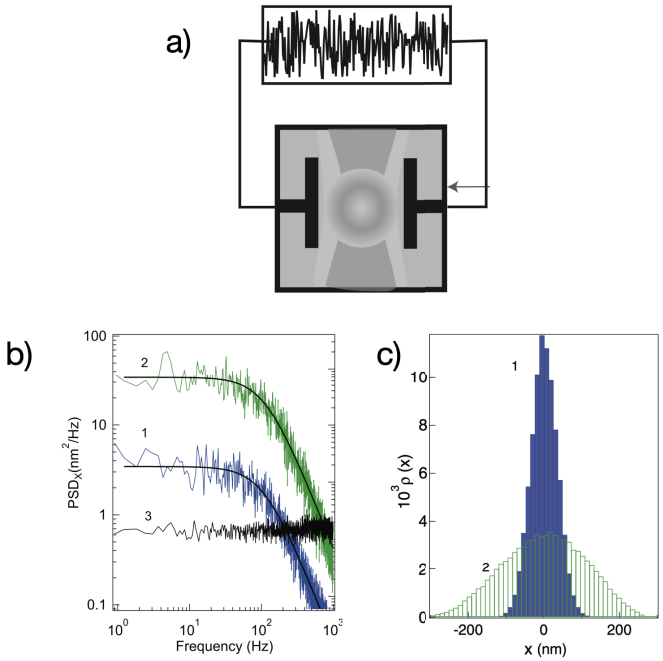

Figure 1.2: a) Polystyrene microsphere trapped in water by optical tweezers. Custom-made electrodes exert a stochastic force through electrostatic interactions with the residual surface charges of the microsphere. b) Position power spectral density (PSD) of the microsphere without the action of the additional stochastic force in blue and after the addition of this force in green. The superimposed curves in black correspond to Lorentzian fits. The PSD of the stochastic force, measured from the input of the electrodes, corresponds to the black spectrum. This verifies the effective "white noise" action of the electrostatic forcing. c) Histograms of the position of the microsphere in the absence and presence of the extra stochastic force. Same color code. The change in the variances of the corresponding Gaussian distribution is interpreted as a change in the effective temperature. Reproduced from ref. [33].

microsphere is trapped in water and, through the action of an additional stochastic force produced by a time-dependent electric field, the temperature of its center of mass increases compared to the expected temperature considering only the action of the surrounding water. In panel b), the nature of this white noise force is characterized by its power spectral density (PSD), in black, that it is flat up to a frequency of 10^3 Hz. Due to the effect of this additional force, the position PSD of the trapped microsphere in blue is transformed into the green one, in which there is a significant increase in the position PSD area. Both spectra display the same characteristic frequency, confirming that the temperature modification does not change the trapping potential. Such an increase in area, directly linked to the increase in position variance, is evident in panel c) from the increase in the variance of the position distribution. The increase in variance is interpreted via equipartition as rise in temperature.

When the temperature is changed by controlling the amplitude of an external stochastic force, relevant time scales, such the bandwidth in which this force is considered as a white noise, sampling frequency, and characteristic time of relaxation of the system under study need to be taken into account carefully [36]. Temperature control makes it possible, for instance, to investigate asymmetries between heating and cooling processes [37], thermalization process towards equilibrium [38], memory effects such like Kovacs [39] and Mpemba [40] effects, and the implementation of colloidal thermal machines [41], in which exchanges of thermal and mechanical energy are investigated [35, 42, 43].

The case of the Kovacs effect is, in this sense, interesting to analyze. Initially observed in attempts to accelerate thermalization through different "heat treatments" in polymer glass systems [44], it was recently verified in the dynamics of an optically trapped nanoparticle at atmospheric pressure (around 1 bar), as described in Figure 1.3. There, the dynamics of the particle, which shows just small deviations from the spectral point of view with respect to the overdamped motion, panel b), attests the need to consider additional state variables to explain such memory effects [45]. In this case, the resonance frequency of the trap is $2\pi \times 159$ kHz, related to the relaxation time of potential energy, and the dissipation rate is $2\pi \times 399$ kHz, related to the relaxation of kinetic energy. This implies that, throughout the thermalization process, the non-equilibrium nature of both degrees of freedom must be taken into account.

The memory effect is observed when a sequential change in temperature is performed, starting from a situation where the center of mass is hot $T_{\mathrm{H}} = 2450$ K, followed by an evolution toward a cold temperature $T_{\mathrm{C}} = 298$ K, and then to a intermediate warm temperature, $T_{\mathrm{W}} = 1290$ K. The change $T_{\mathrm{C}} \to T_{\mathrm{W}}$ is made after a time interval t_{W}, chosen as the instant when the potential energy of the particle reaches the expected value for equilibrium with a target temperature T_{W}. This process results in a

non-monotonic evolution of the potential energy – see red curve in panel d). Whereas the light blue curves in panel c) and d) correspond to the relaxation processes for temperature T_W in diamonds and T_C in triangles, both relaxation processes are monotonic and they have the same characteristic thermalization time. When the Kovacs protocol is used, this experiment shows that the cooling process is not accelerated by using the lowest possible temperature T_C from $t = 0$ to $t = t_W$, and a non-monotonic evolution

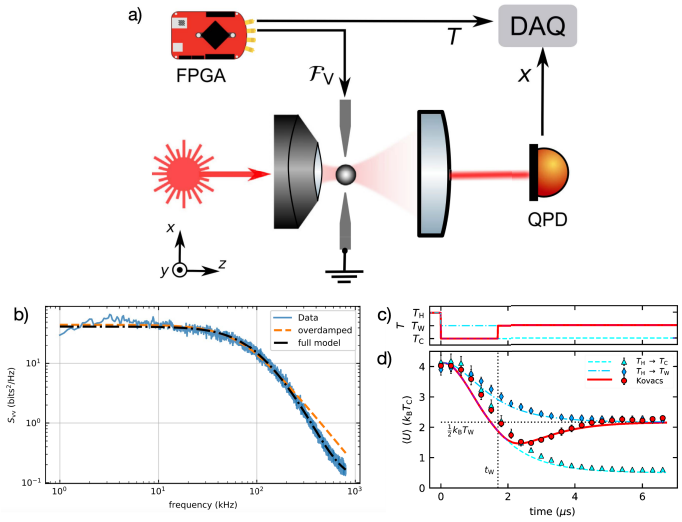

Figure 1.3: a) Experimental scheme for trapping a silica nanosphere in which the temperature of its center of mass is altered by two electrodes, which in turn are controlled by a field-programmable gate array (FPGA). b) Position PSD in which the complete model, considering a second-order differential equation of motion for position, is compared with the PSD expected for the overdamped regime. c) Protocols for changing the temperature $T_H > T_W > T_C$ as a function of time. In light blue, a single change is considered, where the dash-dotted line corresponds to $T_H \to T_W$ and the dashed line to $T_H \to T_C$. The Kovacs protocol corresponds to two temperature changes, in red. d) Evolution of the potential energy for the three previous protocols in which the curves correspond to those expected by the theoretical model, same color code as before. The measurement of the processes $T_H \to T_W$ correspond to diamonds, $T_H \to T_C$ to triangles and the red circles to the Kovacs protocol. While the vertical dashed line corresponds to the instant of change $T_C \to T_W$ for the Kovacs protocol, the horizontal dashed line correspond to the expected potential energy when the particle is in equilibrium with the temperature T_W. Reproduced from ref. [39].

of the potential energy, measured from the position variance, is verified. The Kovacs protocol is an example of how the flow of thermal to kinetic and potential energy, analyzed from Brownian particle dynamics, is still an interesting research topic to be explored.

In those systems in which the center of mass of a trapped particle gets hotter, temperature is linked to the amplitude of a stochastic force described by a Gaussian distribution and with a flat spectrum. Although any physical process that produces stochastic forces necessarily has an associated characteristic time scale associated with, since the fluid molecules that drive the Brownian particle are very fast, the white noise approximation for this stochastic force is sufficient to describe the dynamics of a Brownian particle in equilibrium. In this case, the thermal bath does not add any characteristic time scale to the Brownian dynamics. However, when the time scale of the stochastic forces is comparable to the time scale of the Brownian particle, or when the distribution of the stochastic force is not Gaussian [46, 47, 48], the characteristic times of the Brownian dynamics are altered, and one of the consequences is the emergence of processes with anomalous diffusion [49, 50]. In such cases, the system is said to be immersed in an "active bath".

Engineering the properties of the thermal bath in the context of active matter is thus of primary importance. Using these techniques, for instance, it becomes feasible to verify the dependence of the efficiency of molecular motors, such as the kinesin molecules moving along a microtubule, with respect to the properties of the thermal bath [51]. By applying external noise forces that mimic the intracellular environment, faster motions of these molecular motor were observed, demonstrating direct connections between the efficiency of molecular motors and the fluctuation properties of the thermal bath.

In this thesis, the focus will be directed towards engineering the thermal bath using a stochastic force with a flat spectrum and an effective Gaussian distribution, aiming for a thermodynamic description of state-to-state transitions.

1.2 Acceleration and optimization of Brownian systems

The ability to control the state of a Brownian particle using external parameters naturally leads to the study of the evolution between two equilibrium states, as in the case of the Kovacs protocol discussed in the previous section. Here we will discuss a few specific strategies for speeding up transitions between two equilibrium states.

The process of accelerating such transitions is one of the main goal of the research

area "shortcut to adiabaticity " for quantum systems [52] or swift state-to-state transformations in the classical regime [53]. Within this framework, time is explicitly incorporated to the thermodynamic discussion as a dynamical variable. To illustrate these acceleration processes, we will provide some details of the paradigmatic case called *engineered swift equilibration* (ESE) [54], initially developed in the overdamping regime, adapted to combine thermal and confinement changes [55] and, more recently, applied in the underdamping regime [56], as described in Figure 1.4. In this work, a nanosphere is trapped in a low pressure chamber (5 mbar) and the intensity of the trapping laser is controlled by an acousto-optic modulator (AOM). In the upper panel a), the process of changing the stiffness $\kappa_i \to \kappa_f$ is schematized, where the relaxation time t_{relax}, associated with a discontinuous change in the stiffness, is displayed together with $t_{\text{f}} < t_{\text{relax}}$, the transition time obtained when the acceleration process is carried out.

When the dissipation is weak enough, the Brownian particle responds to an external stimulus with a cyclical transfer between potential and kinetic energies, as can be seen in the blue curves of panel b), when a discontinuous change on the confinement potential $\kappa_i \to \kappa_f$ is produced. Consequently, after t_{relax} that span several oscillations, the position standard deviation $\sigma_x(t)$ increases to compensate the reduction in κ induced by the protocol. Conversely, after this same characteristic time, the velocity standard deviation $\sigma_{v_x}(t)$ returns to its initial value, since a change on the velocity distribution is not expected after equilibrium is reached in an isothermal process.

By introducing an ESE protocol, which in this context corresponds to a polynomial function obtained as an ansatz satisfying a system of differential equations plus equilibration boundary conditions [57], the equilibration of the Brownian particle is reached after a time $t_{\text{f}} < t_{\text{relax}}$. Specific details of the system's out-of-equilibrium evolution can be seen in panel c). While $\alpha(t)$ is associated with the evolution of the instantaneous potential energy, $\beta(t)$ refers to the evolution of the kinetic energy, and $\delta(t)$ captures the correlation between position and velocity. Such acceleration strategies require an additional energy input to suppress non-equilibrium fluctuations, or in this context, also the oscillations produced by the external stimulus, in which a trade-off relationship between the cost and the accelerated relaxation t_{f} is anticipated. In these ESE protocols that accelerate the transition, their derivation is based on the condition that the Browinain particle reaches equilibrium at the time interval t_{f}; however, the relationship between t_{f} and the thermodynamic cost associated with this processes is not taken into account. Naturally, this gives rise to the issue of optimization in which some methods have been proposed.

To do in the realm of both isothermal [58] and non-isothermal processes [59], the concept of "instantaneous equilibrium" has been introduced. The energetic expen-

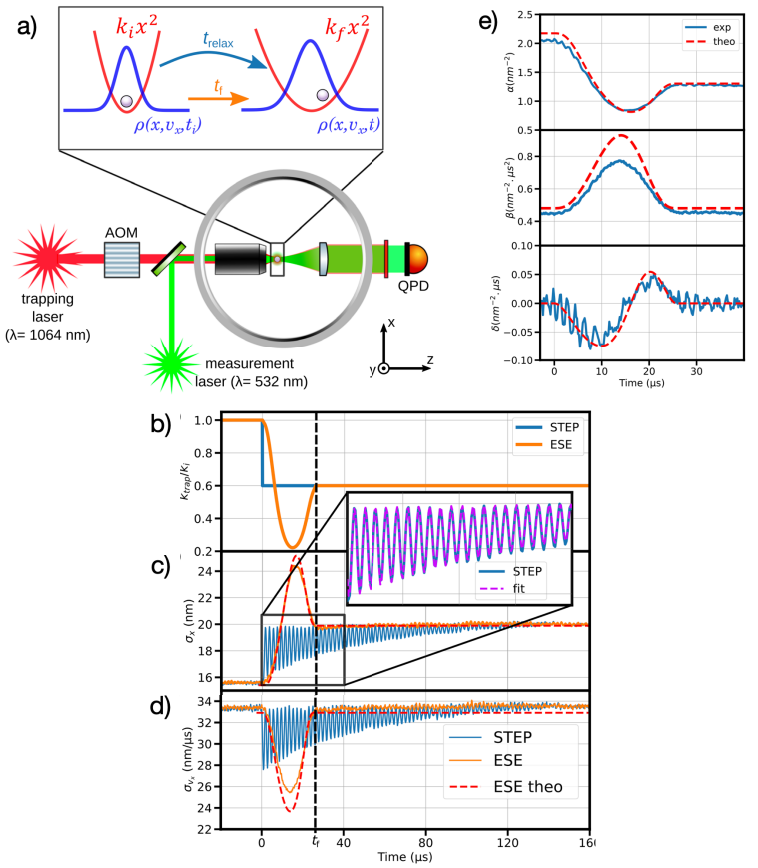

Figure 1.4: a) Experimental scheme where a nanosphere is subjected to the action of two lasers: one that traps the particle (in red), whose intensity is controlled by an acousto-optic modulator (AOM), and another used to detect the position of the microsphere (in green). Two times are considered in the expansion process $\kappa_i \rightarrow \kappa_f$, t_{relax} related to a discontinuous change in potential, and t_f when accelerated expansion is considered $t_f < t_{\text{relax}}$. b) Temporal evolution of the stiffness for the case of a discontinuous change (in blue) and the ESE acceleration protocol (in orange). c) and d) Temporal evolution of the standard deviation of position $\sigma_x(t)$ and speed $\sigma_{v_x}(t)$ for the two protocols, with the same color code. The stabilization time corresponds to $t_f = 26$ μs. Inset: close-up of the oscillations in $\sigma_x(t)$. e) Evolution of the coefficients $\alpha(t)$, $\beta(t)$, and $\delta(t)$ that determine the evolution of the potential energy, the kinetic energy, and the correlation between position and speed. Measured values correspond to the continuous curves and theoretical model values to the dashed curves. Reproduced from ref. [56].

diture, intrinsically associated with the acceleration, is evaluated by introducing an auxiliary potential that quantifies the cost of keeping the Brownian particle in an instantaneous equilibrium state during an acceleration protocol. In these works, the relationship between cost and transition time is evaluated, but no trade-off relationship is established.

Alternative strategies focus on the direct minimization of the transition time [60, 61, 62] in which "bang-bang" protocols, forcing the control parameter (stiffness or temperature of the bath) to undergo maximum changes during the transition, serve this purpose. Other approaches involve protocols for minimizing the transition time in the "slow drive" regime, in which the modulations of the control parameters are slower than the system's intrinsic relaxation time. These techniques relay on the formalism of information geometry [63]. The optimization problem is then directly linked to the determination of a geodesic path [64], which is defined using the concept of thermodynamic length [65], which in turn quantifies "distance between distributions". In these contexts, there is no direct relationship between transition time and relative cost that allows the derivation of a state-to-state optimal transfer protocol.

By considering isothermal processes in which the cost of a transition can be identified directly as the work dissipated throughout the process, in the references [66, 67, 68] an energy dissipation functional, for a given transition time, is constructed. In this context therefore, the optimal protocol corresponds to minimizing this functional. These approaches are directly related to the strategies proposed and developed in this thesis, where the focus is put on the optimization state-to-state transition involving temperature changes.

1.3 Content of this thesis

This thesis aims to present the experimental and theoretical methods to produce and describe both dynamically and thermodynamically isothermal and isochoric processes, implemented on a Brownian particle in the overdamped regime. These procedures are described throughout three chapters:

- **Chapter 2**: in this chapter the experimental methods used to implement the bath engineering techniques are presented. Starting with a discussion on the time scales involved in the description of a microsphere in an aqueous solution (overdamped regime), confined by a harmonic potential, the experimental platform for trapping, monitoring and adding external optical forces is presented. An important development of this experimental platform is the control of the statistical properties of the laser that exerts radiation pressure on the trapped

microsphere. The methods for introducing such procedures using an acousto-optic modulator will be presented in details, together with the description of the dynamics of this microsphere, via the Langevin equation. This formalism allows the description of processes in which the amplitude of the additional stochastic force changes in time. The case of discontinuous changes and protocols that speeds up state-to-state transitions are presented.

- **Chapter 3**: the thermodynamic description of isothermal and isochoric processes in which the internal energy of the system is defined solely from the potential energy is developed in this chapter. The description of such processes is based on the introduction of state functions when the system is out of equilibrium. While the extension of the internal energy to non-equilibrium states is straightforward, this is not the case for the entropy of the system. Therefore, a new definition of entropy associated with a stochastic trajectory is introduced. To quantify the cost of out-of-equilibrium processes, dissipative energy and entropy production are introduced and discussed in detail when discontinuous changes in the control parameters are considered.

- **Chapter 4**: exploiting the functional approach, we address in this last chapter state-to-state transitions by balancing the trade-off between cost and transition time of isochoric processes. This methodology enables us to derive optimal transformations with associated time-entropy constraints. Building on the thermodynamic framework introduced in Chapter 3, we characterize isochoric transformations influenced by time-varying modulations in the amplitude of the external stochastic radiation pressure force. In addition, we explore the asymmetries between heating and cooling processes along three different aspects: for abrupt changes in temperature, for different acceleration techniques, and finally comparing the cost for heating and cooling processes as a function of the transition time and the total temperature change produced in the optimal isochoric process.

1.4 List of publications

The core of this has shaped the following article:

- Pires, L. B., Goerlich, R., da Fonseca, A. L., Debiossac, M., Hervieux, P. A., Manfredi, G., & Genet, C. (2023). Optimal time-entropy bounds and speed limits for Brownian thermal shortcuts. Physical Review Letters **131**, 097101.

The experimental developments of the platform in relation to bath engineering using radiation pressure has been central to the following work:

- Goerlich, R., Pires, L. B., Manfredi, G., Hervieux, P. A., & Genet, C. (2022). Harvesting information to control nonequilibrium states of active matter. Physical Review E, **106**(5), 054617.

Along this thesis a few other works have been published in collaboration with my previous colleagues at Federal University of Rio de Janeiro (UFRJ):

- Pires, L. B., Ether, D. S., Spreng, B., Araújo, G. R. D. S., Decca, R. S., Dutra, R. S., Borges, M., Rosa, F.S.S., Ingold, G.-L., Moura, M. J. B., Frases, S., Pontes, B., Nussenzveig, H. M., Reynaud, S., Viana, N. B. & Neto, P. M. (2021). Probing the screening of the Casimir interaction with optical tweezers. Physical Review Research, **3**(3), 033037.

- Martínez-Tibaduiza, D., Pires, L., & Farina, C. (2021). Time-dependent quantum harmonic oscillator: A continuous route from adiabatic to sudden changes. Journal of Physics B: Atomic, Molecular and Optical Physics, **54**(20), 205401.

- Gómez, F., Dutra, R. S., Pires, L. B., Araújo, G. R. D. S., Pontes, B., Neto, P. M., Nussenzveig, H. M., & Viana, N. B. (2021). Nonparaxial Mie Theory of Image Formation in Optical Microscopes and Characterization of Colloidal Particles. Physical Review Applied, **15**(6), 064012.

There are also two other articles in the final process of publication:

- Goerlich, R., Li, M., Pires, L. B., Hervieux, P. A., Manfredi, G., & Genet, C. (2023). Experimental test of Landauer's principle for stochastic resetting. arXiv preprint arXiv:2306.09503

- da Fonseca A. L., Diniz, K., Monteiro, P. B., Pires, L. B., Moura, G. T., Borges, M., Dutra, R. S., Ether Jr, D. S., Viana, N. B., & Maia Neto, P. A. (2023). Tailoring bistability in optical tweezers with vortex beams and spherical aberration.

Chapter 2

Time dependent temperature in an optical trap

This chapter details the experimental platform on which the stochastic dynamics of a Brownian particle trapped in an optical tweezers is probed and controlled. An essential development of this platform is the addition of a laser that exerts radiation pressure on such a particle. This addition allows to fix and tune the properties of the thermal bath via the mere control of an external parameter.

After presenting the power spectrum and position distribution associated with the stochastic trajectory of the Brownian particle in a stationary state, the dynamical description of time dependent temperature protocols that connect two different stationary states will be presented.

2.1 Introduction

2.1.1 Characteristic times

Temperature is a common concept linked to the "thermal sensation" of hot or cold. This perception only makes sense in the range of meters and seconds since for objects at the micrometer length scales, "thermal sensation" corresponds to a completely different effect. Particles at these length scales are subjected to collisions with fluid molecules with variable intensities, which result in erratic trajectories of these particles known as Brownian motion. From a fundamental point of view, these collisions have a characteristic time related to the frequency at which they occur. This frequency, in turn, depends on the average speed of the fluid molecules, typically 600 m/s for water at room temperature T_{RT}. The other parameter entering the definition of this time is the average distance between molecules, of the order of 0.3 nm, leading to a typical time interval between successive collisions of water molecules of 0.5×10^{-12} s.

Then, the diffusion of a Brownian particle confined in a potential is characterized by additional times associated with its dynamic variables, position $x_j(t)$ and velocity $v_j(t)$. While the first characteristic time τ_x corresponds to the average time the particle spends in each energy level, which determines the correlation between successive measurements of $x_j(t)$, the second characteristic time τ_v describes how far on average the particle continues moving in a direction before collisions randomize that direction, which in turn determines the correlation between successive velocity measurements $v_j(t)$. Such characteristic times can be estimated when the drag force is linear with the velocity, $f_{\text{vis}}(t) = -\gamma v_j(t)$ and the confining force is associated with a harmonic potential, that is linear with the displacement, $f_{\text{trap}}(t) = -\kappa x_j(t)$. In this case, for a micrometric particle in water, $\tau_x = \gamma/\kappa \sim 10^{-3}$ s and $\tau_v = m/\gamma \sim 10^{-6}$ s, where m is the mass of the trapped Brownian particle.

With such time scales in mind, the fundamental question of this chapter can be formulated: how does the dynamics of a Brownian particle measured on the millisecond time scale $t_{\text{meas}} \sim 10^{-3}$ s evolve when subjected to a change of its "thermal sensation"? To answer this question, an experimental platform that makes it possible to measure such dynamics is not sufficient. It is also necessary to have a technique at hand by which it is possible to alter the "thermal sensation" of the Brownian particle in a reliable and repetitive manner. To be more precise, this technique should be capable of changing the statistical properties of the random variables $(x_j(t), v_j(t))$, while keeping the confining potential constant. Note that these random variables are described by probability distributions that in turn are related with Boltzmann distributions when the trapped particle is in thermal equilibrium with the fluid. In the case of a harmonic trapping potential, these distributions are Gaussian, being entirely determined by variances of position s and velocity s_v only.

To solve the dynamics of the Brownian particle in time, it is necessary to define, in addition to t_{meas}, the rate at which the position of the particle is measured, f_{aq}. This rate will lead to define another characteristic time, $1/f_{\text{aq}} = dt \sim 0.015$ ms, when sampling typically at $f_{\text{aq}} = 2^{16}$ Hz. Under this rate, it is possible to

of $x_j(t)$, since $2\pi \times f_{\text{aq}} \gg 1/\tau_x$, but not those of $v_j(t)$. In an overdamped dynamic, the consequences imposed by f_{aq} are appropriate, as they can be understood by Einstein's argument for free Brownian motion: from an initial position at $t = 0$, the position variance of a free Brownian particle increases as $s(t) \propto t$ [69]. To make it short, if we introduce the root mean square velocity as $v_{\text{rms}}(t) = \sqrt{s(t)}/t$, it will lead to $v_{\text{rms}}(t) \propto 1/\sqrt{t}$. As $t \to 0$, the denominator approaches zero and therefore v_{rms} diverges leading to a ill-definition of velocity at very short time scales. These considerations thus justify making the entire description of the dynamics of the Brownian particle only in terms of "instantaneous" positions $x_j(t)$. In turn, this allows us

to interpret the particle as a thermometer whose position variances can be used as a measure of the fluid temperature T, when in equilibrium, through the equipartition theorem setting that $T = \kappa s/k_{\mathrm{B}}$.

2.1.2 From stochastic variables to mobility distributions

Usually, it is standard to define $x(\tau)$ or x_t as a stochastic variable associated with a physical process - see typically [5] and [70]. Note that in this last reference the notation used for a stochastic physical process corresponds to X_t. This lead to define a trajectory associeted to a given process as a temporal series of position recorded over a time interval $[0, t_{\mathrm{meas}}]$ as $x_{[0,t_{\mathrm{meas}}]} = \{x_t\}_{t\in[0,t_{\mathrm{meas}}]}$, that is a succession of time ordered stochastic realizations of the stochastic variable x_t. For each time, x_t takes on values in the set $\mathcal{X} = \mathbb{R}$. Elements of this set are denoted by $x \in \mathcal{X}$, while for this process, it is possible to introduce a probability density $\mathcal{P}(x_{[0,t_{\mathrm{meas}}]})$. Here a different notation will be used for the stochastic variable $x_j(t)$, to highlight the difference between measuring the distribution of this variable over time, which corresponds to $\mathcal{P}(x_{[0,t_{\mathrm{meas}}]})$ and measuring the distribution obtained from an ensemble $\{j\}$ of independent realizations of the variable $x_j(t)$, for the same time t. In this case, this distribution is necessarily Gaussian and given by $p(x, s(t))$. One of the outstanding aspects of the Brownian particle model is the possibility to measure the evolution of the stochastic trajectory for the same process $x_j(t)$, thus determining $\mathcal{P}(x_{[0,t_{\mathrm{meas}}]})$, and the probability distribution associated with the stochastic variable $x_j(t)$ for each instant of time, thus determining $p(x, s(t))$, even for the case in which the instantaneous $s(t)$ position variance evolve in time.

From these basic notations, the experimental technique and procedures to carry out both the measurements and the controls over the Brownian particle will be presented. Once the stationary situation is characterized, the methods that make it possible to study the change in the statistical properties of $x_j(t)$ in time will be described. Then, the mathematical description of processes that connect two stationary states, defined through their probability distributions as $p(x, s_i = k_{\mathrm{B}}T_i/\kappa)$ and $p(x, s_f = k_{\mathrm{B}}T_f/\kappa)$ will provide the right framework to introduce the thermodynamic description of out-of-equilibrium processes that will be carried out in the next chapters.

2.2 Optically trapped Brownian particles

2.2.1 Experimental platform

The optical part of the experimental setup is shown in Figure 2.1. It can be divided into 4 blocks that together allow the manipulation of polystyrene microspheres (Duke Scientific Corp 3 μm in diameter) in aqueous solution. Each block corresponds to a

function: block 1 illuminating the focal region (yellow laser), block 2 optically trapping the microspheres (red laser), block 3 detecting motion (orange laser) and block 4 corresponds to the fourth laser responsible for applying radiation pressure (brown laser).

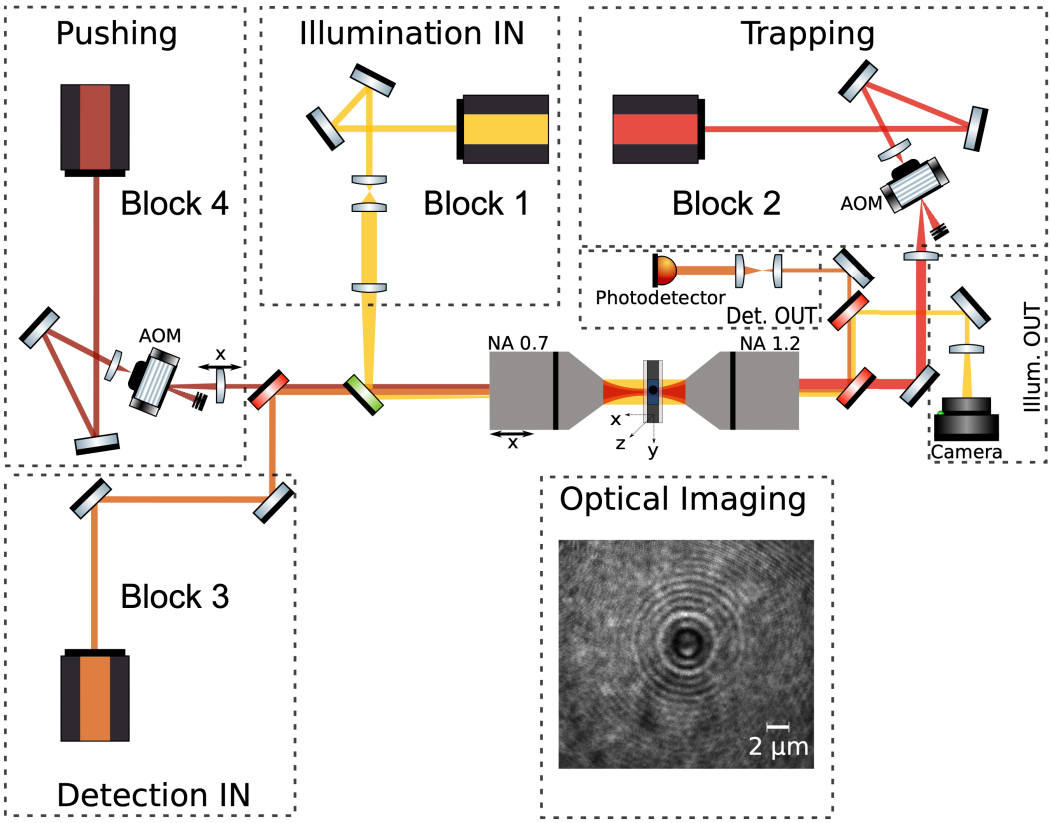

Figure 2.1: Sketch of the optical part of the experimental setup. This setup is divided into 4 blocks that correspond to illumination (594 nm, yellow laser), trapping (785 nm, red laser), detection (639 nm, orange laser) and a laser that exerts radiation pressure (tuned at 800 nm, brown laser), on a Brownian particle, trapped in the focal region of both the two objectives placed in the center of the panel. The divergence and waist of each beam are controlled by telescopes and the intensity of the red and brown lasers can be controlled using acousto-optic modulators (AOM). The yellow laser is directed to a CCD camera providing an image of the focal region, as in the image illustrated on the bottom right panel. When scattered by a trapped particle, the intensity of the detection laser (orange) is modulated by the Brownian motion of the trapped particle, measured using a fast photodetector.

Optical imaging system (block 1)

To form an image of a Brownian particle shown in the bottom right panel of Figure 2.1 we use the yellow laser (594 nm, Excelsior-594-50-CDRH). This laser is first expanded by a telescope and then focused on the back focal plane of a microscope objective (Nikon Plan-fluo extra large working distance 60×, NA=0.7), resulting in a plane wave in the sample region. This can be understood from the concept of front and back focal planes for paraxial rays [71]: while a collimated beam incident on the back focal plane of an objective is focused at the front focal plane, a beam with a center of divergence in the back focal plane is collimated after passing through the objective. This condition is met by the yellow laser when using a converging lens of focal length 30 cm, positioned at this separation distance from the back focal plane of this objective. To produce an image, another objective is used (Nikon Plan Apochomat 60×, NA = 1.2), in a situation in which both focal planes coincide. Then, this second objective collects the collimated beam, along with the light scattered by microspheres diffusing within this shared focal region. The interference pattern is then projected onto a CCD camera (Allied Guppy Pro, 1292×964 pxl^2). The objective of NA = 1.2 will be referred to as objective 1 and the objective of NA=0.7 will be referred to as objective 2 henceforth.

Trapping system (block 2)

In optical tweezers, the condition for trapping dielectric objects having a refractive index larger than that of the surrounding medium [72, 73], is the presence of a gradient force, proportional to the spatial intensity distribution of a highly focused laser beams, $f_{\text{grad}} \propto \partial I(x, y, z)/\partial x$ [74]. This gradient force must be stronger than the inevitable radiation pressure, that in turn is proportional to the laser intensity, $f_{\text{rad}} \propto I(x, y, z)$. This condition requires the use of lenses with large numerical apertures, such as objective 1. When examining displacements around the equilibrium position that are significantly smaller than the radius of the trapped microsphere, one can approximate the optical potential as a harmonic potential. This is a significant simplification, as it implies a linear relationship between the trapping force and the displacement from the equilibrium. The validity of this harmonic approximation has been proven through various experimental results [75, 76, 77]. Notably, by observing the position distribution of trapped microspheres, as shown in Figure 2.5, we find it to closely resemble a Gaussian distribution, a hallmark of a harmonic potential. We note however that nonlinearities can also emerge from the interplay between gradient forces (conservative) and radiation pressure forces (non-conservative) in overdamped [78] and underdamped [79] regimes.

The trapping laser that we use, (785 nm, 110 mW OBIS Coherent, CW) has a Gaussian intensity profile, and is expanded by a telescope system so that its waist satisfies the overfilling condition at the entry of objective 1. This condition maximizes the ratio $f_{\text{grad}}/f_{\text{rad}}$. Under such conditions, polystyrene microspheres in water (refractive indices $n_{\text{poly}} = 1.59$ and $n_{\text{wat}} = 1.33$) are attracted towards the focal region of the laser. The microspheres are dispersed in a volume of 18 μL between two glass slides, separated by a spacer (Grace Bio-Labs) of thickness 120 μm. The microsphere solution is diluted to 0.5×10^{-4} %, thus ensuring that mainly one microsphere is found inside the trapping region during the experiments.

Detection system (block 3)

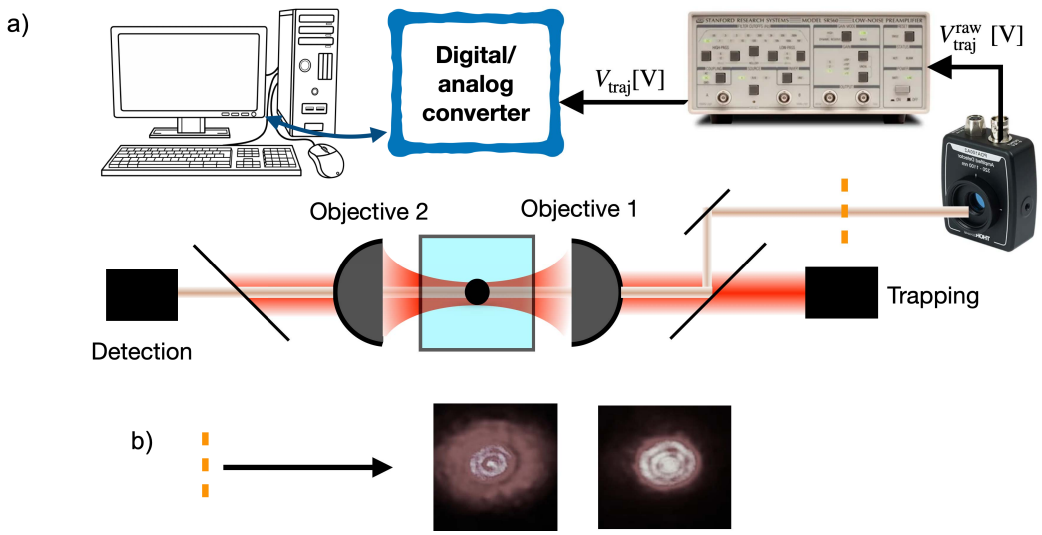

Figure 2.2: Sketch of the detection system. a) The orange laser passing through objectives 2 and 1 is separated from the red one by a dichroic mirror and directed to a photodiode. This signal is amplified and frequency filtered by a low-noise preamplifier and sent to a digital-to-analog conversion board. The digital signal is then saved on a computer. The dashed line corresponds to the position of a bulkhead, used to take a picture of the laser spot and roughly align the detection laser in relation to the trapped microsphere. This bulkhead allows us to see the intensity distribution with and with out a microsphere on its way. b) Intensity pattern of the orange laser scattered by a microparticle (left) and without scattering (right) obtained from a photograph of the spot of this laser on the bulkhead.

The detection laser (639 nm, Thorlabs HL632MG CW) is directed by objective 2 towards the microsphere trapped by objective 1. Both incident beam and scattered light are collected by objective 1 and separated from the trapping laser by a dichroic mirror. A sketch of the detection process, together with a photograph of the projection of this laser onto a bulkhead – which plays the role of an image plane represented by a vertical dashed orange line before the photodetector – are shown in Figure 2.2, respectively on panels a) and b). Panel b) shows the difference on the intensity distribution, viewed by a simple photograph, when this laser is scattered by a trapped particle (image on the left), to the case in which there is no particle on the optical path of the detection laser (image on the right). For the case in which the detection laser is scattered by a trapped particle, the light spreads over a large area, when compared to the case in which there is no particle scattering light along the optical path.

Due to the inherent nature of Brownian motion, the spatial relationship between the trapped microsphere and the focal position of the detection laser is continuously fluctuating over time. This continuous spatial fluctuation induces a time-varying modulation in the detected intensity. This modulation is quantitatively captured in real time by the photodiode as an instantaneous voltage signal, represented as $V_{\text{traj}}^{\text{raw}}(t)$. This raw signal then undergoes a series of processing steps to refine its utility and accuracy.

First, it is routed to an amplifier and bandpass filter (Stanford Research, SR560). This selective filtering effectively isolates a specific bandwidth $[0.3; 100.000]$ Hz from $V_{\text{traj}}^{\text{raw}}$. The high-pass component of the filter serves to eliminate low-frequency components, which are predominantly influenced by drift effects as for example mechanical oscillations of optical elements that are not entirely neutralized by the pneumatic mechanical filtering stage of the optical table, or even subtle drifts in the optical pathways of the lasers. On the other end of the frequency spectrum, the low-pass filter prevents aliasing during the analog-to-digital conversion process executed by the acquisition card (specifically, the National Instrument PCI-6251 paired with BNC-2110).

Radiation pressure (block 4)

The last block sketches a Spectra Physics 3900S Ti:Sapphire CW laser, tuned at 800 nm. This Ti:Sapphire is used to exert unidirectional radiation pressure on the trapped sphere, the pushing laser. The details of the intensity control of this laser using an acousto-optic modulator (AOM - 3200 S Gooch & Housego) will be discussed in a following section.

Force diagram

When under control of this experimental platform, the dynamics of a single Brownian particle can be understood from the force diagram shown in Figure 2.3 [80], in which the forces depicted are the trapping force, exerted by the trapping laser $f_{\mathrm{trap}}(t)$, and a time dependent external force $f_{\mathrm{ext}}(t)$, defined by the intensity of the pushing laser. By the action of the fluid, the Brownian particle is subject to the unavoidable viscous force $f_{\mathrm{vis}}(t)$ and thermal force $f_{\mathrm{ther}}(t) = \sqrt{2k_{\mathrm{B}}T_{\mathrm{RT}}\gamma}\xi_j(t)$, connected through the fluctuation dissipation theorem [81]. Here $\xi_j(t)$ is a stochastic variable with zero mean $\langle\xi_j(t)\rangle = 0$ and delta correlated $\langle\xi_j(t)\xi_{j'}(t')\rangle = \delta_{jj'}\delta(t-t')$. The sub index j accounts for a label taken on the ensemble of different realization of this stochastic variable, at the same instant of time t and $\langle ...\rangle$ correspond to the ensemble average over those different $j-$trajectories, for the same time instant.

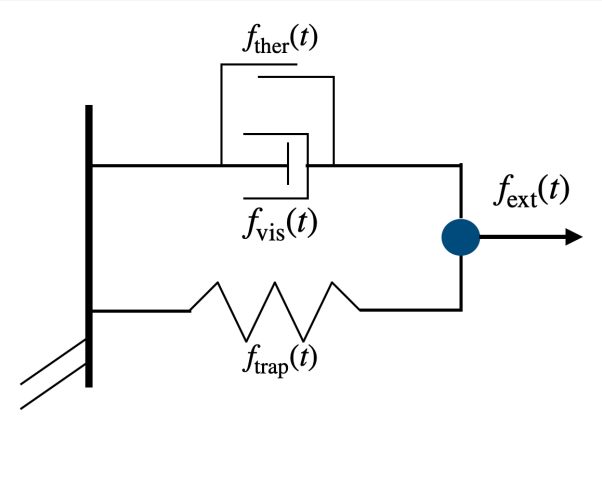

Figure 2.3: Force diagram that determines the dynamics of the Brownian particle. While the trapping force $f_{\mathrm{trap}}(t)$ and the external force $f_{\mathrm{ext}}(t)$ respectively correspond to the action of the trapping laser and the laser exerting unidirectional radiation pressure, the pair viscous force $f_{\mathrm{vis}}(t)$ and thermal force $f_{\mathrm{ther}}(t)$ are connected by the fluctuation dissipation theorem.

2.2.2 Observables

The processed time series $V_{\mathrm{traj}}(t)$, derived from the raw signal $V_{\mathrm{traj}}^{\mathrm{raw}}(t)$ after filtering and amplification, is depicted in Figure 2.4, panel a). Captured at an acquisition rate $f_{\mathrm{aq}} = 2^{15}$ Hz, this series acts as a primary measurement, in which all observables are derived from. A brief interlude is taken to explain the method of position and stiffness calibration [82], based on a linear relation between the microsphere displacements and

the scattered laser intensity ($x_j(t) = V_{\text{traj}}(t)/\beta$, with β a constant calibration factor), using the Power Spectral Density ($PSD(f)$) of $V_{\text{traj}}(t)$, that in turn is measured from a discrete Fourier transform [83].

A discrete Fourier transform consists into the mapping of the time series $V_{\text{traj}}(t) = V_{\text{traj}}(k/f_{\text{aq}})$, where k spans from 0 to $N-1$, and $N = 655.360$ is the total of measurements over a total acquisition time $t_{\text{meas}} = N/f_{\text{aq}} = 20$ s, to the series $\tilde{V}_{\text{traj}}(mf_{\text{aq}}/N)$, with m ranging from 0 to $N/2$, by the transformation:

$$\tilde{V}_{\text{traj}}\left(\frac{m}{N}f_{\text{aq}}\right) = \sum_{k=0}^{N-1} V_{\text{traj}}\left(\frac{k}{f_{\text{aq}}}\right) \exp\left(-2\pi i \frac{mk}{N}\right). \tag{2.1}$$

From this, the $PSD(f)$ can be measured as $PSD_V(f) = |\tilde{V}_{\text{traj}}(f)|^2$, illustrating the signal's power distribution across frequencies. Effectively, $PSD(f)$ provides a comprehensive frequency component spectrum of the signal, highlighting dominant contributors.

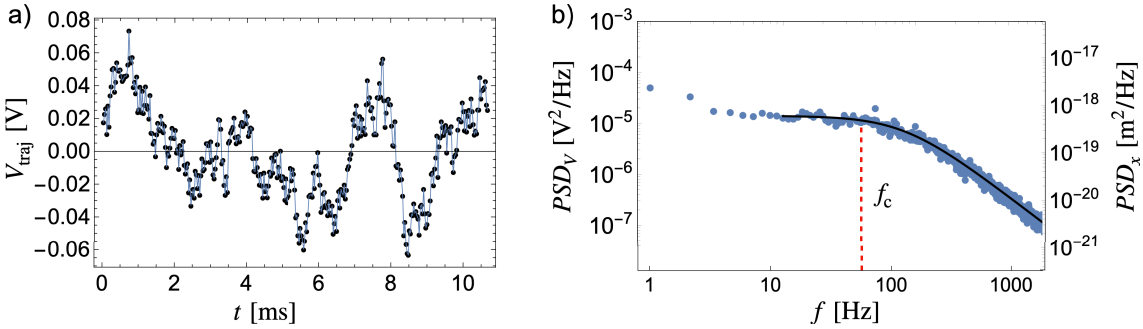

Figure 2.4: a) Trajectory of a Brownian particle in Volts measured using the setup shown in Figure 2.2 at $f_{\text{aq}} = 2^{15}$ Hz. b) $PSD_V(f)$ measured for this time series. In black a Lorentzian function is fitted in the typical interval $[10; 10^3]$ Hz, in which f_c is measured (dashed line in red). For frequencies lower than 8 Hz, the $PSD_V(f)$ deviates from the Lorentzian behavior, due to low-frequency drift, but this deviation can be excluded from the analysis by decreasing the bandwidth used to perform the Lorentzian fit.

At equilibrium, the associated $PSD_x(f)$ of $x_j(t)$ corresponds to a Lorentzian profile, determined by its area (time series variance) and the roll-off frequency $f_c = 1/(2\pi\tau_x)$ in Hz. Thus, using the Lorentzian profile $PSD_V(f) = G_V/(\pi^2(f_c^2 + f^2))$, it is possible to relate the integrals as: $\int_0^\infty PSD_x(f)\, df = (1/\beta^2)\int_0^\infty PSD_V(f)\, df = k_{\text{B}}T/\kappa$. Those measurements are shown in panel b). While the left axis corresponds to the $PSD_V(f)$ in units of V^2/Hz, on the right axis the calibration factor β was used, turning to

$PSD_x(f)$ in units of m^2/Hz. The black curve corresponds to the Lorentzian fit from which G_V and f_c are determined.

Uncertainty of the direct measurement

In order to estimate the error obtained for converting volts into units of length, with $\beta = \sqrt{\gamma G_V / k_B T}$, the variability of the G_V is important to account for. We do so from the standard deviation of 3 independent measurements of $PSD_V(f)$, in which $G_V = 0.86 \pm 0.03$ V^2/Hz. In addition to the uncertainty related to the determination of G_V, we also take into account room temperature uncertainty $T_{RT} = 293 \pm 1$ K that impact on the drag coefficient $\gamma = 6\pi\eta(T_{RT})r$[1], which in turn depends on the viscosity of the water, $\eta(T_{RT})$, and the radius of the microsphere r. The error in γ can thus be estimated as $\delta\gamma = \gamma\sqrt{(\delta\eta/\eta)^2 + (\delta r/r)^2}$, that in turn, by considering $\delta\eta = (\eta(T = 292) - \eta(T = 294))/2$, $\eta = 1.00 \pm 0.02$ mPa.s and the size dispersion of the microspheres given by the manufacturer $r = 1.50 \pm 0.02$ μm, is evaluated as $\gamma = 2.70 \pm 0.07 \times 10^{-8}$ kg/s. This implies finally that, $\beta = 2.3 \pm 0.1 \times 10^6$ V/m, is determined with a relative error of $\delta\beta/\beta = 5$ %. This uncertainty means that, even with a large number of independent measurements of $x_j(t)$ that minimize the statistical errors associated with a finite sample, the measurement of observables obtained from this time series will necessarily have a relative error greater than 5%.

The characteristic frequency, also obtained from a set of 3 $PSD(f)$, is $f_c = 79 \pm 2$ Hz, which corresponds to a characteristic time $\tau_x = 1/(2\pi f_c) = 2.01 \pm 0.06$ ms. Consequently, this sets the error on the trap stiffness $\kappa = 13.1 \pm 0.5$ fN/nm. One of the advantages of using the position spectrum to determine such measurements is that non-thermal noises that necessarily deviate from the Lorentzian spectrum are easily identified, and can therefore be disregarded from the analysis, straightforwardly. In general, a bandwidth of $[10; 10^3]$ Hz is chosen to perform the fitting of $PSD_V(f)$ with a Lorentzian function.

Trapping characteristic time signature

To interpret the characteristic time τ_x, it is worth analyzing the panel a) in Figure 2.4. On a time scale of $t_{meas} = 5\tau_x$, the correlation of the data is evident. For $t_{meas} < \tau_x$, successive measurements of $x_j(t)$ are close to each other and grouped into clusters with length of ~ 0.01 V that corresponding to a spatial extension of 4 nm. Over this time scale, the dynamics of the Brownian particle is dominated by the high-frequency components of the thermal force $f_{ther}(t)$, which are not capable

[1]Valid in the regime of small Reynolds numbers and when a spherical object is far enough from any surface.

of producing significant displacements. When measuring $x_j(t_1)$, the probability that another measurement $x_j(t_2)$ made on this short time interval, $t_2 - t_1 < \tau_x$, is in the neighbourhood of $x_j(t_1)$, at a distance of the order of 4 nm is larger when compared to separation distances > 4 nm. On the other hand, for $t_2 - t_1 > \tau_x$, the correlation between measurements of $x_j(t_1)$ and $x_j(t_2)$ decreases, and it is equally probable to find $x_j(t_2)$ on the neighbourhood of $x_j(t_1)$, or at slightly larger distances. In this second case, low frequency components of $f_{\text{ther}}(t)$ start to contribute on this time scale, making significant displacements more likely.

Position distributions

While a power spectral density requires measuring the particle dynamics over only $t_{\text{meas}} \sim \tau_x$ at a high rate, the series represented in Figure 2.5 is measured on a larger time scale, $t_{\text{meas}} \gg \tau_x$.

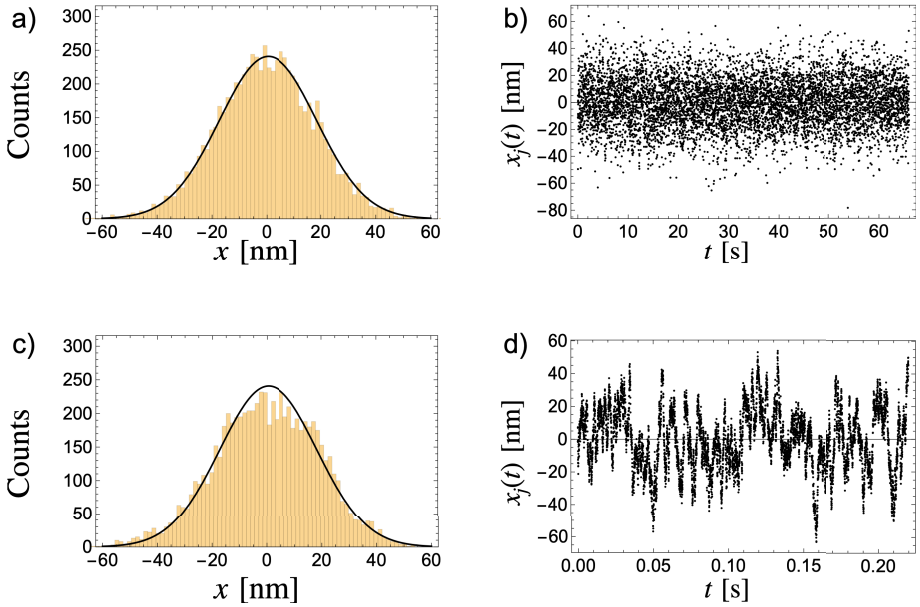

Figure 2.5: a) Position distribution with a Gaussian fit built from the temporal series shown on panel b). b) Successive points, in a total of 7200, that correspond to position measurements taken over successive time intervals of $4.5\tau_x = 9.2$ ms, thus corresponding to successive *uncorrelated* measurements. c) Position distribution using the time series shown on panel d), superimposed by the Gaussian fit obtained from panel a). d) Successive points, totaling also 7200, correspond to position measurements made at each time interval of $0.015\tau_x = 0.031$ ms, thus corresponding this time to successive *correlated* measurements.

Over such time-scale, it is possible to measure the position distribution $\mathcal{P}(x_{[0,t_{\rm meas}]})$ - here $N = 7200$ events - associated with the temporal series of the stochastic variable $x_j(t)$. Such distributions are displayed in panel a) and c) and their respective time series shown in b) and d).

For $t_{\rm meas} \sim \tau_x$, the Brownian particle, initially at a position $x_j(0)$, has no time to explore by diffusion the entire spatial region associated with the Boltzmann distribution, $p(x, k_{\rm B}T/\kappa) = \sqrt{\kappa/(2\pi k_{\rm B}T)}\exp(-\kappa x^2/(2k_{\rm B}T))$, determined by the macroscopic parameters κ, T. In panel a) and c), these regimes are considered: in panel a), $t_{\rm meas} = 33000\tau_x$, while in panel c), $t_{\rm meas} = 100\tau_x$. These distributions will be analyzed in order to clarify the relation between probability distribution measurements and correlation, in other words, the necessity to have enough statistically independent measurements of $x_j(t)$ to probe $p(x, k_{\rm B}T/\kappa)$.

Since the time difference between successive measurements of $x_j(t_1)$ and $x_j(t_2)$ in panel a) and b) corresponds to a time separation $t_2 - t_1 = 4.5\tau_x = 9.2$ ms, successive measurements of $x_j(t)$ are uncorrelated. As a consequence, fewer realizations of $x_j(t)$ are sufficient to determine the stationary distribution associated with this stochastic variable. For the panels c) and d), the time difference between successive measurements is $t_2 - t_1 = 0.015\tau_x = 0.031$ ms leading to high correlation between successive measurements. We compare the two distributions in panels a) and c), constructed with $N = 7200$ measurements of $x_j(t)$ by the kurtosis of 100 distributions with the same N. While for the set of cases measured under the same conditions as panel a), the kurtosis is 3.04 ± 0.04, for panel c) we get 3.0 ± 0.4. Although the two distributions are Gaussian on average, there is a higher dispersion around the Gaussian behavior for the case in which successive measurements are correlated, when compared to the case of a set of uncorrelated data. From now on, the effect of correlation on the measurement of the position distribution will not be relevant since position distributions will be measured from the $\{j\}$ ensemble of statistically independent trajectories, not from time averages.

2.3 Bath engineering

When the system is at equilibrium, the temperature of the thermal bath defines through equipartition the normalisation condition, $s = k_{\rm B}T/\kappa$, for both $PSD(f)$ and position distributions. In this way, the reverse process can be used to determine the temperature of the thermal reservoir: the measurements of κ and s, when the system is at equilibrium, can be used to determine T in a situation where external forces produce extra fluctuations, thus increasing the value of s, compared to the one expected if only room temperature $T_{\rm RT}$ is considered.

In order to extra fluctuations be considered as analogous to a change in temperature, the temporal distribution of the magnitude of this external fluctuation must not inject correlations into the dynamics of the Brownian particle. From a practical point of view, this condition requires a physical system with a response time much shorter than the characteristic times of the Brownian particle. This section will discuss the methods developed to add additional fluctuations to the dynamics of the Brownian particle by controlling the intensity of a laser that exerts random radiation pressure directly on the particle.

2.3.1 Acousto-optic modulator (AOM)

Intensity modulations are implemented in the experimental set-up using an AOM by which a laser beam is diffracted by an optical medium (tellurium dioxide) within a spatial inhomogeneity in the refractive index produced by the presence of sound waves

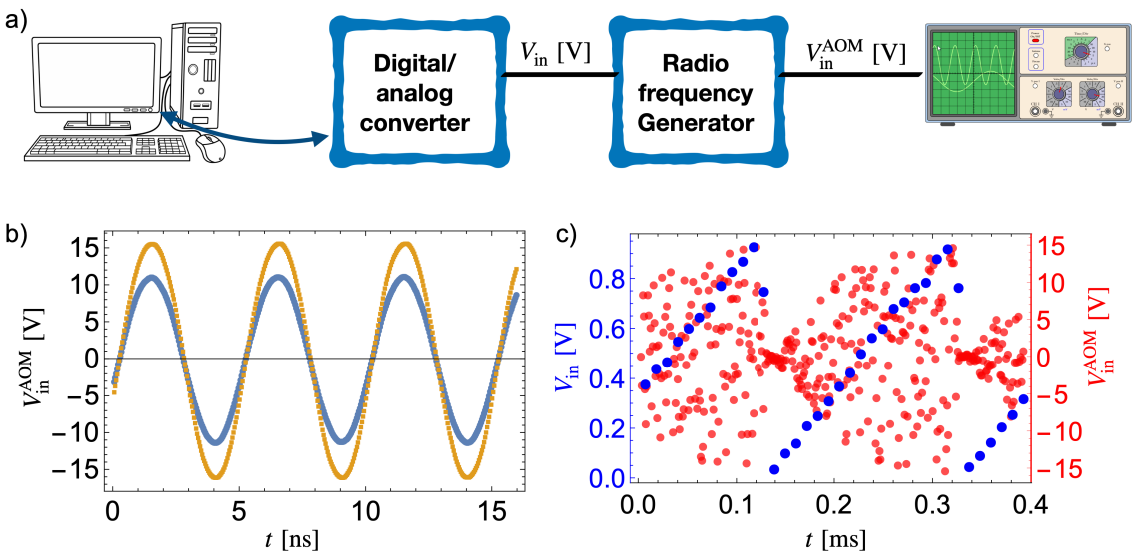

Figure 2.6: a) Diagram for controlling the radio frequency generator (RFG) through an input voltage V_{in}. Its output $V_{\text{in}}^{\text{AOM}}$ is measured by an oscilloscope. b) Time response of the RFG for V_{in} constant in time with an intensity of 1.0 V in orange and 0.5 V in blue. The oscillation period is 5 ns. c) Linear variation of V_{in} in time and associated response $V_{\text{in}}^{\text{AOM}}$ of the RFG. Since the periods of the two signals have a few orders of magnitude of difference and the trigger on the oscilloscope was set on the linear variation of V_{in}, it is not possible to resolve the fast oscillations shown in b) for $V_{\text{in}}^{\text{AOM}}$. As a consequence, this signal corresponds to a series of uncorrelated points with amplitudes that change in time.

in this medium, the so-called acousto-optic effect [84]. In the case of an AOM, the sound waves are produced by a piezoelectric transducer, powered by a radio frequency generator (RFG), with driving frequency $f_{\text{drive}} = 200$ MHz, that limits the maximum bandwidth for intensity modulation. The wavelength of the sound wave in the optical medium defines regions of higher and lower density, which in turn generate modulation in the refractive index with the same characteristic length as these waves.

As the optical oscillation frequency $\sim 5\times10^{16}$ Hz is much higher than the frequency at which the properties of the medium change, it is possible to use an adiabatic approach to describe the response of the laser beam to the effect of the inhomogeneity of the optical medium at each time instant. Thus, the incident light beam experiences a periodic network in which, for an angle of incidence that satisfies Bragg's condition, the beam is reflected with an efficiency proportional to the amplitude of variation of the effective refractive index, defined by the amplitude of the sound wave.

The RFG control is illustrated in Figure 2.6. In panel a), a digital signal corresponding to a time series with values in Volts, at a generation frequency $f_{\text{gen}} = 2^{15}$ Hz is sent to a digital analog converter (same model as in Figure 2.2). The analog signal $V_{\text{in}}(t)$ is then sent to the RFG. An oscilloscope was used[2] to visualise the output signal from the RFG, which in turn will be sent to the piezoelectric transducer of the AOM, $V_{\text{in}}^{\text{AOM}}$. In panel b), $V_{\text{in}}^{\text{AOM}}$ is measured for $V_{\text{in}} = 0.5$ V, blue dots, and $V_{\text{in}} = 1.0$ V, orange dots. In panel c), we see that the amplitude of the GRF output signal varies non-linearly for a time linear input signal V_{in}, in blue. While the period of V_{in} is 200 μs, the period of a single oscillation of $V_{\text{in}}^{\text{AOM}}$ is 5 ns. Since the amplitude of $V_{\text{in}}^{\text{AOM}}$ changes in time, it cannot be used as a trigger for the oscilloscope. Using V_{in} as a trigger, the difference in time scales between these two signals leads the rapid oscillations of $V_{\text{in}}^{\text{AOM}}$ that corresponds to the scattering of red dots in panel c).

AOM calibration

An important procedure for controlling the intensity of a laser using an AOM is to determine a function $p_{\text{calib}}(V_{\text{in}})$ that allows the functional behavior of V_{in} and V_{out} to be identical, schematized in Figure 2.7. The diagram in panel a) shows how to measure V_{out}, proportional to the intensity of the light beam diffracted by the AOM. The measurement of V_{in} and V_{out} for a linear variation of V_{in} in time with a frequency of 1 Hz is shown in panel b). While the unit of V_{in} is relevant since this quantity determines the amplitude of $V_{\text{in}}^{\text{AOM}}$ (the input voltage range to control the RFG is $[0; 1.0]$ V), the unit of V_{out}, measured by a photodiode, is arbitrary. The axis on the left is then normalized and varies between $[0; 1.0]$. This can be understood as a

[2]The RFG output signal of the order of 30 V is too intense to be acquired by our conversion board directly.

relative measurement of the diffracted light amplitude produced by the AOM, that varies between 0 % to 100 %. The AOM calibration procedure is thus based on the relation between V_{in} and V_{out}, measured both at the same time. This relation is shown by the blue points and axis in panel c).

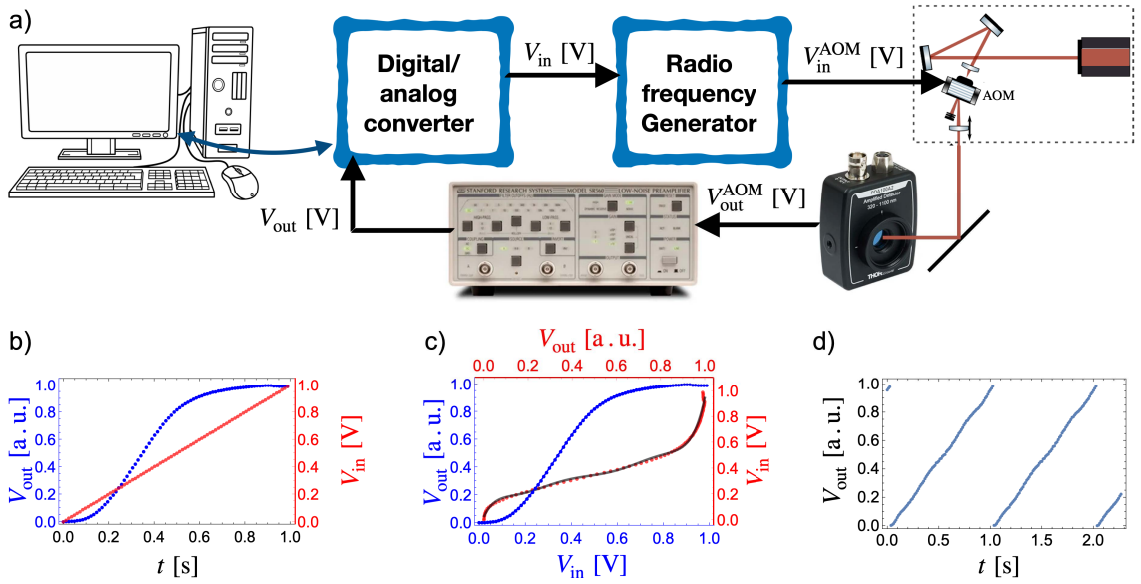

Figure 2.7: a) Diagram displaying how the diffraction efficiency of an AOM is controlled. It also shows the consequent intensity modulation of a diffracted beam via the output V_{out} of a photodiode, after this signal has been amplified and filtered by a preamplifier. This setup is used to perform the AOM calibration and to characterize the statistical properties of the brown laser intensity discussed on the Figure 2.8. b) For a signal that controls the RFG with V_{in} linear in time (in red) the intensity of the diffracted laser is measured in blue. While the red axis on the right corresponds to V_{in}, in Volts, sent to the RFG, the blue axis on the left corresponds to the V_{out} normalized between $[0; 1.0]$. As the two measurements are taken at the same time instants, the black axis is shared among them. c) The measurement of V_{out} as a function of V_{in} and its respective axes are represented in blue. This measurement is inverted, in red, and a polynomial of degree 7, p_{calib}, is fitted to this red curve. d) As a consequence, when sending the signal $p_{\text{calib}}(V_{\text{in}})$ to the RFG, where V_{in} corresponds to a signal that varies linearly in time, V_{out} measured in blue has the same functional behavior. The oscillations produced by the calibration procedure corresponds to a deviation smaller than 1 % in average, with respect to a linear fit implemented on these data.

In the same panel, in red, the relation $V_{\text{out}} = f(V_{\text{in}})$ is inverted. Then, the input control V_{in} is expressed as a function of the relative diffracted intensity V_{out}, corresponding to the axis on the right and on the top in panel c). On this curve, a polynomial of degree 7 is fitted in black. This fit corresponds to p_{calib}. Thus, using the same linear dependence in time but sending $p_{\text{calib}}(V_{\text{in}})$ to the GRF, in panel d) the intensity of the laser diffracted by the AOM is measured, again in arbitrary units. It is possible to verify the linearity of this signal, that follows the same functional time dependence of V_{in}, but with some oscillations, generated by the calibration process. These oscillations correspond on average to a deviation of less then 1 % in with respect to the linear function used to fit these data, see panel d).

2.3.2 Bath engineering exploiting radiation pressure

The effect of the laser that exerts radiation pressure on the Brownian particle can be divided into two contributions, one associated with its average intensity, responsible for producing a shift in the equilibrium position of the particle, the larger the more intense this laser is, and a contribution related to its time dependence. While external harmonic forcing result in the appearance of a peak on $PSD(f)$, at a the frequency corresponding to the modulation of the external force, it is possible to imagine that the consequence of an external force that has components on several frequencies is to produce a shift on $PSD(f)$, where, for each frequency, the shift is proportional to the intensity of the external force for this particular frequency. This is the simple spectral picture that will lead us to the concept of effective temperature of the bath, and thereby its control.

External noise characterization

In order to change such an effective temperature of the bath in which the Brownian particle is immersed using an external force, the spectral distribution of this force must have the same properties as the *heat reservoir* itself. These spectral properties correspond to a force in which "all" frequency components have the same amplitude. While from a spectral point of view this property corresponds to a constant spectrum, from a temporal point of view it corresponds to a series that has a $\delta(t-t')$ correlation: the intensity of this force does not depend on previous instants.

In practice, these considerations are only valid over a finite bandwidth, that in the case considered here, should be broad enough to produce the same change on the spectral properties of $x_j(t)$. The setup presented in Figure 2.7 is used to probe the characteristic features of $f_{\text{ext}}(t)$, when emulating an effective bath. In Figure 2.8, a temporal series of V_{out}, proportional to $f_{\text{ext}}(t)$, is measured in panel a) and b). While

V_{in} is generated at $f_{\text{gen}} = 2^{15}$ Hz as a uniform random distribution, it is acquired at $f_{\text{aq}} = 2^{18}$ Hz.

Since $f_{\text{aq}} > f_{\text{gen}}$, it can be seen that V_{out} corresponds to a plateau of constant value, at time intervals of 0.03 ms, which corresponds to the green spectrum measured and shown in panel c). The frequency f_{gen} separates two regimes. For $f < f_{\text{gen}}$, *i.e.* between different plateaus, there is no correlation and the PSD intensity is constant.

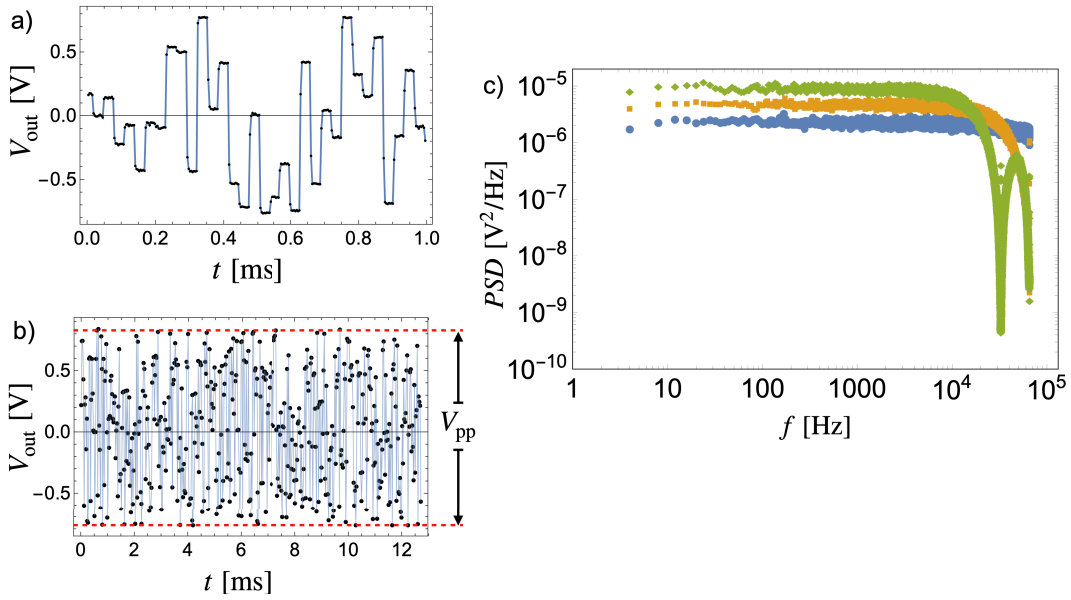

Figure 2.8: a) Time series of the laser diffracted by an AOM with a constant average and uniformly distributed in time. The AOM diffraction efficiency changes at a rate of $f_{\text{gen}} = 2^{15}$ Hz while it is acquired at a rate of $f_{\text{aq}} = 2^{18}$ Hz. Due to the difference between these rates, expected constant intensity plateaus with a duration of 30.5 μs are observed. b) Same time series as a), but over a total measurement time of $t_{\text{meas}} = 12.3$ ms, where the constancy of the peak-to-peak voltage V_{pp}, can be verified. c) Power spectrum of V_{out} for different f_{gen}. Green, $f_{\text{gen}} = 2^{15}$, yellow $f_{\text{gen}} = 2^{16}$ and blue $f_{\text{gen}} = 2^{17}$, measured at a rate $f_{\text{aq}} = 2^{18}$ Hz. Since the bandwidth over which V_{out} is considered as a white noise, defined by a constant power spectrum, increases as high generation frequencies are considered, the value of the corresponding plateau should decrease. This is why the blue spectrum, that has the highest f_{gen}, corresponds to the lower power spectrum plateau. For frequencies $f > f_{\text{gen}}$, it is possible to verify the correlation in V_{out} as measured by the decrease in spectral intensity for these frequencies.

For $f > f_{\text{gen}}$, the measured bandwidth is associated with time intervals small enough to probe the variation of V_{out} at points that correspond to the same plateau, *i.e.* completely correlated. Thus, $PSD(f > f_{\text{gen}}) \ll PSD(f < f_{\text{gen}})$. When V_{in} is generated at higher rates, yellow curve $f_{\text{gen}} = 2^{16}$ Hz and blue curve $f_{\text{gen}} = 2^{17}$ Hz in panel c), it is possible to see a decrease in the plateau of the $PSD(f)$, for $f < f_{\text{gen}}$. As for these cases the variance $\langle V_{\text{out}}^2 \rangle$ must be constant, the wider the bandwidth is, the lower the plateau for $PSD(f < f_{\text{gen}})$ must be. As the effective temperature T is a function of $\langle V_{\text{out}}^2 \rangle$, and frequencies of the order of $f \sim 1/\tau_x$ have a more significant impact than $f > 1/\tau_x$, the signal with $f_{\text{gen}} = 2^{15}$ Hz was chosen to modify this effective temperature T in order to produce higher ones for the same $\langle V_{\text{out}}^2 \rangle$.

Another factor that affects $\langle V_{\text{out}}^2 \rangle$ is the distribution used to generate the digital random signal $V_{\text{in}}(t)$. While a normal distribution is defined by its mean and standard deviation, a uniform distribution is defined by its maximum and minimum values, which in turn define the peak-to-peak value V_{pp}. Thus, for a given V_{pp}, a uniform distribution will necessarily have a larger variance, compared to a Gaussian distribution with the largest possible variance, for a given V_{pp}. The convergence from a uniform distribution to an effective effect associated with a stochastic force having thus a normal distribution is an interesting topic. We will discuss a few more aspects of this relation below.

In all protocols involving additional stochastic forces, the distribution used to generate V_{in} is uniform, where the effective temperature of the thermal bath will be directly related to V_{pp}, illustrated in panel b).

Temperature calibration

To determine the effective temperature of the particle, when at equilibrium with the thermal bath, we now look at a stationary situation, depicted in Figure 2.9. For $V_{\text{pp}} = 0$, using the same calibration discussed in Figure 2.4, it is possible to determine the relation $x_j(t) = V_{\text{traj}}(t)/\beta$, since in this case the Brownian particle is at equilibrium at a temperature T_{RT}, and trapped with a corner frequency f_c, extracted from the Lorentzian fit, as discussed in the Section 2.2.2. When the particle is subjected to $V_{\text{pp}} \neq 0$, its position spectrum will be shifted, as can be seen in panel a), in which $V_{\text{pp}} = 0$ (blue), $V_{\text{pp}} = 0.5$ V (yellow), and $V_{\text{pp}} = 1.0$ V (green).

Using the adjusted values of β and f_c, it is possible to set T as the only fitting parameter for the Lorentzian function that will describe the $PSD(f)$ in the situations for which $V_{\text{pp}} \neq 0$. The relationship between the adjusted T and the amplitude of V_{in} is shown in panel b). To assess the uncertainty associated with this calibration method, it is possible to measure the average deviation from the linear fit, as we did for the AOM calibration on Section 2.3.1. In this case, $\delta T/T \times 100\ \% = 7.4\ \%$.

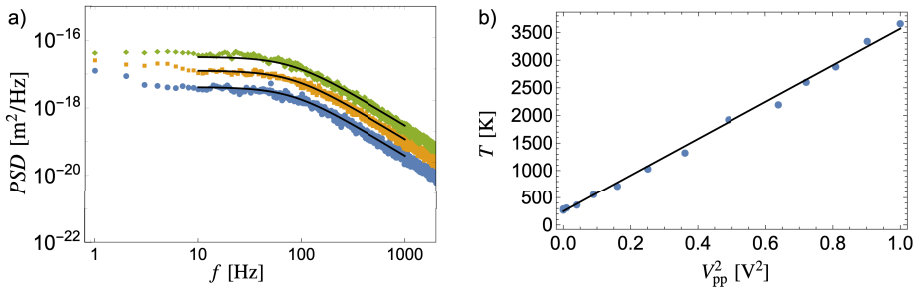

Figure 2.9: a) $PSD(f)$ of $x_j(t)$ for which different $V_{\rm pp}$ of the AOM that controls the radiation pressure intensity are considered, in a stationary situation for the Brownian particle. In blue, $V_{\rm pp} = 0$, in yellow $V_{\rm pp} = 0.5$ V and in green $V_{\rm pp} = 1.0$ V. Using β and f_c measured from the blue data by fitting a Lorentzian function, these parameters are used in the fit for $V_{\rm pp} \neq 0$. For those cases, the only fitting parameter left is the equilibrium temperature T, responsible for the displacement in the spectrum. b) From 3 measurements for $V_{\rm pp} = 0$, and 11 measurements of T with different $V_{\rm pp}$, a linear function is fitted, in which the proportionality coefficient between T and $V_{\rm pp}^2$, $T(V_{\rm pp}^2) = \alpha V_{\rm pp}^2 + T_{\rm RT}$, is measured. From the average deviation of these measurements from the liner adjustment, an uncertainty of $\delta T/T = 7.4$ % is obtained.

Instantaneous temperature

It is important to note that the relationship between the position variance s and the temperature of the thermal bath T is only valid in a stationary situation. But once the relationship has been established, it is possible to define the instantaneous temperature of the heat reservoir, *even when the system is not at equilibrium with it.*

Indeed, by introducing a time dependence $V_{\rm pp} = V_{\rm pp}(t)$, it is legitimate to define a time evolution in the temperature of the thermal bath $T(t) \propto V_{\rm pp}^2(t)$, determined unambiguously for each instant of time, and regardless of the measured value of the instantaneous variance position $s(t)$ for that same instant, as explained in detail below.

In this context, we can propose protocols for changing the temperature of the thermal bath as shown for the case of a discontinuous change of $V_{\rm pp}(t)$ at $t = 0$ in Figure 2.10. As a consequence of this temperature change, the position distribution of $x_j(t)$ will evolve in time, being described by the time dependent probability distribution $p(x, s(t))$, where for each instant of time it is possible to define an instantaneous variance $s(t)$. For this process, initial equilibration for $t < 0$ corresponds to $s_i = k_{\rm B}(T_i + T_{\rm RT})/\kappa$ and, after evolving through a transient region, at a sufficiently long times $t/\tau_x \gg 1$, the Brownian particle must be again in equilibrium with the thermal

bath but at the new temperature, where $s_f = k_B(T_f + T_{RT})/\kappa$. For these two cases, the distributions of position $p(x, s_i)$ and $p(x, s_f)$ can be measured in the same way as in Figure 2.5, but this measurement procedure cannot be used within the transient. In this case, we measure $p(x, s(t))$ from an ensemble $\{j\}$ of independent realizations of the same process $T(t)$, as now explained.

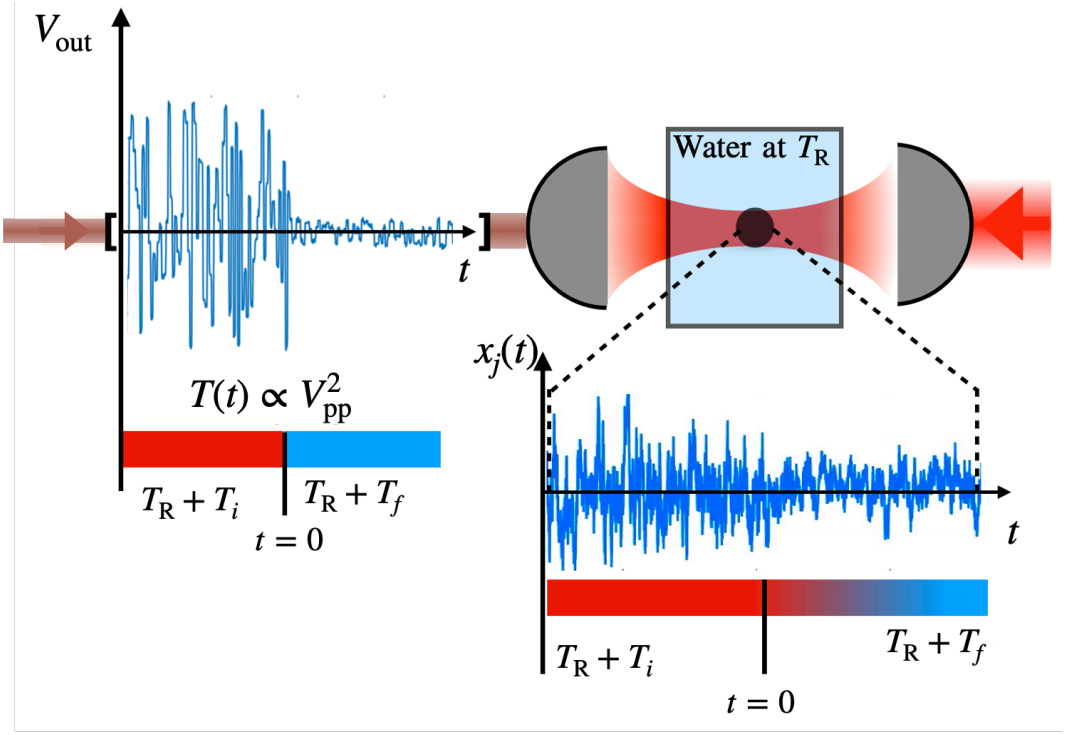

Figure 2.10: The laser (in brown on the left side of the diagram), exerts unidirectional radiation pressure on the harmonically trapped microsphere and adds noise to its diffusive motion. At $t < 0$ the brown laser peak-to-peak intensity V_{pp} is maximum, and the system is at equilibrium with a high temperature bath with $T(t < 0) = T_i + T_{RT}$. At $t = 0$, V_{pp} is changed instantaneously to a lower value, and the temperature of the thermal bath is instantaneously considered to be $T(t \geq 0) = T_f + T_{RT}$. After this time instant, the Brownian particle is considered to be in a non-equilibrium state: the statistical properties of $x_j(t)$, characterized by $s(t)$, will evolve in time through a transient with a natural relaxation time of $2\tau_x$. For $t \gg \tau_x$, the Brownian particle is again at equilibrium, but now with a temperature $T_f + T_{RT}$, different from the initial one. Such abrupt change of effective temperature will be hereafter named "STEP-like $T(t)$ protocol", see Section 2.4.2 below.

Building the ensemble $\{j\}$

To measure $p(x, s(t))$, the protocol $T(t)$ is repeated many thousand times so that it is possible to obtain independent realizations of the stochastic variable $x_j(t)$ to build precisely the distribution $p(x, s(t))$, depicted in Figure 2.11. Initially, a reference signal $V_{\text{ref}}(t)$ is generated, panel a), so that it is possible to reliably identify the start of a protocol. This measurement corresponds to the difference between consecutive measurements $V_{\text{ref}}(t+dt) - V_{\text{ref}}(t)$, and corresponds to the black vertical lines in panel d).

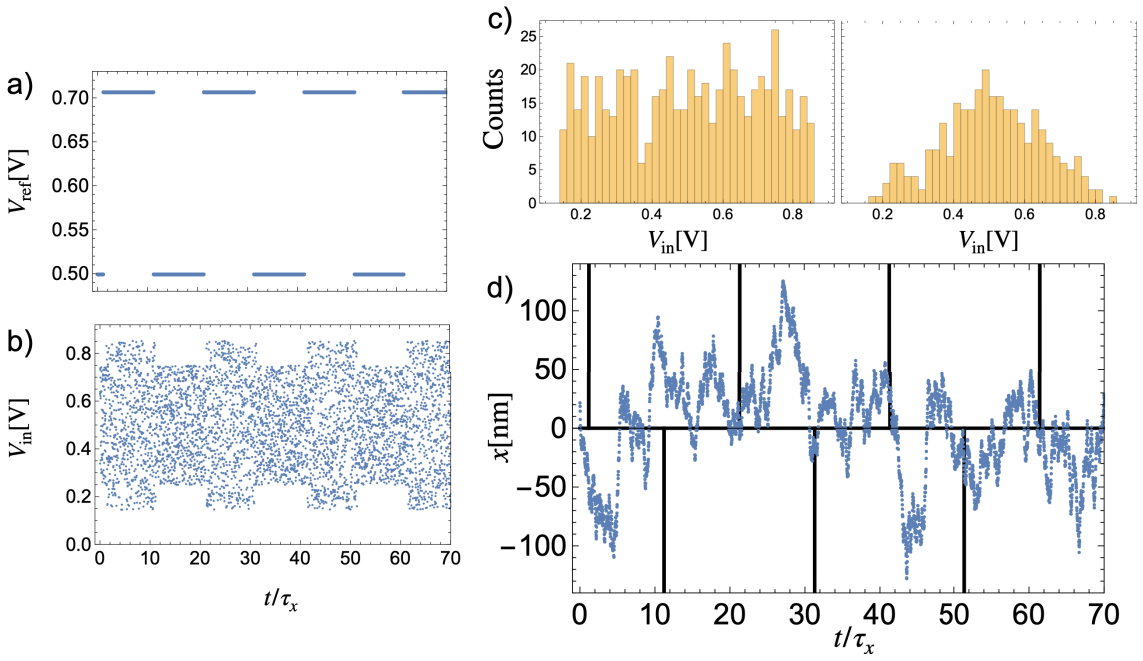

Figure 2.11: a) Reference signal $V_{\text{in}}(t)$ used to generate the time series $V_{\text{in}}(t)$ using Eq. (2.2). The difference between two consecutive values of this signal is used to identify the start time of the protocol $T(t)$ represented in the vertical lines in c). b) Time series $V_{\text{in}}(t)$ sent to the RFG to generate a stochastic force whose amplitude changes discontinuously. This signal controls the intensity of the force that generates radiation pressure on the Brownian particle $V_{\text{in}}(t) \propto f_{\text{ext}}(t)$ c) While the panel on the left corresponds to the distribution of V_{in} for a time interval of $10\tau_x$, an interval in which V_{ref} is constant, the panel on the right corresponds to the average distribution of two consecutive values of V_{in}, considering that same time interval. d) Measurement of the temporal evolution of the Brownian particle's position when subjected to $f_{\text{ext}}(t)$. The vertical black lines correspond to the start of a heating or cooling protocol.

This quantity is used to define the values $V_{\rm pp}$ that will correspond to the maximum and minimum values at which random numbers will be generated Random$[-V_{\rm pp}/2, V_{\rm pp}/2]$, following a uniform distribution, shown on the left panel of c). These values correspond to $V_{\rm in}(t)$, shown in panel b), and are determined by

$$V_{\rm in}(t) = \text{Random}[0.5 - \frac{V_{\rm ref}(t)}{2}, 0.5 + \frac{V_{\rm ref}(t)}{2}], \tag{2.2}$$

in which we set $\langle V_{\rm in}(t)\rangle = 0.5$ V so as not to have $V_{\rm in}(t) < 0$. From this average value, the maximum modulation amplitude $V_{\rm pp} = 1$ V can be implemented, since 1 V corresponds to the maximum voltage value that can be sent to the RFG (our equipment does not allow negative voltages neither).

The time interval in this protocol in which the temperature of the thermal bath is constant corresponds to $10\tau_x$, in which 580 realizations of $V_{\rm in}$ are made, whose distribution is shown in the left-hand c) panel. Otherwise, the time interval between two consecutive impulses of this stochastic force is set to 0.03 ms, and it is legitimate to interpret the effective forcing on the dynamics of the Brownian particle by an average of consecutive realizations of $V_{\rm in}(t)$. Thus, the right-hand c) panel shows the distributions of $V_{\rm in}$ values when considering the average between two consecutive values.

To analyze the relationship between an uniform and normal distribution, it is then convenient to compare the average kurtosis for different distributions of $V_{\rm in}$. When considering 50 uniform distributions, the kurtosis value obtained is 1.80 ± 0.05, as expected. For a distribution obtained from the average of two consecutive values, 2.5 ± 0.2 and, if 5 consecutive points are considered to make the average, 2.7 ± 0.3, already compatible with the description of a Gaussian noise. This analysis shows the relationship between the frequency of generation of the stochastic force added to the system and the effective distribution corresponding to this force. For all intents and purposes, the stochastic force in this work will be implemented from a uniform distribution, but in the theoretical description it will be considered as coming from a Gaussian distribution.

From a total acquisition time of $t_{\rm meas} = 6$ min, a long time series $x(t)$ is obtained. The beginning of this temporal series, that last a few realizations of a cyclical heating and cooling protocols, are shown in panel d). Thus, by identifying the instant of the discontinuity, which the black vertical line corresponds to, the ensemble of realizations of the protocol $T(t)$ is built, and the time dependent ensemble average properties of the stochastic variable $x_j(t)$ can be measured.

For each of these independent realizations, the initial position $x_j(0)$ is a stochastic variable from a distribution $p(x, s_i = k_{\rm B}(T_i + T_{\rm RT})/\kappa)$, defined in a thermal bath with temperature $T_f + T_{\rm RT}$. In order for this initial condition to be realized, before any change in temperature is induced, a waiting time interval of $10\tau_x$ is introduced. This

waiting time ensures that the Brownian particle has enough time to reach equilibrium with $T_i + T_{\mathrm{RT}}$ or $T_f + T_{\mathrm{RT}}$ for both the sequences of heating and cooling protocols. The different realizations $\{j\}$ are combined in such a way that for each time instant, a set of values $x_j(t)$ is obtained, with the same initial condition $p(x, s_i)$, and in such a way that for each instant, it is possible to determine the distribution $p(x, s(t))$ associated to $x_j(t)$.

2.4 From discontinuous changes to finite-time processes

2.4.1 Dynamical description

This section details the mathematical formalism that we will use to describe the dynamical evolution of a Brownian particle between two equilibrium states when subjected to temperature $T(t)$ protocols.

At the level of one trajectory j, the motion $x_j(t)$ of the trapped microsphere along the optical axis $\hat{x}$ of the optical trap is described by a Langevin equation. When subjected to an external force $f_{\mathrm{ext}}(t) = f_{\mathrm{DC}} + \delta f(t)$ of constant mean, $\langle f_{\mathrm{ext}}(t)\rangle = f_{\mathrm{DC}}$ and delta correlated, $\langle \delta f(t)\delta f(t')\rangle \propto \delta(t - t')$, as discussed in the previous section, the particle will see a change in the effective temperature of the heat reservoir. The consequence of this is a change in the magnitude of the resulting stochastic force, that can be quantitatively described in the equation of motion as:

$$\gamma \frac{dx_j}{dt}(t) = -\kappa x_j(t) + \sqrt{2k_{\mathrm{B}}T(t)\gamma}\xi_j(t), \tag{2.3}$$

where the stochastic variable $\xi_j(t)$ has zero mean $\langle \xi_j(t)\rangle = 0$ and delta correlated $\langle \xi_j(t)\xi_{j'}(t')\rangle = \delta_{jj'}\delta(t - t')$. Note that the effect of f_{DC} is to simply induce a change in the equilibrium position x_0, measured from the initial averaged position $\langle x_j(t)\rangle = x_0 = 0$ to $x_0 = f_{\mathrm{DC}}/\kappa$. By incorporating a change of variables $x_j(t) \to x_j(t) + f_{\mathrm{DC}}/\kappa$, and assuming that κ and f_{DC} are constant during the process, the effect of f_{DC} can be incorporated into Eq. (2.3), and the change of variable will corresponds to $\langle x_j(t)\rangle = 0$. Of course, more complex processes can be considered by introducing time dependence on $\kappa(t)$ or $f_{\mathrm{DC}}(t)$, leading to $\langle x_j(t)\rangle \neq 0$.

Eq. (2.3) can be used to describe the temporal evolution of $x_j(t)$ associated with a single trajectory j, or to describe the statistical properties of $x_j(t)$ at one given time t considering an ensemble $\{j\}$ of N realizations of this variable.

Single trajectory evolution

In the first case, the solution for a single stochastic trajectory will depend on the initial condition $x_j(0)$ (since it is a first-order differential equation) and the knowledge of $\xi_j(t)$ for each instant of time. Then, $x_j(t)$ can be obtained in terms of $x_j(0)$, $T(t)$ and $\xi_j(t)$ using a Laplace transform, leading to

$$x_j(t) = x_j(0^-)\exp[-t/\tau_x] + \int_0^t \sqrt{\frac{2k_B T(\zeta)}{\gamma}}\xi_j(\zeta)\exp[(\zeta - t)/\tau_x]d\zeta. \tag{2.4}$$

We emphasize that the non-local nature of the temporal evolution of $x_j(t)$ is made explicit from the correlation introduced by the integral in the time interval $[0, t]$. In addition, the necessity to know a priori the protocol $T(t)$ clearly appear since the stochastic variable $x_j(t)$ at time a t depends on the evolution of the protocol $T(t)$ at previous times.

Variance evolution

In the second case, the description in terms of the position probability distribution $p(x, s(t))$ corresponds to a deterministic evolution in which the temporal correlation relating $x_j(t)$ and $\xi_j(t)$ is no longer made explicit. Due to the Gaussian nature of $x_j(t)$, the definition of $p(x, s(t))$ only demands to determine the average of $x_j^2(t)$, considering independent realizations in the $\{j\}$ ensemble, at each instant of time.

The differential equation describing the evolution of this stochastic quantity is obtained by multiplying Eq. (2.3) by $x_j(t)$ – with $\tau_x = \gamma/\kappa$ the characteristic time with the damped motion of the particle inside the trap, see Section 2.1.1 above

$$\frac{dx_j^2}{dt}(t) = -\frac{2}{\tau_x}x_j^2(t) + \sqrt{\frac{8k_{\mathrm{B}}T(t)}{\gamma}}\xi_j(t)x_j(t), \tag{2.5}$$

where it is possible to determine the autocorrelation for zero lag $\left\langle x_j^2(t)\right\rangle = s(t)$, and the correlation for zero lag for the two stochastic variables $\langle x_j(t)\xi_j(t)\rangle = \sqrt{k_{\mathrm{B}}T(t)/(2\gamma)}$, calculated from Eq. (2.4).

Although the evolution of $x_j(t)$ is non-local in time, since the initial condition $x_j(0)$ is independent of $\xi_j(t)$, and $\xi_j(t)$ is local, the correlation $\langle x_j(t)\xi_j(t)\rangle$ is a local quantity, since it does not depends on the previous values of $x_j(t)$.

Using these relationships, the evolution of the position variance obtained from an ensemble of independent realizations of a protocol $T(t)$ corresponds to

$$\frac{ds(t)}{dt} = \frac{2}{\tau_x}\left(\frac{k_{\mathrm{B}}T(t)}{\kappa} - s(t)\right), \tag{2.6}$$

where the effective nature of $T(t)$ implies that thermal changes affect the diffusion coefficient simply as $D(t) = k_{\mathrm{B}}T(t)/\gamma$ with the relaxation time of the system τ_x remains constant.

To interpret the dynamical impact that $T(t)$ has on $s(t)$, it is convenient to compare Eq. (2.6) with the equation of a RC circuit

$$\frac{dV_{\mathrm{out}}(t)}{dt} = \frac{1}{RC}\left(V_{\mathrm{in}}(t) - V_{\mathrm{out}}(t)\right), \tag{2.7}$$

where the time variation of the output voltage $V_{\mathrm{out}}(t)$ is determined by the characteristic time of the circuit given by its capacitance C and its resistance R and the instantaneous input voltage $V_{\mathrm{in}}(t)$. In this context, by varying the amount of energy per charge carrier in time, defined by $V_{\mathrm{in}}(t)$, $V_{\mathrm{out}}(t)$ will also vary in time, limited by the response time given by RC.

In the case of the Brownian particle, by changing the thermal energy $k_{\mathrm{B}}T(t)$ in a finite time interval, the term $\kappa s(t)$ will evolve in time towards a stationary situation, which corresponds to $ds(t)/dt = 0$. This stationary limit corresponds to the situation in which $k_{\mathrm{B}}T(t) = \kappa s(t)$. If the protocol $T(t)$ has a very slow time dependence with respect to τ_x, in other words, if the time derivative of the temperature protocol $\dot{T} = dT/dt$ obeys the condition $\dot{T}/T \ll 1/\tau_x$, $s(t)$ will correspond to a stationary evolution with a time dependence determined by the protocol $k_{\mathrm{B}}T(t)/\kappa$.

2.4.2 Isochocric discontinous transformations: STEP-like $T(t)$ protocol

We will now look at the evolution $s(t)$ derived from protocols $T(t)$ that connect two stationary states. We start here with the evolution of the motion variance $s(t)$ along the STEP-like temperature protocol plotted in Figure 2.10, $T(t) = (T_{\mathrm{RT}} + T_i) + \Theta(t)(T_f - T_i)$, where $\Theta(t) = 0$, for $t < 0$ and $\Theta(t) = 1$, for $t \geq 0$.

A discontinuous change in a control parameter can be understood as a free evolution starting from an out-of-equilibrium initial condition, since $\left\langle x_j^2(0)\right\rangle \neq k_{\mathrm{B}}T(0)/\kappa$. In this case, the initial probability distribution is set to $p(x, s(0)) = p(x, s_i) = 1/\sqrt{2\pi s_i}\exp[-x^2/(2s_i)]$, where $s_i = k_{\mathrm{B}}(T_{\mathrm{RT}} + T_i)/\kappa$.

The evolution of the probability distribution $p(x, s(t))$ associated with $x_j(t)$ is determined by the initial condition s_i and by the macroscopic parameters κ and $T_{\mathrm{RT}} + T_f$ according to

$$s(t) = s_i \exp[-\frac{2}{\tau_x}t] + \frac{k_{\mathrm{B}}\left(T_f + T_{\mathrm{RT}}\right)}{\kappa}\left(1 - \exp[-\frac{2}{\tau_x}t]\right). \tag{2.8}$$

The procedure outlined by Eq. (2.8) and the kurtosis 2.91 ± 0.03 along the process is

depicted in Figure 2.12. The initial thermal bath temperature is denoted as $T_i + T_{\mathrm{RT}} = 2000 \pm 70\,\mathrm{K}$, transitioning to a final temperature of $T_f + T_{\mathrm{RT}} = 1000 \pm 35\,\mathrm{K}$.

The error bars arise from a χ^2 method, employed to compute a 95% confidence interval, which is applied over an ensemble of $j_{\max} = 17980$ realizations [85]. This method assumes a true variance s_{true} in which the quantity $(j_{\max} - 1)s/s_{\mathrm{true}}$ is associ-

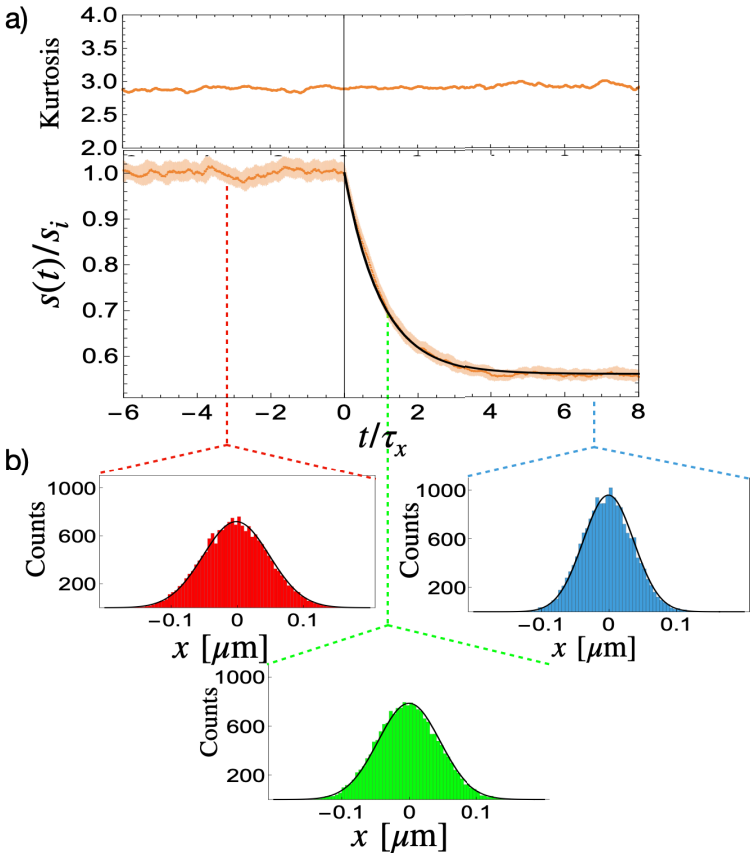

Figure 2.12: a) Kurtosis 2.91 ± 0.03 and evolution of $s(t)$ for a set of 17980 independent realizations of a STEP-like $T(t)$ protocol, as described in Figure 2.10. The vertical line at $t/\tau_x = 0$, in which $\tau_x = 2.01 \pm 0.06$ ms, corresponds to the start of the protocol which is followed by a transient sequence in which $s(t)$ evolves in time with an exponential decay. This evolution towards a new equilibrium state is superimposed to the solution of Eq. (2.8). b) Position probability distribution built from the set of trajectories before (in red), and after equilibrium is reached (in blue), and at a given time within the transient region (in green). While the distributions in red and blue are described by equilibrium Boltzmanns distribution with temperatures $T_i + T_{\mathrm{RT}}$ and $T_f + T_{\mathrm{RT}}$, respectively, the green one remaining Gaussian yields a measure of an instantaneous non-equilibrium distribution.

ated to a χ^2 distribution with $(j_{\max}-1)$ degrees of freedom. With a specified confidence interval, both the minimum $(j_{\max}-1)s/\chi^2_{\text{upper}}$ and maximum $(j_{\max}-1)s/\chi^2_{\text{lower}}$ variances are inferred from the cumulative distribution function of the χ^2 distribution. Computations for these values were done using the software *Mathematica*.

In panel a), the kurtosis displays a deviation of 3% from the expected value of a truly Gaussian distribution. We believe that this deviation is reminiscent of the fact that the distribution of external noise is not Gaussian, or that it can also be related to an experimental residual misalignment between the radiation pressure laser, injected into the optical trap, and the detection laser that slightly distorts the recorded distributions. Since the kurtosis is however clearly constant all along the process, from the initial, through the transient, until the final state, this deviation should not be related to the time dependence of the temperature protocol itself. The instantaneous position distribution $p(x, s(t))$, fitted by a Gaussian, is measured for 3 different times in panel b). These distributions corresponds to an equilibrium situation, before and after the discontinuity, and for one instant taken in the transient, the distribution corresponds to out of equilibrium.

2.4.3 Thermal engineered swift equilibration

In contrast with the case discussed in the previous section where the initial state of the Brownian particle is an out-of-equilibrium state and that, after $t = 0$, freely evolves towards a relaxed, equilibrium state, this section will study a type of $T(t)$ process that speeds up the state evolution and the relaxation towards equilibrium.

The necessary condition behind such protocols that accelerate equilibration is that they must be non-monotonic: the variation in the control parameter must occur with a characteristic time that is shorter than the system's correlation time (where, for overdamped dynamics, it corresponds to the position correlation time $\tau_x = \gamma/\kappa$) and reach an extreme value at a certain instant throughout the protocol. This is what has been coined as engineered swift equilibration (ESE), developed for stiffness-type $\kappa(t)$ protocols [54]. Our purpose here is to adapt such strategies to temperature protocols, aiming at defining thermal engineered swift equilibration processes, hereafter called ThESE.

For such type of protocol, a third-degree polynomial ansatz is used, just like for $\kappa(t)$ protocols. With this ansatz, one describes the temporal evolution of the position variance as $s(t) = At^3 + Bt^2 + Ct + D$, where equilibrium conditions are imposed initially for $t = 0$, with $s(0) = s_i = k_{\text{B}}(T_i + T_{\text{RT}})/\kappa$, and finally at the end of the protocol at $t = \Delta t$, with $s(\Delta t) = s_f = k_{\text{B}}(T_f + T_{\text{RT}})/\kappa$. We also impose stationary conditions at initial and final times of the process with $\dot{s}(0) = \dot{s}(\Delta t) = 0$. These

ingredients are sufficient to determine A, B, C, D leading to the following solution for the time evolution of the motional variance throughout the protocol, at the time interval $0 < t < \Delta t$

$$s(t) = \frac{k_B}{\kappa}\left(-2\Delta T\frac{t^3}{\Delta t^3} + 3\Delta T\frac{t^2}{\Delta t^2} + T_{RT} + T_i\right). \tag{2.9}$$

By substituting Eq. (2.9) and its derivative $\dot{s}(t)$ into Eq. (2.6), the explicit time dependence of the protocol $T(t)$ can be derived. It corresponds here to

$$T(t) = -2\Delta T\frac{t^3}{\Delta t^3} + 3\Delta T\left(-\frac{\tau}{\Delta t} + 1\right)\frac{t^2}{\Delta t^2} + 3\Delta T\frac{\tau t}{\Delta t^2} + T_{RT} + T_i. \tag{2.10}$$

This derivation is valid for heating $T_f > T_i$ and cooling, $T_f < T_i$, processes where the two cases are shown in Figure 2.13. In the upper panels, the protocol $T(t)$ is directly measured from the variation of $V_{pp}(t)$ over time. The transition times are given by $\Delta t = 0.39\tau_x$, for $\tau_x = 1.37 \pm 0.06$ ms in the case of a heating process with $T_i + T_{RT} = 350 \pm 13$ K and $T_f + T_{RT} = 1100 \pm 40$ K and $\Delta t = 0.72\tau_x$, for

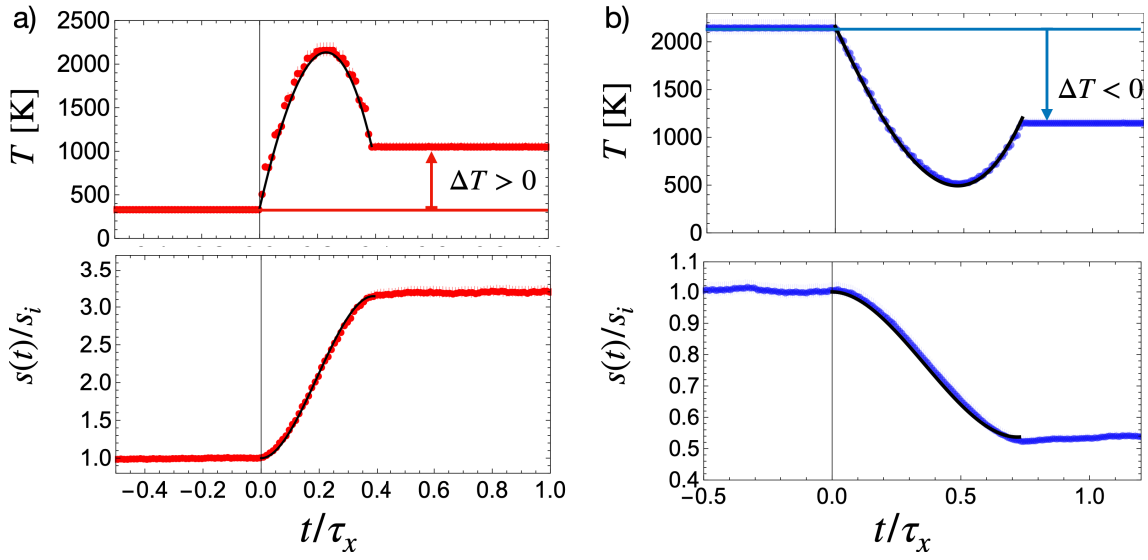

Figure 2.13: a) Temperature protocol (top panel) for a heating process (bottom panel) that accelerates the thermalization with $\Delta t = 0.39\tau_x = 0.53$ ms. For this heating protocol $T_i + T_{RT} = 350 \pm 13$ K and $T_f + T_{RT} - 1100 \pm 40$ K. The top panel shows the effective temperature measured by the peak-to-peak intensity of the fluctuating laser that exerts radiation pressure, V_{pp}, and superimposed to Eq. (2.10). The bottom panel corresponds to $s(t)$, superimposed to Eq. (2.9) over the time interval $[0, \Delta t]$. b) Similar to panel a), but this time for an accelerated cooling process $\Delta t = 0.72\tau_x = 0.85$ ms in which $T_i + T_{RT} = 2160 \pm 76$ K and $T_f + T_{RT} = 1160 \pm 41$ K.

$\tau_x = 1.18 \pm 0.05$ ms in the case of a cooling process with $T_i + T_{\mathrm{RT}} = 2160 \pm 76$ K and $T_f + T_{\mathrm{RT}} = 1160 \pm 41$ K. Eq. (2.10) is superimposed to both protocols, top panels in a) and b), and in the bottom panels, Eq. (2.9) is superimposed on the $s(t)/s_i$ measurements for these same parameters, accordingly.

Based on the idea of "connecting states" for the Brownian particle (states are defined from the particle position distributions), the next chapter will focus on presenting the appropriate thermodynamic formulation that makes it possible to quantify this connection. The great advantage of the formulation we propose in Chapter 3 is that it can also be used to quantify the cost related to connecting states. This asset will be exploited in Chapter 4 when discussing optimization for thermal protocols.

2.5 Conclusion

The control of the Brownian motion of a single particle using one specific platform was presented in this chapter. Specifically, this control corresponds to trapping the particle, tracking its trajectory, and adjusting its dynamics based on the modulation of the trapping potential and the influence of an external radiation pressure force. By controlling the statistical characteristics of this external force, we can perform thermal bath engineering protocols and develop procedures to increase the center of mass temperature of the Brownian particle by several thousand Kelvin.

At the core of this technique is the notion of the center of mass temperature, measured by the position power spectral density (PSD) of the Brownian particle when at equilibrium with the thermal bath. Building on the connection between this temperature and the amplitude of the external force, the bath temperature is considered as a time-dependent control parameter $T(t)$.

The characterization of the Brownian motion was undertaken by analyzing directly the measurement: the time-dependent intensity of a laser scattered by the Brownian particle. By considering a linear relation between this intensity and the instantaneous position displacement of the particle, several observables are built. These include trajectories measured in length units, position distributions, and position PSDs.

An important discussion of the chapter is the relationship between the nature of the stochastic force distribution—be it uniform or normal—and the frequency of its generation. While the center of mass temperature diminishes when the radiation pressure intensity is modified at high generation frequencies, at this limit, a stochastic force with an initially uniform distribution converges towards a normal one. This interplay becomes even more relevant when stochastic forces with other distributions are employed to modify the Brownian dynamics. It's crucial to understand that the distribution and generation frequency of a stochastic force are intertwined and cannot

be consider independently.

Another aspect of bath engineering corresponds to introduce correlation on the stochastic forcing that drives the Brownain particle, that we discuss in details in the case of "active bath" engineering in our publication [48], and it is presented on the PhD thesis of Rémi Goerlich [86].

We them illustrate how the Browinan dynamics can be modified through the action of two $T(t)$ protocols. While a discontinuous temperature change generates a non-equilibrium evolution, where the system's variance $s(t)$ relaxes with an exponential decay towards a final equilibrium state, more intricate temporal dependences on $T(t)$ can be introduced, leading for instance to an accelerated transition and thermalization. The concept of *connecting states* will drive the thermodynamic description for isothermal and isochoric processes that we propose in the next chapter.

Chapter 3

Thermodynamics of a Brownian particle

Considering that the instantaneous variation of the internal energy of a particle is given solely by its potential energy $\Delta U_{\rm sys}(t) = (1/2)(\kappa(t)s(t) - \kappa_i s_i)$*, this chapter will describe how thermodynamic functions are affected when isothermal* $(\kappa(t), T = cte)$ *or isochoric* $(\kappa = cte, T(t))$ *protocols are considered. This description will be based on state functions and path-dependent functions for out-of-equilibrium processes. To this aim, a new definition of the entropy of the system associated with a stochastic trajectory* $\sigma_{\rm sys}(x_j(t))$ *will be considered.*

After determining, on one side state, instantaneous functions of the protocol $(\kappa(t), T = cte)$ *or* $(\kappa = cte, T(t))$ *and of the process, measured through* $s(t)$*, and, on an other side, path-dependent functions as functionals of the protocols* $(\kappa(s), T = cte)$ *or* $(\kappa = cte, T(s))$*, the thermodynamic cost associated with a given protocol that connects two equilibrium states via a discontinuous change of a control parameter will be discussed. The functional formulation introduced here will be exploited in the next chapter when optimal isochoric processes will be derived.*

3.1 From stationary to dynamical state

In both thermodynamics and mechanics, the concept of state refers to the set of parameters or variables that completely describe a given system at a given time. However, the specific meaning and the nature of the variables involved in the description differ from the two fields. While in thermodynamics, the equilibrium state is associated to a set of macroscopic variables, in classical mechanics the state of a system is described by positions and velocities of all the constituent particles in the system at a given time.

In the context of Brownian particle inside a harmonic potential, those two levels of description are mixed. On the one side, the thermodynamic content is imprinted on the collisions between the molecules and the mesoscopic particle and energy is exchanged within the confining potential through work and heat. The heat reservoir is defined by temperature T and the work reservoir with stiffness κ. The mechanical content on the other side relies on the position and velocity of the Brownian particle.

At the level of single trajectories of this Brownian particle, the coupling with the reservoir leads to stochastic quantities $(x_j(t), dx_j(t)/dt = v_j(t))$, for each time instant t and independent stochastic realization j. Those stochastic variables in turn define probability distributions, measured after averaging over an ensemble of $\{j\}$ independent stochastic realizations. At the ensemble average or macroscopic level of description, the whole dynamics related to the harmonic confinement is Gaussian, as discussed in the previous chapter. As a consequence, only the variances of those distributions $\left\langle x_j^2(t)\right\rangle = s(t)$ and $\left\langle v_j^2(t)\right\rangle = s_v(t)$ are needed to define the mechanical state of the Brownian particle.

That state evolves according to the laws of motion in which position and velocity change over time due to forces acting on it. At the stochastic level, the lack of knowledge of the position and velocities of all the surrounding molecules lead to an effective description of a stochastic thermal force that drive the Brownian particle. Otherwise, at the macroscopic level of description, from the time dependence of the control parameters $\chi(t) = (\kappa(t), T(t))$, the trajectories $(s(t), s_v(t))$ are determined unequivocally as a solution of a differential equation. If $\chi(t)$ changes sufficiently slowly so that its instantaneous value is sufficient to determine $(s(t), s_v(t))$, the system will evolve as a succession of equilibrium states within the work and heat reservoirs. Otherwise, the system is considered to perform a non-equilibrium evolution and $(s(t), s_v(t))$ will also depend on the rate of change $\dot{\chi}(t)$ of the control parameters.

3.1.1 Time scales

Since the discussion below is based on such dynamical processes, it is important to define time scales that set how fast $\chi(t)$ changes. We assume it to change over times of the order of the position correlation time (for microspheres in water $\tau_x = \gamma/\kappa \sim$ ms), but at a time scale much larger than the velocity correlation time ($\tau_v = m/\gamma \sim \mu$s). In such conditions, the non-equilibrium discussion will be based only on how potential energy $(1/2)\kappa(t)s(t)$ of the microsphere change in time. With respect to kinetic energy, all processes considered here correspond to a succession of equilibrium states, a quasi-static transformation in which, for each instant of time, $ms_v(t) = k_{\mathrm{B}}T(t)$. This leads to the absence of an energetic cost associated with the change in velocity distribution.

Another important time scale is related to the measurement process itself: the system evolution is followed at discrete time steps dt, corresponding to time intervals between successive measurements. In practical terms, time corresponds to the index in a list of successive values of the control parameter $\chi(t)$ and system and response $x_j(t)$ or $s(t)$, for the micro or macroscale description, respectively. Again, for $dt \gg \tau_v$, it is not possible to reconstruct the time dependence of the particle's velocity. We however ensure $dt \ll \tau_x$.

3.1.2 Connecting states and time dependent processes

A cornerstone of thermodynamic description is the identification of two kinds of quantities: state functions, whose variations depend only on the initial and final states, and path dependent quantities that depend on the actual process that connects those two states. It is therefore convenient to separate the thermodynamic analysis of a process in terms of these two quantities. By considering the initial and final states, defined in turn by the distributions $p(x, s_i = k_\mathrm{B}T_i/\kappa_i)$ and $p(x, s_f = k_\mathrm{B}T_f/\kappa_f)$, the variation of the state functions, such as internal energy ΔU_sys, free energy ΔF and entropy of the system $\Delta\Sigma_\mathrm{sys}$, associated with any protocol $\chi(t)$, are completely defined by (κ_i, κ_f) and (T_i, T_f).

Otherwise, when path-dependent quantities such as the work W, the heat that corresponds to the energy exchanged between the Brownian particle and the thermal reservoir Q, the entropy of the medium Σ_med and the total entropy Σ_gen are considered, these quantities will depend on the $\chi(t)$ protocol, which connects such states. Path dependent quantities measure how far from equilibrium the system is when it is driven by the control parameters $\chi(t)$.

Before defining the thermodynamic quantities along an out-of-equilibrium process $s_i \to s_f$, some considerations will be made on how to measure the infinitesimal variation of the position variance of the Brownian particle ds in a given time interval dt, and along the process $\Delta s(t) = s(t) - s_i$ (see below).

Description in terms of instantaneous values

When a temporal dependence on the state functions is considered, care should be taken to extend their definition to non-equilibrium states. Generalizing the discussion of $T(t)$ protocols introduced in the previous chapter by considering also $\kappa(t)$ ones, an infinitesimal variance change ds, derived from the ensemble average of the dynamical equation of $dx_j^2(t)/dt$, Eq. (2.5), can be obtained. Then, by the instantaneous difference between the the control parameters $\chi(t)$ and $s(t)$, it is possible to measure ds for a given time interval dt as

$$ds = \frac{2}{\gamma}\left(k_{\mathrm{B}}T(t) - \kappa(t)s(t)\right)dt. \tag{3.1}$$

This equation defines ds as an instantaneous deviation from a quasi-static evolution. Stationary solutions means either that there is no time dependence on the control parameters, or that for each successive time increment $k_{\mathrm{B}}T(t) = \kappa(t)s(t)$. We stress that, once ds is used to evaluate an infinitesimal variation of a given state function (for instance system internal energy or system entropy — as discussed below), Eq. (3.1) cannot be used since it only measure a *deviation* from the quasi-static limit and does not give access to the actual variation induced by the protocol $\chi(t)$ on that state function. The protocol to measure ds expressed by Eq. (3.1) can only be used to measure variations on pure dissipative quantities, *i.e.* path dependent quantities that are identically zero for quasi-static processes.

Description in terms of increments

Along the process, measuring $s(t)$ corresponds to the ensemble average of the stochastic quantity $x_j^2(t)$, measured in each time interval dt, by the average of a set of independent trajectories $\{j\}$, subjected to the same protocol $\chi(t)$. All those $\{j\}$ trajectories share the same protocol initial condition $\chi(0)$, but corresponds to a different realization of the stochastic variable $x_j^2(t)$. Once the list of $s(t)$ is measured, by solely considering the difference between consecutive measurements $s(t)$ and $s(t+dt)$, an infinitesimal change on $s(t)$ can be evaluated as $ds = s(t+dt) - s(t) = \dot{s}(t)dt$. This way to measure ds leads to the definition of a time dependent variance difference along a trajectory as $\Delta s(t) = \int_0^t ds$, in which the integral is performed as a cumulative sum of infinitesimal changes $\sum_{n=0}^{N-1}(s((n+1)dt) - s(ndt))$, when N is the number of measurements performed on the time interval $[0, t]$, and $t = Ndt$.

Our method analyses how increments $d\chi = \chi(t+dt) - \chi(t)$ impacts ds. By increments, we mean that $d\chi$ can be in principle arbitrary large between two consecutive measurements. While $\chi(t)$ can be discontinuous, the change on the mechanical response of the system $s(t)$ is a continuous function. Since $d\chi$ and ds are measured independently, a quasi-static transformation corresponds to the case in which, for each dt, the control parameter changes in a sufficiently small amount so that for each intermediary change, measurements of $d\chi$ can be identified as infinitesimal variations, and ds will be obey the relation $ds/s = dT/T - d\kappa/\kappa$. The consequences of a discontinuous change in the control parameters will be considered at the end of this chapter. Before that, the control parameters $\chi(t)$ will be considered to be a continuous function with infinitesimal variations $d\chi$ able to drive the evolution of the system $s(t)$ away from a quasi-static transformation.

Then, using the definition of ds as a difference between successive measurements of $s(t)$, one can discuss an important difference. While state functions depend on the instantaneous values $(\chi(t), s(t))$, path-dependent quantities are defined according to how those quantities are affected by a change in the control parameters $d\chi$. Before introducing the expressions used to determine the thermodynamic functions associated with $\chi(t)$, we will first establish the relationships between the state functions and their corresponding path-dependent functions.

3.2 Isotherm and isochoric processes

This section aims to define thermodynamic quantities, evaluated from ensemble averages of stochastic trajectories, in which protocols of $\kappa(t)$ and $T(t)$ are considered on an equal footing. In terms of control parameters, we define an isotherm protocol as $\chi^{\kappa}(t) = (\kappa(t), T)$ and an isochoric one $\chi^{T}(t) = (\kappa, T(t))$. The control parameters $\chi(t)$ are assumed to change in a finite interval of time Δt, producing an evolution of the system from an initial state, defined by (χ_i, s_i), to a final state (χ_f, s_f), in which equilibrium is verified by the condition $\kappa_i s_i = k_{\mathrm{B}} T_i$ e $\kappa_f s_f = k_{\mathrm{B}} T_f$.

The equilibrium condition can be interpreted from the equality between the instantaneous potential energy of the Brownian particle, identified as its internal energy $U_{\mathrm{sys}}(t) = (1/2)\kappa(t)s(t)$ and the thermal energy identified as the internal energy of the thermal bath $U_{\mathrm{med}}(t) = (1/2)k_{\mathrm{B}}T(t)$. As these quantities are state functions, regardless of the protocol $\chi(t)$ that connects two equilibrium states, $(\chi_i, s_i) \to (\chi_f, s_f)$ it is possible to identify the total variation of these quantities when isothermal or isochoric processes are considered

$$\Delta U^{\kappa}_{\mathrm{sys}} = \Delta U^{\kappa}_{\mathrm{med}} = 0 \to \frac{1}{2}\kappa_i s_i = \frac{1}{2}\kappa_f s_f, \tag{3.2}$$

$$\Delta U^{T}_{\mathrm{sys}} = \Delta U^{T}_{\mathrm{med}} \to \frac{1}{2}\kappa\left(s_f - s_i\right) = \frac{1}{2}k_{\mathrm{B}}\left(T_f - T_i\right). \tag{3.3}$$

Those relations defines the total variation of a state function, ΔU_{sys} (whenever the index κ or T is no shown, the relation is valid for both processes), in terms of the the initial χ_i and final χ_f values of the control parameters $\chi(t)$.

3.2.1 Thermodynamic First law

In contrast, path-dependent energetic quantities, such as work and heat, must be introduced at the differential level, considering infinitesimal changes of the system internal energy, dU_{sys} between two consecutive measurements, with a time difference dt. Since after equilibrium there is no information regarding the evolution of the

control parameter $\chi(t)$ imprinted on ΔU_{sys}, it is necessary to consider the differential first law in order to introduce path dependent quantities. At this differential level, dU_{sys} can be understood as the relation of the rate of change between two path-dependent quantities: 1) the amount of heat discarded into the heat reservoir $đQ$[1], and 2) the total work $đW$ done by the work reservoir[2], at each time interval dt. This relation between rates leads them to the instantaneous change of dU_{sys} as

$$dU_{\text{sys}} = đW - đQ. \tag{3.4}$$

While $đW$ arises from a change in the potential, and thus does not arise from a temperature change, $đQ$ corresponds to a change in the position variance, that in contrast to $đW$ can be provoked by both a potential or a temperature change.

The differential relations account for the fact that the change on control parameters $d\chi$ can be discontinuous for a given dt, leading for this case to discontinuous thermodynamic functions. On the other hand, the mechanical state of the system, described by $s(t)$, has a continuous evolution, since an infinitesimal change of the variance ds is constrained by the position variance relaxation time $2\tau_x$. While for thermodynamic quantities, d accounts for total differential, for the mechanical description, as for ds, d accounts for infinitesimal changes.

Along a non-equilibrium process

Along quasi-static transformations $dU_{\text{sys}} = dU_{\text{med}}$, for each dt, so that the system evolves as a succession of equilibrium states. In contrast, along a non-equilibrium process, $dU_{\text{sys}} \neq dU_{\text{med}}$ and Eqs. (3.2) and (3.3) are valid only in the end of the transformation, after the system is in equilibrium. We then identify the instantaneous potential energy as the system internal energy, even for a non-equilibrium process. Differentiating it as $dU_{\text{sys}} = (1/2)d(s\kappa) = (1/2)sd\kappa + (1/2)\kappa ds$, leads to define the work rate at time dt, $đW = (1/2)sd\kappa$ and the heat rate $đQ = -(1/2)\kappa ds$.

From Eq. (3.4), the signature of a non-equilibrium isothermal process is imprinted on the imbalance between $đW$, that takes into account instantaneous exchange of energy between system and work reservoir, and $đQ$, proportional to ds, that remains constrained by the system natural relaxation time. This is what is sketched on Fig. 3.1 where the arrows represent the flux of energy for an isothermal compression or an expansion of the harmonic potential.

[1] $đ$ means an inexact differential.
[2] Defined on Figure 3.1

3.2.2 Dissipated energy

For the isothermal case, it is convenient to split after equilibrium is reached the total work W into two contributions: one that is path independent and that can be identified as the total difference in the free energy ΔF, and another that is associated with a pure dissipative part, $W_{\rm dis}^{\kappa}$. The former being a free energy is defined as the work extracted if the process $s_i \to s_f$ were performed as a succession of quasi-static transformations $\Delta F = \int_{s_i}^{s_f} dW = (1/2)k_{\rm B}T\ln(\kappa_f/\kappa_i)$. Since this definition involves quasi-static transformations, the infinitesimal work rate is considered to be a total differential dW, that in turn, for each step on this quasi-static protocol, $ds/s(t) = -d\kappa/\kappa(t)$. This split of contributions leads to a new infinitesimal rate equation between two path dependent quantities that yields a state function in the form of the free energy as

$$dF = đW - đW_{\rm dis}^{\kappa}. \tag{3.5}$$

Dissipative work

The total difference in the free energy, ΔF is interpreted for a given temperature, as the reversible amount of energy exchanged with the work reservoir in order to modify the spatial region probed by the Brownian particle as fixed by the total change in variance $\Delta s = s_f - s_i$, once equilibrium conditions are reach.

In contrast, the mechanical interpretation of $W_{\rm dis}^{\kappa}$ is more subtle. This energetic quantity is related to the average imbalance between the three forces involved on the description of the Brownian particle dynamics when a change $d\kappa$ is considered. The three forces are: (i) thermal, provided by the collision of the Brownian particle with the surrounding molecules, (ii) confining, pulling the particle to the center of the trap, and (iii) friction, inevitable since the medium is viscous. Whenever there is an average imbalance between them, dissipative forces oppose the motion.

The dissipative nature of the $W_{\rm dis}^{\kappa}$, can be better understood if a single discontinuity $\kappa_i \to \kappa_f$ is considered. We note here that the sign of $W_{\rm dis}^{\kappa}$ is independent of whether a compression or an expansion is considered, as expected from a pure dissipative quantity.

From an energetic viewpoint, the system can be considered to be in a non-equilibrium state immediately after the discontinuity $\kappa_i \to \kappa_f$ with $U_{\rm sys}(t = 0^+) = (1/2)\kappa_f s_i$, departing from equipartition. From $t = 0$, the system evolution is such that $U_{\rm sys}(t \to \infty) - U_{\rm sys}(t = 0^+) < 0$ for a compression, while $U_{\rm sys}(t \to \infty) - U_{\rm sys}(t = 0^+) > 0$ for an expansion. Such energy fluxes are represented by the vertical arrows on Figure 3.1. From the force perspective, the instantaneous change on stiffness will lead to an imbalance between the averaged trapping force (ii), always directed toward the center of the trap, and the averaged thermal force (i), isotropic. For a compression, the Brownian

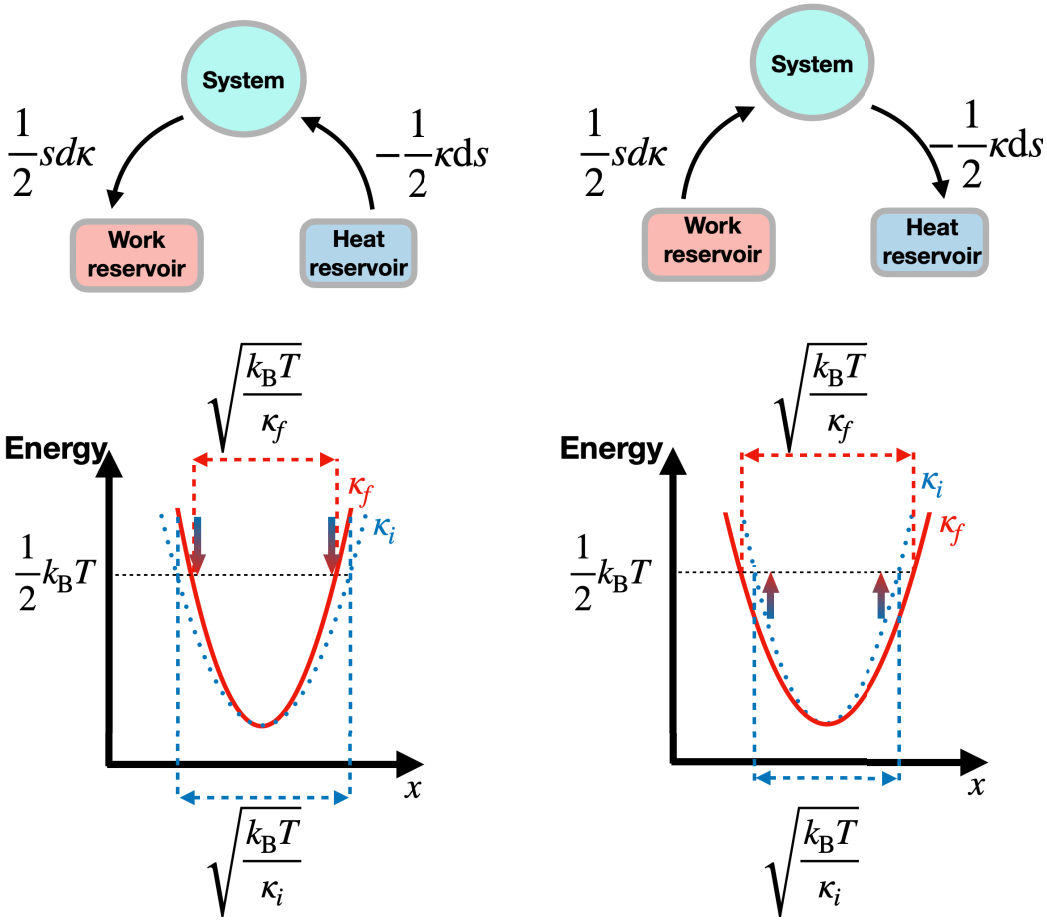

Figure 3.1: Schematic representation of isothermal processes, with a compression on the left panels and an expansion on the right ones. If a discontinuous change $d\kappa = \kappa_f - \kappa_i$ is considered, at the instant of the discontinuity, an amount of energy $đW = (1/2)(\kappa_f - \kappa_i)s_i$ is exchanged between the system and the work reservoir. After this instant, energy is exchanged at a rate $đQ = -(1/2)\kappa_f ds$ between the system and the heat reservoir. The top diagrams represent the flux of energy between work and heat reservoirs and the system, when a change in the control parameter is performed. While for compression the system receives energy from the heat reservoir, in the case of an expansion, the energy is released by the system. The two bottom diagrams represent the consequence of a change $\kappa_i \to \kappa_f$, that will lead, when equilibrium is reached, to a modification of the position variance of the system $s_i \to s_f$. Since the thermal energy is constant for these processes, the initial and final internal energies of the system do not change, as represented by the dashed black lines.

particle is pulled more strongly towards the center of the trap. For an expansion, this pulling is reduced. The net effect of both processes will be to produce a non-vanishing averaged velocity $\langle v_j(t)\rangle \neq 0$, that in turn leads to an extra viscous force (iii), greater than the one necessary to maintain the system in equilibrium. This extra viscous force generates an extra amount of heat dissipated from the trapped bead to the fluid. This dissipation corresponds to $W^{\kappa}_{\rm dis}$, a positive definite quantity.

Thermal work

When isochoric transitions are considered, a similar discussion for the energy dissipated in the medium $W_{\rm dis}$ can be performed. This leads us to introduce the concept of thermal work $W^{T}_{\rm dis}$ induced by a temperature change, as proposed already in [43]. One key aspect is that despite the fact that the processes of heating and cooling, represented in Figure 3.2, are symmetrical from the energetic viewpoint (since the absolute value of total variation on the system internal energy $|\Delta U_{\rm sys}|$ is the same when the absolute variation on the temperature $|\Delta T|$ is considered) $W^{T}_{\rm dis}$ always represents an amount of energy dissipated towards the heat reservoir. This can be understood by looking at the force balance. For heating, the thermal force (i) increases, causing the Brownian particle to move away from the equilibrium position, and in relation to the averaged confining force (ii), generate an instantaneous lack of balance that in turns increases the viscous force (iii). For cooling, the thermal force decreases: the particle is, on average, pulled towards to the center of the trap, and again by the fact that $\langle v_j(t)\rangle \neq 0$, the drag force will produce some dissipation of energy into the medium.

While the first law allowed the definition of ΔF, that in turn led us to identify $W^{\kappa}_{\rm diss}$ as a pure dissipative quantity associated with an isothermal process, the same procedure is not possible for isochoric transformations, since energetic relations for such process only determine the balance between the total heat, accumulated along the process, and the total variation on the system internal energy, according to $\Delta U^{T}_{\rm sys}+Q^{T}=0$. The crucial aspect of isochoric changes is that the exchange of energy between the system and the heat reservoir involves different temperatures along the process. This has an impact on the entropic description of the system and of the heat reservoir. Therefore, the first law must be complemented by an entropic description in order to precisely account for the different nature of the energy exchanges between the system and the heat reservoir when $T(t)$ protocols are considered.

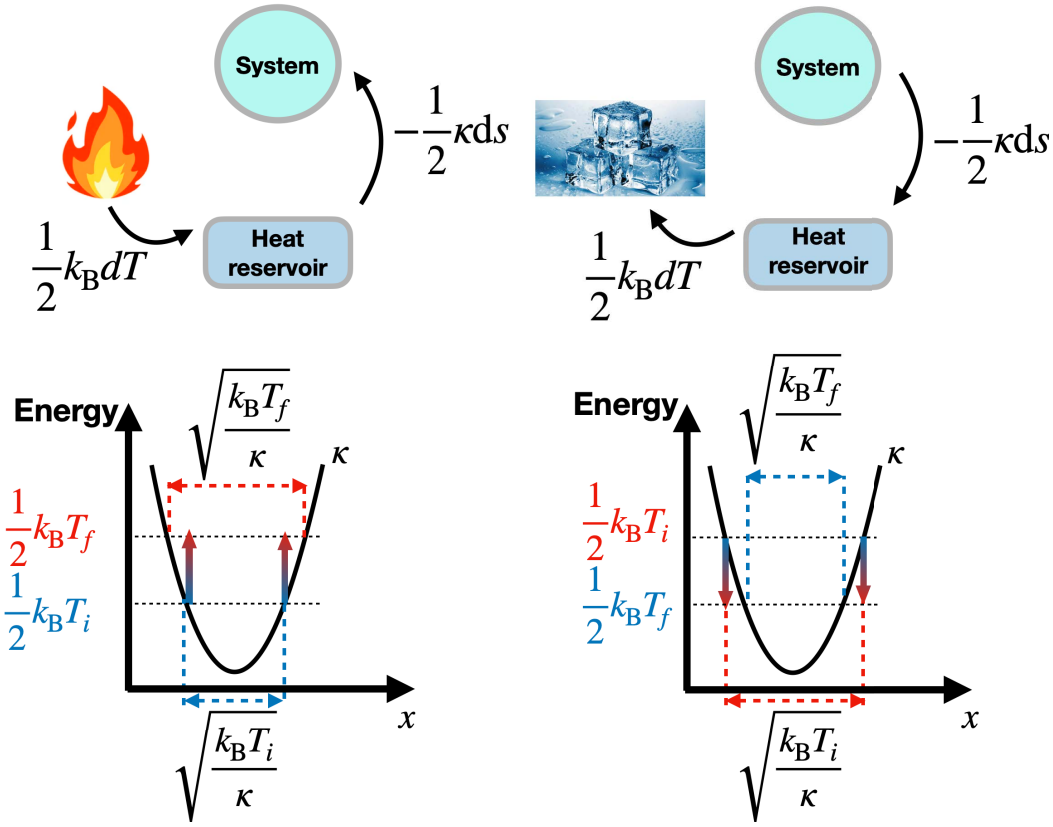

Figure 3.2: Schematic representation of isochoric processes, with a heating process on the left panels and a cooling one on the right ones. If a discontinuous change $dT = T_f - T_i$ is induced, at the instant of the discontinuity, an amount of energy $(1/2)k_B dT$ is instantaneously supplied to, or removed from, the thermal bath, depending on whether a heating or cooling process is considered. After this instant, energy is exchanged at a rate $đQ = -(1/2)\kappa ds$ between the system and the heat reservoir. The top diagrams represent the flux of energy by which an external agent modifies the temperature of the heat reservoir, by the instantaneous change of the control parameter dT. While for a heating process the system receives energy from the heat reservoir, a cooling process sees the energy released by the system. The two bottom diagrams represent the consequence of a change $T_i \to T_f$ that will lead, when equilibrium is reached, to a modification of the position variance of the system $s_i \to s_f$. Since the internal energy of the heat reservoir ΔU_{med} changes for these processes, $\Delta U_{\text{sys}} \neq 0$.

3.2.3 Thermodynamic Second law

First, and following the same approach developed for the first law, we choose to define the state function associated with entropy, so called the system entropy, from the balance between the incremental productions of medium entropy, that accounts for the exchange of energy with the heat reservoir, $đ\Sigma_{\text{med}} = đQ/T$, and a pure dissipative quantity, the total entropy $đ\Sigma_{\text{gen}}$, generated along a non-equilibrium process within a time dt

$$d\Sigma_{\text{sys}} = đ\Sigma_{\text{gen}} - đ\Sigma_{\text{med}}. \tag{3.6}$$

Defining $đ\Sigma_{\text{gen}}$ then demands to identify $d\Sigma_{\text{sys}}$. From the difference between two equilibrium states, connected by a protocol in which the control parameters change from initial to final values $\chi_i \to \chi_f$, the total variation on the system entropy $\Delta\Sigma_{\text{sys}}$ can be derived by analyzing the corresponding quasi-static process, in which $\Delta\Sigma_{\text{sys}} + \Sigma_{\text{med}} = 0$ at all times. This is the same type of analysis used to define the total variation of the free energy ΔF above (see Eq. (3.5)). For such a process, at each infinitesimal change $d\chi$ of the control parameter, the energy exchanged between the system and the heat reservoir corresponds to an infinitesimal increment of a specific state function. For an isothermal process, it corresponds to an infinitesimal change dF of free energy. For an isochoric process, it corresponds to an infinitesimal change of the internal energy dU_{sys}.

The corresponding quasi-static processes (with $đ\Sigma_{\text{gen}} = 0$) provides an approach to define the total variation on the system entropy $\Delta\Sigma_{\text{sys}}$ related to two equilibrium states defined by s_i and s_f. These states are connected by an isothermal $\kappa(t) = k_{\text{B}}T/s(t)$ or isochoric $T(t) = \kappa s(t)/k_{\text{B}}$ protocol, in which Eqs. (3.2) and (3.3) are valid for each time instant along the process $s_i \to s_f$. For these processes, the infinitesimal heat turns to be a total differential $đQ \to dQ = -(1/2)\kappa ds$, and the medium entropy associated to those quasi-static processes can be determined as $\Sigma_{\text{med, QS}} = -(k_{\text{B}}/2)\int_{s_i}^{s_f} ds/s$. Then, the total variation of the system entropy $\Delta\Sigma_{\text{sys}}$ for any isothermal and isochoric processes connecting two equilibrium states is given by

$$\Delta\Sigma_{\text{sys}} = \frac{k_{\text{B}}}{2} \ln \frac{s_f}{s_i}. \tag{3.7}$$

From entropy to dissipative energy

For an isothermal process, integrating Eq. (3.4) between two equilibrium states, leads to the total work associated to the process equal to the total heat $W = Q$. The integration of Eq. (3.5) can be rewritten as $\Delta F = Q - W_{\text{dis}}^{\kappa}$. Then, as $T(t) = cte$, those relations can be interpreted as entropic ones by solely dividing them by T, even after integration. The total variation on the medium entropy is given by the total heat

divided by the temperature $\Sigma_{\text{med}} = Q/T$ and the total change in the free energy divided by temperature is the opposite of the system entropy $\Delta F/T = (k_{\text{B}}/2)\ln(\kappa_f/\kappa_i) = -\Delta\Sigma_{\text{sys}}$, since $\kappa_f/\kappa_i = s_i/s_f$ when equilibrium states at the beginning and at the end of an isothermal process is considered.

The comparison between energetic quantities with entropic ones, leads to the relation $\Sigma^{\kappa}_{\text{gen}} = W^{\kappa}_{\text{dis}}/T$ between the total dissipative work W^{κ}_{dis} and the total entropy production $\Sigma^{\kappa}_{\text{gen}}$. By analogy with this isothermal case, a similar relation between energetic and entropic quantities can be set between the total thermal work W^{T}_{dis} and the generated entropy Σ^{T}_{gen}, when isochoric processes are considered. But, since in this case temperature is modified along the non-equilibrium process, this relation should be evaluated as $W^{T}_{\text{dis}} = \int T(t) đ\Sigma^{T}_{\text{gen}}$.

Two aspects will be clarified below. After the system reaches equilibrium, ΔF and $\Delta\Sigma^{\kappa}_{\text{sys}}$ are equivalent quantities, but a subtle point emerges since it is not necessarily the case for a non-equilibrium intermediary state. The first aspect to be clarified corresponds to the difference between the instantaneous variation of the free energy $\Delta F(t) = F(t) - F(0)$ and system entropy $\Delta\Sigma_{\text{sys}}(t) = \Sigma_{\text{sys}}(t) - \Sigma_{\text{sys}}(0)$ along a non-equilibrium process. The second aspect corresponds to the explicit dependence of the dissipative and thermal work for a given time dependence on the control parameter $\chi(t)$.

3.3 Non-equilibrium state functions

Extending in the previous section the definition of $\Delta U_{\text{sys}}(t)$ to non-equilibrium processes was straightforward, since for each time instant $U_{\text{sys}}(t) = (1/2)\kappa(t)s(t)$ is defined as the potential confinement energy of the Brownian particle. However, such extension is not trivial for state function variations like $\Delta F(t)$ and $\Delta\Sigma_{\text{sys}}(t)$. Variations of those state functions through a transition between two equilibrium states $s_i \to s_f$ have been defined above at the limit of quasi-static transformations. In this section, we propose a stochastic version of the system entropy $\sigma_{\text{sys}}(t)$, along a trajectory $x_j(t)$ to quantify the pure dissipative quantities associated with isothermal and isochoric processes.

3.3.1 Non-equilibrium free energy

In order to define the instantaneous free energy associated with a non-equilibrium state when a isothermal process is considered, M. Espositio and C. van den Broeck [87] introduce the relative entropy between the non-equilibrium distribution, $p(x, s(t))$ and the corresponding equilibrium one $p_{\text{eq}}(x, \kappa(t), T)$ as the "[...] *amount of information $I(t)$ that needs to be processed to switch from the known equilibrium distribution*

$p_{\rm eq}(x,\kappa(t),T)$ *to the distribution* $p(x,s(t))$ *under consideration.*" For us, those two probabilities distributions are defined as:

$$p(x,s(t)) = \frac{1}{\sqrt{2\pi s(t)}} \mathrm{e}^{-\frac{x^2}{2s(t)}}, \tag{3.8}$$

$$p_{\rm eq}(x,\kappa(t),T) = \frac{1}{\sqrt{2\pi \frac{k_{\rm B}T}{\kappa(t)}}} \mathrm{e}^{-\frac{\kappa(t)x^2}{2k_{\rm B}T}}. \tag{3.9}$$

While Eq. (3.8) defines the non-equilibrium evolution of the system, imprinted on the time dependence of the position variance $s(t)$, Eq. (3.9) is a probability distribution defined by the instantaneous value of the external control parameters, the protocol $\kappa(t)$, in this case. Eq. (3.9) defines the equilibrium position distribution defined by the macroscopic parameters $(\kappa(t),T)$, as required by the definition of equilibrium state in thermodynamics, as discussed at the beginning of this chapter. Eq. (3.9) also defines the partition function for isothemal protocos as $Z^{\kappa}(t) = \sqrt{2\pi k_{\rm B}T/\kappa(t)}$. While the actual *process* $s(t)$ performed by the Brownian particle defines Eq. (3.8), the *protocol* $\kappa(t)$ defines Eq. (3.9).

In this context, corresponding equilibrium means that, for each instant of time t there is an instantaneous position variance that corresponds to the one expected *if the system were in equilibrium*, $s_{\rm eq}(t) = k_{\rm B}T/\kappa(t)$. This variance of course is different from the measured value $s(t)$ for a non-equilibrium state.

Then the two probability distributions, which in turn are associated with a single instantaneous state, are used to determine the difference between the non-equilibrium free energy $F_{\rm non-eq}(t)$, and the equivalent equilibrium free energy $F_{\rm eq}(t)$, as follows

$$F_{\rm non-eq}(t) - F_{\rm eq}(t) = k_{\rm B}TI(t) \tag{3.10}$$

$$I(t) = \int_{-\infty}^{\infty} p(x,s(t)) \ln \frac{p(x,s(t))}{p_{\rm eq}(x,\kappa(t),T)} dx. \tag{3.11}$$

This is precisely how information plays its role according [87] since one recognize $I(t) \equiv D_{\rm KL}(p \parallel p_{\rm eq})$ as the Kullback-Leibler divergence measuring the "distance" between the two distributions Eqs. (3.8) and (3.9).

If a quasi-static $\kappa(t)$ protocol is considered, one recovers for each time instant that $p(x,s(t)) = p_{\rm eq}(x,\kappa(t),T)$, leading to the identification of $F_{\rm non-eq}(t) = F_{\rm eq}(t)$. If not, substituting Eqs. (3.8) and (3.9) into Eq. (3.11) yields the free energy of a non-equilibrium state as

$$F_{\rm non-eq}(t) = F_{\rm eq}(t) + \frac{k_{\rm B}T}{2} \ln \frac{k_{\rm B}T}{\kappa(t)s(t)} + \frac{1}{2}\left(\kappa(t)s(t) - k_{\rm B}T\right). \tag{3.12}$$

Based on these definitions, it is possible to identify the instantaneous equilibrium free energy as $F_{\rm eq}(t) = -k_{\rm B}T \ln Z^{\kappa}(t)$ and then infinitesimal variation of those functions. The infinitesimal variation in the out-of-equilibrium free energy $dF_{\rm non-eq}$ from $dF_{\rm eq} = (k_{\rm B}T/2)(d\kappa/\kappa)$ and $dU^{\kappa}_{\rm sys} = (1/2)d(\kappa s)$ leads to $d\Sigma^{\kappa}_{\rm sys,\ non-eq} = (dU^{\kappa}_{\rm sys} - dF_{\rm non-eq})/T = (k_{\rm B}/2)(ds/s)$. Thus, Eq. (3.12) allows to identify the variation of the system entropy along an out-of-equilibrium process as an extension to a non-equilibrium evolution $s_f \to s(t)$, obtained by differentiating Eq. (3.7) in relation to $s(t)$. In fact, this definition for $d\Sigma^{\kappa}_{\rm sys\ non-eq}$ is also obtained if the entropy along a stochastic trajectory introduced in [88] is considered.

In Section 3.4, we will discuss how to relate entropic quantities, starting from the First Law, Eq. (3.27), and based on the Langevin equation, in an approach similar to that introduced by Ken Sekimoto [89], Eqs. (3.37) and (3.38). In these discussions, when the infinitesimal variation of the system's energy is defined as $dU_{\rm sys} = \frac{1}{2}d(\kappa s)$, a different definition for $d\Sigma_{\rm sys}$ needs to be considered. Therefore, we propose to carry out the thermodynamic description for non-equilibrium processes based on a new definition of the system entropy $\sigma_{\rm sys}(t)$, considered at the stochastic level.

3.3.2 Non-equilibrium system entropy

Udo Seifert [88] suggests to define a trajectory-dependent entropy for a Brownian particle at the stochastic level as $\sigma^{\rm Seifert}_{\rm sys}(t) = -k_{\rm B} \ln p(x_j(t), s(t))$ by evaluating the probability distribution $p(x, s(t))$, Eq. (3.8), along the stochastic trajectory $x_j(t)$. He then defines rate equations for the system and medium entropies leading to the full entropy production rate. For this definition, $p(x_j(t), s(t))$ can be interpreted as a stochastic probability distribution, since it corresponds to the probability to find the system at position $x = x_j(t)$ for a given stochastic realization.

Here we suggest a different definition to evaluate the system entropy along a stochastic trajectory $x_j(t)$, when only one control parameter $\chi(t)$ is varied, whether the trap stiffness or the bath temperature, respectively:

$$\sigma^{\kappa}_{\rm sys}(t) = -k_{\rm B} \ln \sqrt{\frac{\kappa(t)}{2\pi k_{\rm B}T}} e^{-\frac{\kappa(t)x_j^2(t)}{2k_{\rm B}T}}, \tag{3.13}$$

$$\sigma^{T}_{\rm sys}(t) = -k_{\rm B} \ln \sqrt{\frac{\kappa}{2\pi k_{\rm B}T(t)}} e^{-\frac{\kappa x_j^2(t)}{2k_{\rm B}T(t)}}. \tag{3.14}$$

While U. Seifert suggests to evaluate $x_j(t)$ along Eq. (3.8), we suggest here to evaluate $x_j(t)$ along Eq. (3.9). For the case of an isothermal process, $p_{\rm eq}(x_j(t), \kappa(t), T)$ is no longer interpreted as probability distribution, since it is not even normalized. This assumption implies that the Boltzmann weight still applies to a non-equilibrium state $\exp(-u_{\rm sys}(x_j(t), \kappa(t))/(k_{\rm B}T(t))) = \exp(-\kappa(t)x_j^2(t)/(2k_{\rm B}T(t)))$. An interpretation for

$p_{\rm eq}(x_j(t),\kappa(t),T)$ is thus that it relates a system microstate $x_j(t)$ at a given time, distributed accordingly to $p(x,s(t))$, with the corresponding equilibrium distribution $p_{\rm eq}(x,\kappa(t),T)$ defined by the instantaneous value of the external control parameter $\kappa(t)$.

The condition that only one control parameter can be time-dependent in order to define $\sigma_{\rm sys}(t)$ by Eqs. (3.13) and (3.14), corresponds to the fact that non-equilibrium states of the system are unambiguously defined only by the instantaneous values $(\kappa(t),T,s(t))$ or $(\kappa,T(t),s(t))$. If a protocol with two simultaneously changing control parameters $(\kappa(t),T(t))$ is considered, $(\kappa(t),T(t),s(t))$ does not completely define the non-equilibrium state of the system.

This more general case goes beyond the discussion we want to develop here. Note however that the consideration of velocity distribution on overdamped system has been discussed recently in the literature, for example in [90] in which the *"Kinetic energy estimates are obtained from measurements of the mean square velocity of the trapped bead sampled at frequencies several orders of magnitude smaller than the momentum relaxation frequency."* In this case, the equipartition theorem that relates $s_v(t)$ to the instantaneous temperature $T(t)$ is modified in order to consider the under-sampling rate of experimental measurements, in which the acquisition frequency is much smaller than the inverse of the velocity correlation time $2\pi f_{\rm aq} \ll 1/\tau_v$. The fact that the kinetic energy should be considered in a thermodynamic description is a topic that is currently under debate [91, 92]. Here we will stick to the thermodynamic discussion limited only to isothermal and isochoric processes for which the definition of $\sigma_{\rm sys}(t)$ given by Eqs. (3.13) and (3.14) is valid.

Infinitesimal changes

Back to isothermal and isochoric processes, it is convenient to relate the change in the system entropy $d\sigma_{\rm sys}$ associated with an increment of a control parameter $d\chi$, by differentiating Eq. (3.13) with respect to $(x_j(t),\kappa(t))$ and Eq. (3.14) with respect to $(x_j(t),T(t))$. Then, an infinitesimal change on the system entropy $d\sigma_{\rm sys}$ produced when an isothermal change $d\kappa$ or an isochoric change dT is applied on the confining potential or on the temperature of the thermal reservoir corresponds to

$$d\sigma^{\kappa}_{\rm sys}(t) = \frac{\kappa(t)x_j(t)}{T}dx_j + \frac{k_{\rm B}}{2}\left(\frac{\kappa(t)x_j^2(t)}{k_{\rm B}T} - 1\right)\frac{d\kappa}{\kappa(t)}, \tag{3.15}$$

$$d\sigma^{T}_{\rm sys}(t) = \frac{\kappa x_j(t)}{T(t)}dx_j - \frac{k_{\rm B}}{2}\left(\frac{\kappa x_j^2(t)}{k_{\rm B}T(t)} - 1\right)\frac{dT}{T(t)}. \tag{3.16}$$

While the first terms on the right hand side of Eqs. (3.15) and (3.16) are identified as a medium entropy $-đ\sigma_{\rm med}(t) = -đq(t)/T(t)$, that can be a positive or negative

quantity, the other terms given by $d\sigma_{\text{sys}} + đ\sigma_{\text{med}}$ describes the entropic impact of the external parameters $\chi(t)$ on the change of $d\sigma_{\text{sys}}$ when a non-equilibrium process is performed. Independently whether a compression/expansion or a heating/cooling process is considered, this term corresponds to a positive quantity identified as $đ\sigma_{\text{gen}}$, the infinitesimal production of entropy associated with such non-equilibrium processes.

In order to characterize the system entropy associated to protocols at the macroscopic level, in which the system is described by $\langle x_j^2(t)\rangle = s(t)$, as measured on Figures 2.12 and 2.13, in Chapter 2, the ensemble averaged system entropy $d\Sigma_{\text{sys}}(t) = \langle d\sigma_{\text{sys}}\rangle$ can be evaluated for each time instant for a given variation of the control parameters $d\chi$ as

$$d\Sigma_{\text{sys}}^{\kappa}(t) = \frac{\kappa(t)}{2T} ds + \frac{k_{\text{B}}}{2}\left(\frac{\kappa(t)s(t)}{k_{\text{B}}T} - 1\right)\frac{d\kappa}{\kappa(t)}, \tag{3.17}$$

$$d\Sigma_{\text{sys}}^{T}(t) = \frac{\kappa}{2T(t)} ds - \frac{k_{\text{B}}}{2}\left(\frac{\kappa s(t)}{k_{\text{B}}T(t)} - 1\right)\frac{dT}{T(t)}. \tag{3.18}$$

Pure dissipative quantities

The infinitesimal second law introduced on Eq. (3.6) will be now considered to interpret the different contributions of $d\Sigma_{\text{sys}}(t)$. From the Eqs. (3.17) and (3.18), the total differential $d\Sigma_{\text{sys}}$ is decomposed into two non-exact differentials. The first terms on the right hand side on both Eqs. (3.17) and (3.18) are identified as the negative of the medium entropy $đ\Sigma_{\text{med}} = đQ/T = -(1/2T)\kappa ds$ for each process. Based on this identification, the remaining terms on the right hand side on Eqs. (3.17) and (3.18) will be defined as infinitesimal variations of the total entropy $đ\Sigma_{\text{gen}}(t)$ for an infinitesimal isothermal or isochoric change. This pure dissipative entropic quantity is then related to the pure dissipative energetic quantities by $T đ\Sigma_{\text{gen}}$ according to

$$đW_{\text{dis}}^{\kappa}(t) = \frac{1}{2}\left(\kappa(t)s(t) - k_{\text{B}}T\right)\frac{d\kappa}{\kappa(t)}, \tag{3.19}$$

$$đW_{\text{dis}}^{T}(t) = -\frac{1}{2}\left(\kappa s(t) - k_{\text{B}}T(t)\right)\frac{dT}{T(t)}. \tag{3.20}$$

Eqs. (3.19) and (3.20) should be interpreted as how much energy is dissipated in a time interval dt, for an infinitesimal variation on the control parameter $d\chi$. It is important to stress that Eq. (3.20) corresponds to a new energetic quantity, that is not described by the first law, and that accounts for the energetic cost of an isochoric transition.

Those pure dissipative quantities corresponds to evaluating the change in thermodynamic functions by the action of a protocol. Another possibility to measure dissipative quantities is to consider the rate of change of these quantities over time, as for example

to determine the temporal evolution of entropy production $\Sigma_{\text{gen}}(t)$, that in turn obeys a differential equation [93]. In opposition to this formalism of rate equations, the pure dissipative quantities introduced here associate these quantities with a change in the control parameter $d\chi$ produced in the time interval dt.

Since $\chi(t)$ does not correspond experimentally to a continuous function, but rather to increments in either the intensity of the trapping laser or the amplitude of the stochastic radiation pressure (that in turn is also associated to a change in intensity of a laser), the measurement of entropy production or energy dissipation over the course of a protocol, $\Sigma_{\text{gen}} = \int đ\Sigma_{\text{gen}}$ or $W_{\text{dis}} = \int đW_{\text{dis}}$ requires a more detailed discussion. Such a discussion will be made at the end of this chapter based on a functional formulation of these functions. Before that, a brief digression will be made on the consistency of the definition of $\sigma_{\text{sys}}(t)$ given in Eqs. (3.13) and (3.14).

3.4 Thermodynamics consistence

The consistency required for the definition of $\sigma_{\text{sys}}(t)$ will be discussed through two approaches. The first consists of obtaining the Second Law from the First Law by considering the instantaneous values of thermodynamic functions, assuming that $\chi(t)$ is a piece-wise continuous function. This condition is necessary so that the integration of the thermodynamic functions that depend directly on the variation of the control parameter $d\chi$ can be rewritten from an integration by parts, to integrals determined by the infinitesimal ds plus a surface term. The second approach follows the thermodynamic interpretation of the Langevin equation, introduced by Ken Sekimoto [89], rewritten here to handle properly the relation between the different entropic quantities.

3.4.1 From the first to the second law

Since there is no ambiguity in the definition of the instantaneous value of the difference in internal energy $\Delta U_{\text{sys}}(t)$, this quantity can be determined by integrating the total differential $\Delta U_{\text{sys}}(t) = \int_0^t d(\kappa s)$, from an initial state at $t = 0$ to a generic state at time t, not necessarily in equilibrium. Thus, when considering an isothermal or isochoric process, we write

$$\Delta U^{\kappa}_{\text{sys}}(t) = \frac{1}{2}\int_{s_i}^{s(t)} d(\kappa(t)s(t)) = \frac{1}{2}\left(s(t)\kappa(t) - s_i\kappa_i\right), \tag{3.21}$$

$$\Delta U^{T}_{\text{sys}}(t) = \frac{\kappa}{2}\int_{s_i}^{s(t)} ds(t) = \frac{\kappa}{2}\left(s(t) - s_i\right). \tag{3.22}$$

For an isothermal protocol $\kappa(t)$, Eq. (3.21) is related to two path-dependent functions, the work and the heat. In contrast, for an isochoric protocol $T(t)$, the work is

zero $W^T = 0$, and Eq. (3.22) can then also be used to determine $-Q^T(t)$.

It is also possible to analyze how entropic quantities vary throughout these processes. Despite the First Law for this type of isochoric process does not contain any dissipative quantities, since $đQ^T \to dQ^T$, it is possible to derive inexact differentials by dividing $dU^T_{\rm sys}$ and dQ^T by $T(t)$.

First, considering just the heat, it immediately yields the entropy of the medium $đ\Sigma^T_{\rm med} = dQ^T/T$, as a functional of the process $s(t)$ and the protocol $T(t)$. Likewise for isothermal changes, both medium entropy for isothermal and isochoric processes along a non-equilibrium process is determined as

$$\Sigma^{\kappa}_{\rm med}(t) = -\frac{1}{2T}\int_{(s_i,\kappa_i)}^{(s(t),\kappa(t))} \kappa(t)ds, \tag{3.23}$$

$$\Sigma^{T}_{\rm med}(t) = -\frac{\kappa}{2}\int_{(s_i,T_i)}^{(s(t),T(t))} \frac{ds}{T(t)}. \tag{3.24}$$

Entropic exact differentials

By analyzing the inexact differential $dU_{\rm sys}/T(t)$, this quantity can be identified as part of an exact differential, in which isothermal and isochoric protocols, when considered individually, lead to the following respective expressions

$$d\left(\frac{U^{\kappa}\text{sys}}{T}\right) = d\left(\frac{\kappa(t)s(t)}{2T}\right) = \frac{\kappa(t)ds}{2T} + \frac{s(t)}{2T}d\kappa, \tag{3.25}$$

$$d\left(\frac{U^{T}\text{sys}}{T}\right) = d\left(\frac{\kappa s(t)}{2T(t)}\right) = \frac{\kappa ds}{2T(t)} - \frac{\kappa s(t)}{2T^2(t)}dT, \tag{3.26}$$

in which the isotherm case considered in Eq. (3.25) correspond to the same relation given by Eq. (3.4).

The dimensionless version of the total differential Eqs. (3.25), (3.26) obtained by normalizing the terms by $k_{\rm B}$, can be interpreted as the infinitesimal variation of the ratio between system and medium internal energies $d(U_{\rm sys}/U_{\rm med})$. As discussed in the Figure 3.2 the difference $\Delta U_{\rm sys}(t) \neq \Delta U_{\rm med}(t)$ is the instantaneous signature of a non-equilibrium state.

Entropic inexact differentials

By considering then the infinitesimal change $d(U_{\rm sys}/U_{\rm med})$, two kinds of non-exact differentials are derived:

- one that takes into account the change in the system's state defined by the instantaneous variation on the process performed of the Brownian particle, $\kappa ds/(2T)$ that is the first term on the right hand side of Eqs. (3.25) and (3.26).

- another related to the external drive $\chi(t)$, that depends if a isothermal or isochoric process is considered.

For an isothermal transformation, the second term on the right hand side of Eq. (3.25) is identified as the infinitesimal work divided by temperature $đW/T = s\delta\kappa/(2T)$. The last term on the right hand side of Eq. (3.26), by analogy, should them have the same nature, but this time associated with isochoric processes. This quantity was measured in [43] and indeed characterizes the non-equilibrium nature of a time dependent temperature $T(t)$.

Returning to the analysis of the isochoric case, Eq. (3.26) can be used to rewrite the relation $\int(dU_{\text{sys}} + dQ)/T = 0$ over the course of a process as follows

$$\frac{\kappa}{2}\left(\frac{s(t)}{T(t)} - \frac{s_i}{T_i}\right) + \Sigma^T_{\text{med}}(t) = -\frac{\kappa}{2}\int_{(s_i,T_i)}^{(s(t),T(t))} \frac{s(t)}{T^2(t)} dT, \tag{3.27}$$

where the first term on the left-hand side corresponds to the integral of the total differential given by Eq. (3.26). Eq. (3.24) was used to replace the term related to the entropy of the medium.

At this point, Eq. (3.27) relates entropic quantities, but cannot be identified as the Second Law for isochoric processes. As discussed in Eq. (3.6), the Second Law relates two quantities that are a *functional* of the $\chi(t)$ protocol, Σ_{med} and Σ_{gen}, to a quantity that is a instantaneous *function* of $\chi(t)$, $\Delta\Sigma_{\text{sys}}(t)$. In the case where the time dependence of the Second Law is given explicitly for isochoric processes, Eq. (3.27) needs to be modified so that it is possible to identify $\Delta\Sigma_{\text{sys}}(t)$ along an out-of-equilibrium process. This quantity cannot be identified in Eq. (3.27) since the only term that is an instantaneous function of $s(t)$ and $T(t)$, the term on the left hand side, is only different from zero when the system is out of equilibrium and it does not have the features required for the instantaneous variation of the system entropy $\Delta\Sigma_{\text{sys}}(t)$. This issue will be solved below.

Entropy along a process

In order for Eq. (3.27) to be interpreted as the second law, it is necessary to identify the right features for $\Delta\Sigma_{\text{sys}}(t)$. To do so, Eqs. (3.17) and (3.18), derived from the definition of $\sigma_{\text{sys}}(t)$, once integrated over isothermal and isochoric processes, lead to

the respective expressions

$$\Delta\Sigma^{\kappa}_{\rm sys}(t) = \frac{1}{2T}\int_{(s_i,\kappa_i)}^{(s(t),\kappa(t))} \kappa(t)ds + \frac{1}{2T}\int_{(s_i,\kappa_i)}^{(s(t),\kappa(t))} s(t)d\kappa - \frac{k_{\rm B}}{2}\int_{\kappa_i}^{\kappa(t)}\frac{d\kappa}{\kappa}, \tag{3.28}$$

$$= \frac{1}{T}\left(U_{\rm sys}(t) - U_{\rm sys}(0)\right) - \frac{k_{\rm B}}{2}\ln\frac{\kappa(t)}{\kappa_i}, \tag{3.29}$$

$$\Delta\Sigma^{T}_{\rm sys}(t) = \frac{\kappa}{2}\int_{(s_i,T_i)}^{(s(t),T(t))}\frac{ds}{T(t)} - \frac{\kappa}{2}\int_{(s_i,T_i)}^{(s(t),T(t))}\frac{s(t)}{T^2(t)}dT + \frac{k_{\rm B}}{2}\int_{T_i}^{T(t)}\frac{dT}{T(t)}, \tag{3.30}$$

$$= \left(\frac{U_{\rm sys}(t)}{T(t)} - \frac{U_{\rm sys}(0)}{T_i}\right) + \frac{k_{\rm B}}{2}\ln\frac{T(t)}{T_i}, \tag{3.31}$$

where Eqs. (3.29) and (3.31) can be obtained from the combination of the two first integrals on Eq. (3.28) and (3.30) respectively, using integration by parts. From this combination, a surface term (coming from $\int d(\kappa s/T)$) is obtained. Then, only Eq. (3.31) leads to the definition of $\Delta\Sigma^{T}_{\rm sys}(t)$ which can be substituted in Eq. (3.27), leading to an expression with the required features for the Second Law.

It is important to point out that identifying the total entropy variation of the system Eq. (3.7), derived for initial and final states in equilibrium, to non-equilibrium states as $s_f \to s(t)$, does not lead to a consistent definition of the entropy of the system when Eq. (3.27) is taking into account. Here, since the stochastic system entropy is defined in a different manner, its instantaneous value at the macroscopic level is given by Eqs. (3.29) and (3.31), depending on the protocol. On those equations, the property of $\Delta\Sigma_{\rm sys}(t)$ being a state function is obvious, since this quantity only depends on the instantaneous values of the process $s(t)$, the values of the control parameters $\chi(t)$ and the initial condition.

The production of entropy along a non-equilibrium process can be evaluated based on the sum of Eqs. (3.29) and (3.23) in the case of an isothermal process $\Sigma^{\kappa}_{\rm gen}(t) = \Delta\Sigma^{\kappa}_{\rm sys}(t) + \Sigma^{\kappa}_{\rm med}(t)$, and by the sum of Eqs. (3.31) and (3.24) $\Sigma^{T}_{\rm gen}(t) = \Delta\Sigma^{T}_{\rm sys}(t) + \Sigma^{T}_{\rm med}(t)$, in the case of an isochoric process. These relationships will be explored in more detail in the following sections and in the next chapter.

Instantaneous free energy difference

When isothermal processes are considered, it is necessary to define an expression for $\Delta F(t)$ throughout the processes consistent with $\Delta U^{\kappa}_{\rm sys}(t)$, Eq. (3.21) and $\Delta\Sigma^{\kappa}_{\rm sys}(t)$, Eq. (3.29). At an infinitesimal level, those quantities are related, with

$$d\left(\frac{U^{\kappa}_{\rm sys} - F}{T}\right) + \frac{đQ^{\kappa}}{T} = \frac{đW^{\kappa}_{\rm dis}}{T}, \tag{3.32}$$

obtained from the combination of Eqs. (3.4) and (3.5).

While the second term on the left-hand side of Eq. (3.32) is identified as the entropy of the medium $đ\Sigma^{\kappa}_{\text{med}} = đQ/T$, the term on the right-hand side is identified as the entropy production $đ\Sigma^{\kappa}_{\text{gen}} = đW^{\kappa}_{\text{dis}}/T$. Thus, the first term on the left hand side of Eq. (3.32) corresponds to $d\Sigma_{\text{sys}}$, Eq. (3.17). As a consequence, an infinitesimal change on the free energy should be explicitly calculated as $dF = (k_{\text{B}}T/2)d\kappa/\kappa$, and one integrated along the process, its instantaneous variation at all times is given by $\Delta F(t) = (k_{\text{B}}T/2)\ln(\kappa(t)/\kappa_i)$.

Comparing $\Delta F(t)$ with Eq. (3.29) clearly reveal the difference between this quantity and $\Delta\Sigma_{\text{sys}}(t)$ for a transient non-equilibrium state. In an isothermal process, there is a change in the instantaneous value of the internal energy of the system if the conditions of equilibrium are not met. If a transition moving the system from a non-equilibrium state toward an equilibrium one is considered, that difference in internal energy should be accounted for. If only transitions between equilibrium states are considered, $\Delta\Sigma^{\kappa}_{\text{sys}}(t) = \Delta F(t)$.

3.4.2 Ken Sekimoto's approach to non-equilibrium system entropy

Ken Sekimoto's seminal work [89], endowed the Langevin equation with a thermodynamic interpretation, providing a mechanical description for thermodynamic processes at the level of stochastic trajectories. The general idea was to transform a relation between thermal, viscous and confining forces into energetics relations, when the system is subjected to an infinitesimal displacement dx_j, ending writing the Langevin equation in this energetic form

$$0 = \left(\gamma\frac{dx_j(t)}{dt} - \sqrt{2k_{\text{B}}T\gamma}\xi_j(t)\right)dx_j + \kappa x_j(t)dx_j. \tag{3.33}$$

Stochastic first law

For the particular case in which there is no time dependent external parameters $\chi(t) = cte$, that in turn describes an equilibrium state, the differential stochastic version of the system internal energy $du_{\text{sys}} = d(\kappa x_j^2/2) = \kappa x_j dx_j$ is identified as the last term on the left hand-side, because this term corresponds to a total differential. Then, the combination of a source of energy, provided by the collisions between the surrounding molecules of the medium and the Brownian particle, and accompanied by energy dissipation when the particle moves across the medium, defines the stochastic heat discarded by the system into the heat bath

$$đq = \left(-\sqrt{2k_{\text{B}}T\gamma}\xi_j(t) + \gamma\frac{dx_j(t)}{dt}\right)dx_j, \tag{3.34}$$

we stress that this incremental term is a non-exact differential and it can not be expressed as a simple gradient of another function.

To recover the first law, let us consider an isothermal process. Since $u_{\rm sys} = (1/2)\kappa x_j^2$, it is necessary to add on both sides of Eq. (3.33) the stochastic work $đw = (1/2)x_j^2 d\kappa$, playing the role of a "missing term" needed to recover a total differential

$$du_{\rm sys} = đw - đq, \tag{3.35}$$

$$\frac{1}{2}x_j^2(t)d\kappa + \kappa(t)x_j(t)dx_j = \frac{1}{2}x_j^2(t)d\kappa - \left(-\sqrt{2k_{\rm B}T\gamma}\xi_j(t) + \gamma\frac{dx_j(t)}{dt}\right)dx_j. \tag{3.36}$$

Stochastic second law

When temperature becomes a time dependent parameter, a *"new contribution to the energy change has to be taken into account"* as stated in [43]. To identify this new contribution, the approach is to transform the energetic relation expressed on Eq. (3.36) into an entropic relation, dividing each term by the temperature T. Just like the case of an isothermal process, in which the identification of the first law consists in building a total differential quantity, the same procedure will be performed here. But now by the dividing action, the total differential must also take into account the temperature change. It will corresponds to the stochastic version of Eqs. (3.25) and (3.26) for isothermal and isochoric processes, respectively.

As discussed at the macroscopic level, on Eq. (3.6), the Second Law can be formulated as a relation between one term that describes the exchange of energy between the system and the heat reservoir, in the form of the stochastic medium entropy $đ\sigma_{\rm med} = đq/T$, a second term that is a total differential, the stochastic system entropy $d\sigma_{\rm sys}$, and a third term corresponding to a purely dissipative quantity, characterizing the stochastic entropy production $đ\sigma_{\rm gen}$. By dividing Eq. (3.36) by T, and also add on both sides $-(k_{\rm B}/2)d\kappa/\kappa$ or $(k_{\rm B}/2)dT/T$, respectively for the case of isothermal or isochoric processes, it is possible to identify a purely dissipative quantity (different from zero only when a non-equilibrium process is considered), leading to the following definitions for an infinitesimal change on the system stochastic entropy $d\sigma_{\rm sys}$

$$d\sigma_{\rm sys}^{\kappa} = \frac{k_{\rm B}}{2}\left(\frac{\kappa(t)x_j^2(t)}{k_{\rm B}T} - 1\right)\frac{d\kappa}{\kappa(t)} + \frac{\kappa(t)x_j(t)}{T}dx_j = đ\sigma_{\rm gen}^{\kappa} - đ\sigma_{\rm med}^{\kappa}, \tag{3.37}$$

$$d\sigma_{\rm sys}^{T} = -\frac{k_{\rm B}}{2}\left(\frac{\kappa x_j^2(t)}{k_{\rm B}T(t)} - 1\right)\frac{dT}{T(t)} + \frac{\kappa x_j(t)}{T(t)}dx_j = đ\sigma_{\rm gen}^{T} - đ\sigma_{\rm med}^{T}, \tag{3.38}$$

that are consistent with Eqs. (3.15) and (3.16), that in turn were derived directly from the definition of $\sigma_{\rm sys}(t)$, Eqs. (3.13) and (3.14).

3.5 Functional approach

In this section, we will explain the discussion mentioned above (at the end of Section 3.3) in which the pure dissipative quantities, such as the total entropy Σ_{gen}, the dissipative work and the thermal work, W^{κ}_{dis} and W^{T}_{dis}, can be considered as a function of the protocol $\chi(t)$ that connects two states, s_i and s_f, not necessarily in equilibrium.

For the case of Σ_{gen}, such a functional corresponds to the sums of Eqs. (3.29) and (3.23) or Eqs. (3.31) and (3.24)

$$\Sigma^{\kappa}_{\text{gen}}[s_i, s_f; \kappa(s)] = \frac{1}{2T}\left(s_f\kappa_f - s_i\kappa_i\right) - \frac{k_{\text{B}}}{2}\ln\frac{\kappa_f}{\kappa_i} - \frac{1}{2T}\int_{s_i}^{s_f}\kappa(s)ds, \tag{3.39}$$

$$\Sigma^{T}_{\text{gen}}[s_i, s_f; T(s)] = \frac{\kappa}{2}\left(\frac{s_f}{T_f} - \frac{s_i}{T_i}\right) + \frac{k_{\text{B}}}{2}\ln\frac{T_f}{T_i} - \frac{\kappa}{2}\int_{s_i}^{s_f}\frac{ds}{T(s)}. \tag{3.40}$$

If either s_i or s_f does not correspond to an equilibrium state, the first term on the right-hand side of Eqs. (3.39) and (3.40), interpreted as a surface term, will be non-zero. The second term, $\ln(\chi_f/\chi_i)$, is independent of the details of the $\chi(t)$ protocol and depends only on the value of the control parameter at the start and at the end of the process under study. The third term $\int_{s_i}^{s_f}\kappa ds/(2T)$, corresponds to an integral of the protocol χ, parameterized by the evolution of the system $\chi(s)$, through its variance.

To illustrate how the functional relationship $\Sigma_{\text{gen}}[s_i, s_f; \chi(s)]$ can be used to quantify the cost of a specific process, Eqs. (3.39) and (3.40) will be used to characterize the cost of a discontinuous change $\chi_f \to \chi_i$ where s_i and s_f correspond to equilibrium states. Since, in this case, $s_i = k_{\text{B}}T_i/\kappa_i$ and $s_f = k_{\text{B}}T_f/\kappa_f$, the surface term will be identically zero and the integrals can be easily calculated, leading to

$$\Sigma^{\kappa}_{\text{gen, STEP}} = -\frac{k_{\text{B}}}{2}\ln\frac{\kappa_f}{\kappa_i} - \frac{k_{\text{B}}}{2}\left(1 - \frac{\kappa_f}{\kappa_i}\right), \tag{3.41}$$

$$\Sigma^{T}_{\text{gen, STEP}} = \frac{k_{\text{B}}}{2}\ln\frac{T_f}{T_i} - \frac{k_{\text{B}}}{2}\left(1 - \frac{T_i}{T_f}\right). \tag{3.42}$$

Some consequences of Eqs. (3.41) and (3.42) will be explained by analyzing Figure 3.3, in which these equations are plotted on a Linear $\times$ Log scale for the interval $\chi_f/\chi_i = [0.1; 10]$. As expected, for any physical process $\Sigma_{\text{gen}} > 0$. The asymmetry of this quantity for expansion *vs.* compression and cooling *vs.* heating is evident.

Another analysis that can be made from Eqs. (3.41) and (3.42) are the conditions under which a discontinuous transformation can be considered quasi-static in a more quantitative way. This analysis consists in determining the relationship between a variation $d\chi = \chi_f - \chi_i$ and the equivalent entropy production $\Sigma_{\text{gen, STEP}}$. In the case where $(\chi_f - \chi_i)/\chi_i \ll 1$, it is possible to expand Eqs. (3.41) and (3.42), where the

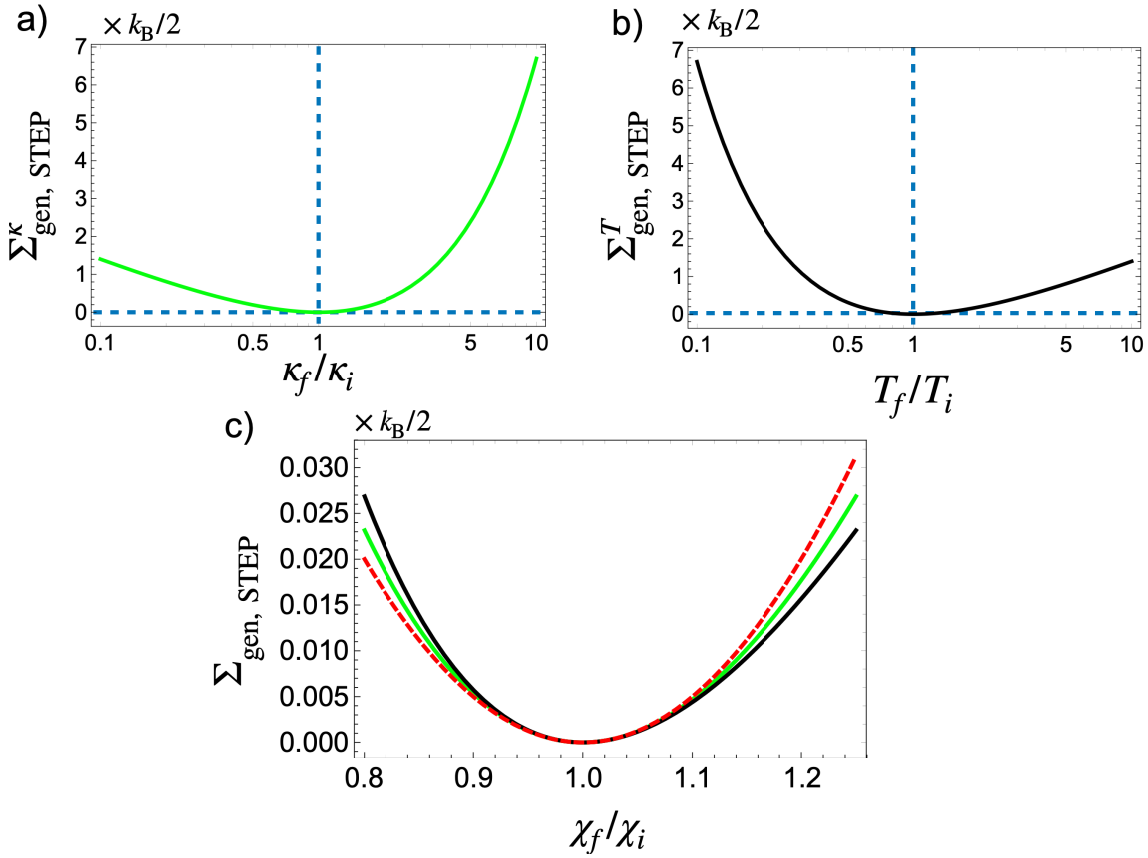

Figure 3.3: Plot of Eqs. (3.41), in green, and (3.42), in black , a) and b) respectively, in Linear × Log scale. It corresponds to the generated entropy for a given ratio between final and initial values of the control parameter χ_f/χ_i for a instantaneous change $\chi_i \to \chi_f$. The horizontal dashed lines correspond to $\Sigma_{\text{gen}} = 0$ and the vertical lines to $\chi_f = \chi_i$. a) In the vicinity of the region $\chi_f/\chi_i = 1$, the approximation given by Eq. (3.43), in red, is verified for all the processes (here a Linear × Linear scale is used).

first non-zero term corresponds to a symmetrical relationship between complementary processes (compression *vs.* expansion and cooling *vs.* heating), as seen in panel c)

$$\Sigma_{\text{gen, QS}} = \frac{k_B}{4}\left(\frac{\chi_f}{\chi_i} - 1\right)^2. \tag{3.43}$$

The same functional analysis done for $\Sigma_{\text{gen}}[s_i, s_f; \chi(s)]$ is compatible with purely dissipative energy quantities. These quantities can be expressed from an integration

by parts of Eqs. (3.19) and (3.20)

$$W^{\kappa}_{\rm dis}[s_i, s_f; \kappa(s)] = \frac{1}{2}\left(\kappa_f s_f - \kappa_i s_i\right) - \frac{k_{\rm B}T}{2}\ln\frac{\kappa_f}{\kappa_i} - \frac{1}{2}\int_{s_i}^{s_f}\kappa(s)ds, \tag{3.44}$$

$$W^{T}_{\rm dis}[s_i, s_f; T(s)] = -\frac{\kappa}{2}\left(s_f \ln\frac{T_f}{T_{\rm Ref}} - s_i \ln\frac{T_i}{T_{\rm Ref}}\right) - \frac{k_{\rm B}}{2}\left(T_f - T_i\right) + \frac{\kappa}{2}\int_{s_i}^{s_f}\ln\frac{T(s)}{T_{\rm Ref}}ds, \tag{3.45}$$

where in the case of an isochoric transformation, Eq. (3.45), a constant with temperature unit $T_{\rm Ref}$ was introduced to make the argument of the logarithmic function dimensionless.

While for the isothermal case, Eq. (3.44) is completely analogous to Eq. (3.39), for the isochoric case significant differences exist between Eq. (3.45) and (3.40). For the surface term present in $W^{T}_{\rm dis}$, this term is non-zero, even if the final and initial states are in equilibrium. The second term on the right-hand side of Eq. (3.45) corresponds to the change in the internal energy of the medium, which is given by $\Delta U_{\rm med} = (1/2)k_{\rm B}(T_f - T_i)$. Finally, the integral corresponding to the third term on the right-hand side of Eq. (3.45) corresponds to a functional with a different structure from the one considered in Eq. (3.40). This discrepancy in the functional approach for entropy and energy is only found in the case of isochoric processes. For isothermal ones, there is a close analogy in the entropic Eq. (3.41) and energetic Eq. (3.44) functionals.

3.6 Conclusion

This chapter aimed to relate thermodynamic functions, both from the stochastic viewpoint described by the stochastic variable $x_j^2(t)$, and from its average behavior, depicted through the evolution of the position variance $s(t)$, when considering isothermal processes, described by $(\kappa(t), T, s(t))$, or isochoric processes, described by $(\kappa, T(t), s(t))$. The relationships constructed here are rooted in the initial hypothesis that the system's internal energy is described by its potential energy. Consequently, functional relationships quantifying both the energetic and entropic costs associated with non-equilibrium processes. As will be discussed in the next chapter, this approach to cost quantification, when associated with a transition between equilibrium states occurring over a specific time interval Δt, allows for the determination of an optimal protocol through the minimization of a functional defined by the trade-off between such cost and Δt.

An essential aspect considered was the infinitesimal variations of thermodynamic state functions, like internal energy, free energy, and system entropy, occurring over a

specific time span, such as the interval dt between two consecutive measurements of $x_j^2(t)$, or even an arbitrary time instant t, where the initial condition is specified from the Gaussian position distribution $p(x, s_i = \langle x_j^2(0) \rangle)$.

In this context, while state functions correspond to instantaneous functions of the protocol $\chi(t)$ and the process $s(t)$, path-dependent functions are determined by functionals $J[s_i, s(t); \chi(s)]$. To illustrate this methodology, we discussed how these functionals enable the determination of dissipated energy and generation of entropy, when discontinuous changes in control parameters $d\chi = \chi_f - \chi_i$ are produced over an interval dt.

The difference in nature of the path dependent thermodynamic functions, if their infinitesimal variations depend on the change in position variance ds, like heat and environment entropy, or on the change in control parameters $d\chi$, such as work, its dissipative contributions, and the production of entropy, are pivotal when considering the temporal evolution of such functions. While on the one hand

- the energy exchange rate between the system and the heat reservoir corresponds to a continuous process, limited by the position variance relaxation time $2\tau_x$, that in turn constrain the variation ds, on the other hand,

- the energy exchanges with the work reservoir and the variation on the internal energy of the heat reservoir depend on $d\kappa$ and dT respectively, quantities whose variation is not limited by relaxation processes.

This different nature of how energy exchanges happen, is fundamental when considering the evolution of the thermodynamic functions developed here.

To make these definitions consistent with each other, we introduced a new definition of system entropy. An essential property characterized by an entropy measure is the relationship between micro and macro states. In our definition, such a relationship is measured over a stochastic trajectory from the microstate $x_j^2(t)$ and the corresponding position variance defined from the instantaneous values of the control parameter $s_{\text{eq}}^{\kappa}(t) = k_{\text{B}}T/\kappa(t)$ for isothermal processes, and $s_{\text{eq}}^{T}(t) = k_{\text{B}}T(t)/\kappa$ for isochoric processes. This measure can be executed when one can define averages in the ensemble $\{j\}$ of trajectories that share the initial condition $p(x, s_i = \langle x_j^2(0) \rangle)$.

An interesting aspect of the simultaneous dynamic and thermodynamic discussion of the Brownian motion developed here is, for example, the possibility of relating the dissipated energy in non-equilibrium processes from the balance of trapping forces, stochastic forces, and viscous force: when some protocol $\chi(t)$ is fast enough to generate an increase $ds(t) > 0$ or decrease $ds(t) < 0$ in position variance.

When these processes occur, the average collision force in the interval dt is not counteracted by the trapping force, causing the average speed in this time interval to

differ from zero. As a result, energy is dissipated by the viscous force. This system serves as a didactic model to discuss thermodynamic processes where the time scale of processes and the quasi-static limit, which in this case corresponds to processes where the average speed is zero, can be discussed from a mechanical approach, from the analysis of force balance.

Chapter 4

Isochoric transformation

In this chapter the techniques presented in Chapter 2 and the thermodynamic analysis and interpretation methodology developed in Chapter 3 will be used to characterize the entropy and energy exchanges involved in isochoric transformations performed on a Brownian particle. In such processes, the amplitude of the stochastic force produced by the radiation pressure changes over time, generating an evolution of the temperature of the center of mass of the Brownian particle.

First, we will derive the protocol that minimizes the production of entropy for a given transition time Δt. Next, the thermodynamic characterization for a discontinuous change in the temperature of the heat reservoir will be presented, in which the asymmetry between heating and cooling processes will be explored. Finally, optimal protocols will be presented, in which a new dimension - the time Δt of the transition - also presents asymmetry between heating and cooling processes. Different acceleration rates will be considered, and the optimal protocols derived here will be compared with the ThESE acceleration protocols derived in Chapter 2.

4.1 Optimal isochoric finite time transformations

Isochoric processes are characterized by a change in the system internal energy at constant volume: there is no work performed in this type of process. The First Law guarantees that the total amount of heat exchanged between the system and the heat reservoir corresponds to the change in internal energy, which leads to an apparent contradiction about how to deal with the energy dissipated in a non-equilibrium process. How is it possible to quantify the dissipated energy? This question was resolved in Chapter 3 by resorting to an entropic analysis.

This analysis consisted in quantifying the difference between i) the variation in

the instantaneous system entropy $\Delta\Sigma_{\rm sys}(t)$[1] and *ii*) with the entropy produced by the exchange of energy between the system and the medium throughout a process, quantified by the entropy of the medium $\Sigma_{\rm med}(t)$. Based on this comparison, whenever there is an imbalance between these quantities, entropy is generated according to $\Delta\Sigma_{\rm sys}(t) + \Sigma_{\rm med}(t) = \Sigma_{\rm gen}(t)$.

To establish the relationship between these entropic quantities, Chapter 3 also considered that within a time interval dt along a protocol, the instantaneous temperature of the heat reservoir is given by $T(t)$, and an increase in entropy production is proportional to the temperature variation $đ\Sigma_{\rm gen} \propto dT$. Thus, in this approach, it is possible to quantify an increase in dissipated energy, so-called thermal work, as $đW_{\rm dis} = T(t)đ\Sigma_{\rm gen}$. By determining such purely dissipative quantities *over an entire protocol*, we can then write these quantities as a *functional of a process*. Such functionals can then be used to quantify the cost of a given process that connects two states, be then in equilibrium or not. This idea is the basis for deriving the optimal protocols developed in this section.

4.1.1 Optimal protocol derivation

As discussed in Chapter 3, the entropy production and energy dissipation (dissipative work) functionals for isothermal processes have the same structure. However, for isochoric processes, this is not the case. Here, we will choose the entropy production functional as a way to quantifying the cost of connecting two states, defined by the initial s_i and final s_f position variance, which we recall

$$\Sigma_{\rm gen}[s_i, s_f; T(s)] = \frac{\kappa}{2}\left(\frac{s_f}{T_f} - \frac{s_i}{T_i}\right) + \frac{k_{\rm B}}{2}\ln\frac{T_f}{T_i} - \frac{\kappa}{2}\int_{s_i}^{s_f}\frac{ds}{T(s)}. \tag{4.1}$$

This expression is valid even if s_i and/or s_f do not correspond to equilibrium states. In this case, T_i and T_f correspond to the temperature of the heat reservoir associated with the considered states, not the one given by the initial and final position variance of the Brownian particle, $\kappa s_{i,f} \neq k_{\rm B}T_{i,f}$. Here we will consider processes in which the initial and final states are in equilibrium, then the conditions $s_i = k_{\rm B}T_i/\kappa$ and $s_f = k_{\rm B}T_f/\kappa$ are obeyed.

An important aspect of the functional formulation given by Eq. (4.1) is the implicit nature of time evolution: in this formulation, the protocol $T(s)$ can be expressed through $s(t)$, for each time instant t, given the monotonic nature of $s(t)$. In order to parameterize $T(s(t))$ in this way, only one parameter can change over time.

[1]Since only isochoric processes will be considered in this chapter, we will suppress from now the index ^{T}.

In parallel, we introduce a functional for the total process time Δt for a given transition from s_i to s_f, using the approach developed in [68] for isothermal transformations, for isochoric processes with

$$\Delta t = \int_0^{\Delta t} dt = \frac{1}{2}\int_{s_i}^{s_f} \frac{\gamma ds}{k_{\mathrm{B}}T(s) - s\kappa}, \tag{4.2}$$

where the differential relation $ds = (2/\gamma)(k_{\mathrm{B}}T(t) - \kappa s(t))dt$ deduced in Chapter 2 and discussed in Chapter 3 is written here as an integral.

Once combined, Eqs. (4.1) and (4.2) allow to identify the optimal protocol $T_{\mathrm{opt}}(t)$. This protocol corresponds to the minimal entropy production Σ_{gen} when the states s_i and s_f are connected in a given time interval Δt, determined by minimizing the functional

$$\int_{s_i}^{s_f} L[s, T(s)]ds = \int_{s_i}^{s_f} \left(\frac{\gamma}{k_{\mathrm{B}}T(s) - s\kappa} - \frac{\lambda\kappa}{k_{\mathrm{B}}T(s)} \right) ds, \tag{4.3}$$

which combines the transition time and the entropic cost on an equal footing by the Lagrange multiplier λ/k_{B}. This expression corresponds to the adaptation for isochoric transformations of the methodology proposed in [68] for isothermal ones. While in the latter case the cost was addressed as work, here we framed it as entropy.

The minimization of the functional given by Eq. (4.3) is performed using the Euler-Lagrange equation $d/ds(\partial L/\partial T') - \partial L/\partial T = 0$, with $T' \equiv dT/ds$. This equation will lead to

$$\left(1 - \frac{\lambda}{\tau_x}\right) T^2 + 2\frac{\lambda}{\tau_x}\frac{\kappa s}{k_{\mathrm{B}}} T - \frac{\lambda}{\tau_x}\left(\frac{\kappa s}{k_{\mathrm{B}}}\right)^2 = 0. \tag{4.4}$$

This minimization procedure yields two families of optimized thermal protocols $T_{\mathrm{h/c}}(s)$ in which the sub-index "h" refers to heating $T_i < T_f$ and the sub-index "c" refers to cooling $T_i > T_f$. Such families are based on the fact that Eq. (4.4) is a second-order polynomial equation for $T(s)$. As each of the solutions are related to different processes, the Lagrange multiplier that regulates the relationship between cost and transition time corresponds to different functions when heating and cooling processes are considered.

Thus, the two roots of Eq. (4.4) determine the functions $T_{\mathrm{h/c}}(s)$, with their respective Lagrange multiplier $\lambda_{\mathrm{h/c}}$

$$T_{\mathrm{h}}(s) = \frac{\kappa s}{k_{\mathrm{B}}\left(1 - \sqrt{\tau_x/\lambda_{\mathrm{h}}}\right)}, \tag{4.5}$$

$$T_{\mathrm{c}}(s) = \frac{\kappa s}{k_{\mathrm{B}}\left(1 + \sqrt{\tau_x/\lambda_{\mathrm{c}}}\right)}, \tag{4.6}$$

where the $k_{\mathrm{B}}T \equiv \kappa s$ quasi-static limit corresponds to $\tau_x = \gamma/\kappa \ll \lambda_{\mathrm{h/c}}$.

In order to implement optimal protocols experimentally, it is necessary to obtain explicit time dependent solutions. Such solutions $s_{\mathrm{h,c}}(t)$ can be obtained by integrating Eq. (4.2) up to an intermediate instant t using $T_{\mathrm{h/c}}(s)$ given by Eqs. (4.5) and (4.6). The optimal heating and cooling processes then correspond to

$$s_{\mathrm{h}}(t) = s_i \exp\left[-\frac{2t}{\tau_x}\left(1 - \frac{1}{1-\sqrt{\tau_x/\lambda_{\mathrm{h}}}}\right)\right], \tag{4.7}$$

$$s_{\mathrm{c}}(t) = s_i \exp\left[-\frac{2t}{\tau_x}\left(1 - \frac{1}{1+\sqrt{\tau_x/\lambda_{\mathrm{c}}}}\right)\right]. \tag{4.8}$$

Another way of expressing these optimal solutions is through the transfer time Δt itself. For a given Δt for both heating and cooling processes, different values are required for λ_{h} and λ_{c}. Thus, by changing the parameterization of Eqs. (4.7) and (4.8) and also using the initial $s_{\mathrm{h,c}}(0) = s_i = k_{\mathrm{B}}T_i/\kappa$ and the final $s_{\mathrm{h,c}}(\Delta t) = s_f = k_{\mathrm{B}}T_f/\kappa$ equilibrium conditions, it is possible to write the Lagrange multipliers as

$$1 - \sqrt{\tau_x/\lambda_{\mathrm{h}}} = \left(1 + \frac{\tau_x}{2\Delta t}\ln\frac{T_f}{T_i}\right)^{-1}, \tag{4.9}$$

$$1 + \sqrt{\tau_x/\lambda_{\mathrm{c}}} = \left(1 + \frac{\tau_x}{2\Delta t}\ln\frac{T_f}{T_i}\right)^{-1}. \tag{4.10}$$

Eqs. (4.9) and (4.10) allow us to parameterize the process $s_{\mathrm{h,c}}(t)$ into a single expression, which we define as the optimal isochoric process

$$s_{\mathrm{opt}}(t) = s_i\left(\frac{T_f}{T_i}\right)^{t/\Delta t}. \tag{4.11}$$

From the explicit time dependence given by Eq. (4.11) and Eqs. (4.9) or (4.10), for heating and cooling respectively, which define the Lagrange multipliers as a function of transition time Δt and the initial and final equilibrium temperatures, T_i and T_f, it is possible to determine the time dependence of the optimal protocol $T_{\mathrm{opt}}(t)$.

Equilibrium conditions between the system and the heat reservoir need to be guaranteed at the beginning and end of the optimal protocol. To ensure that the initial temperature, at $t = 0$, and the final temperature, at $t = \Delta t$, of the heat reservoir correspond to that expected by the instantaneous variance of the system, $\kappa s_i/k_{\mathrm{B}}$ and $\kappa s_f/k_{\mathrm{B}}$, two discontinuous transitions are supplemented on this protocol, just like in the case of optimal isothermal processes [66, 67, 68]. The T_{opt} protocol is then divided into three steps

$$T_{\mathrm{opt}}(t) = \begin{cases} \frac{\kappa s_i}{k_{\mathrm{B}}} & \text{at,} \quad t = 0, \\ \frac{\kappa s_{\mathrm{opt}}(t)}{k_{\mathrm{B}}}\left(1 + \frac{\tau_x}{2\Delta t}\ln\frac{T_f}{T_i}\right) & \text{for,} \quad \Delta t > t > 0, \\ \frac{\kappa s_f}{k_{\mathrm{B}}} & \text{at,} \quad t = \Delta t. \end{cases} \tag{4.12}$$

In general, acceleration protocols involve an overshooting ("os") in the control parameter. In the case of the optimal protocol derived here, it corresponds to $k_{\mathrm{B}}T_{\mathrm{os}} = \kappa s_f(1+\tau_x/(2\Delta t)\ln(T_f/T_i))$. In the case of heating processes, the minimum value of Δt experimentally accessible will then depend only on the maximum temperature that can be implemented. For cooling processes, the minimum value of Δt accessed experimentally is also constrained by the experimental technique used, but in contrast to the heating case, an asymmetry arises associated with the fundamental limit temperature $T = 0$ K. This limit implies that for the cooling case, the maximum acceleration that can be reached corresponds to

$$\Delta t_{\mathrm{min}} = \frac{\tau_x}{2}\ln\frac{T_i}{T_f}. \tag{4.13}$$

The asymmetry related to Δt_{min} will be discussed below in the context of entropy production for different accelerations $\Sigma_{\mathrm{gen}}(\Delta t)$. For now, Eqs. (4.11) and (4.12) will be used to determine Σ_{min} from Eq. (4.1).

4.1.2 Time-entropy bound

In this section we will derive the expression for the minimum entropy production, Σ_{min} for a given system entropy variation $\Delta\Sigma_{\mathrm{sys}} = (k_{\mathrm{B}}/2)\ln(T_f/T_i)$, and transition time Δt. The derivation needs to take into account the 3 stages of the optimal protocol; the two discontinuities at the beginning $t = 0^- \to 0^+$ and at the end $t = \Delta t^- \to \Delta t^+$ of the protocol, and the entropic evolution along the process $s_{\mathrm{opt}}(t)$ between those discontinuities. The minimal entropy production is the result of the sum of those three intermediate steps:

- from $t = 0^-$ to $t = 0^+$. In this first step, $T(0^-) = T_i$ and $T(0^+) = T_i[1+\tau_x/(2\Delta t)\ln(T_f/T_i)]$, while $s(0^-) = s(0^+) = s_i$. Thus, by substituting these quantities into Eq. (4.1), one gets:

$$\Sigma^{(1)}_{\mathrm{min}} = \frac{k_{\mathrm{B}}}{2}\ln\left(1+\frac{\tau_x}{2\Delta t}\ln\frac{T_f}{T_i}\right) + \frac{k_{\mathrm{B}}}{2}\left(\frac{1}{1+\frac{\tau_x}{2\Delta t}\ln\frac{T_f}{T_i}} - 1\right). \tag{4.14}$$

- from $t = 0^+$ to $t = \Delta t^-$. In this second step, $T(0^+) = T_i[1+\tau_x/(2\Delta t)\ln(T_f/T_i)]$ and $T(\Delta t^-) = T_f[1+\tau_x/(2\Delta t)\ln(T_f/T_i)]$, while $s(0^+) = s_i$ and $s(\Delta t^-) = s_f$. During this step, the time dependence of $s_{\mathrm{opt}}(t)$ and $T_{\mathrm{opt}}(t)$ are described by Eqs. (4.11) and (4.12) and, again, by substituting these quantities into Eq. (4.1), one arrives at:

$$\Sigma^{(2)}_{\mathrm{min}} = \frac{k_{\mathrm{B}}}{2}\ln\frac{T_f}{T_i} - \frac{k_{\mathrm{B}}\ln\frac{T_f}{T_i}}{2\left(1+\frac{\tau_x}{2\Delta t}\ln\frac{T_f}{T_i}\right)}. \tag{4.15}$$

- from $t = \Delta t^-$ to $t = \Delta t^+$. In this last step, the second discontinuity is produced with $T(\Delta t^-) = T_f[1 + \tau_x/(2\Delta t)\ln(T_f/T_i)]$ and $T(\Delta t^+) = T_f$, while $s(\Delta t^-) = s(\Delta t^+) = s_f$. Finally, by substituting these quantities into Eq. (4.1):

$$\Sigma_{\rm min}^{(3)} = \frac{k_{\rm B}}{2}\ln\left\{\frac{1}{1+\frac{\tau_x}{2\Delta t}\ln\frac{T_f}{T_i}}\right\} + \frac{k_{\rm B}}{2}\left(1 - \frac{1}{1+\frac{\tau_x}{2\Delta t}\ln\frac{T_f}{T_i}}\right). \tag{4.16}$$

It is interesting to note that connecting states in equilibrium necessarily yields $\Sigma_{\rm gen} \geqslant 0$, but that when one of the states (initial or final) is not in equilibrium, it is possible that $\Sigma_{\rm gen} < 0$. This can be checked with Eqs. (4.14) and (4.16), since $\Sigma_{\rm min}^{(1)} = -\Sigma_{\rm min}^{(3)}$. This situation however will not be explored in this work since for our protocols only intermediate states are out of equilibrium.

The minimal entropy production associated with the optimal protocol is then evaluated as $\Sigma_{\rm min} = \Sigma_{\rm min}^{(1)} + \Sigma_{\rm min}^{(2)} + \Sigma_{\rm min}^{(3)} = \Sigma_{\rm min}^{(2)}$. Using the definition of the total variation of the system entropy $\Delta\Sigma_{\rm sys} = (k_{\rm B}/2)\ln(T_f/T_i)$ associated with two equilibrium states with different temperatures, it is possible to write this minimal entropy production associated with the optimal protocol as

$$\Sigma_{\rm min} = \frac{\Delta\Sigma_{\rm sys}}{1 + \frac{k_{\rm B}}{\tau_x}\frac{\Delta t}{\Delta\Sigma_{\rm sys}}} \tag{4.17}$$

We emphasize that this expression is valid both for cooling and heating protocols but with different thermodynamic consequences, as discussed below.

4.2 Thermodynamic analyses of isochoric transformations

4.2.1 STEP-like $T(t)$ protocol

In Section 2.4.2 and Figures 2.10 and 2.11, we discussed the methods for producing and measuring over time the evolution of the position variance of the Brownian particle $s(t)$ when subjected to a discontinuous change in the amplitude of a stochastic radiation pressure force. Here, we will present the methods used for describing the thermodynamic observables associated with these processes. This corresponds to the description of the entropic and energetic evolutions, respectively shown in Figure 4.1 and Figure 4.2, in which the asymmetries between heating (when the amplitude of the modulation of the external stochastic force increases) and cooling (when the amplitude decreases) are discussed.

The thermodynamic observables associated with these measurements depend on the trap stiffness $\kappa = 13.1 \pm 0.5$ fN/nm, the position correlation time $\tau_x = \gamma/\kappa =$

2.01 ± 0.06 ms and the time series acquired for monitoring the position variance $s(t)$ and the temperature $T(t)$. While $s(t)$ is measured from a set of $j_{\max} = 17980$ independent realizations of the stochastic trajectory $x_j(t)$, subjected to the protocol $T(t) = T_i + \Theta(t)(T_f - T_i)$, where $\Theta(t < 0) = 0$ and $\Theta(t \geq 0) = 1$, the series $T(t)$ is measured from the peak-to-peak signal $V_{\rm pp}^2(t)$ sent to the AOM, which in turn determines the modulation amplitude of the laser exerting radiation pressure on the Brownian particle. The uncertainties of these time series, $\delta s(t)/s(t) = 0.04$ are determined within a confidence interval of 95% based on a χ^2 distribution with $j_{\max}$ degrees of freedom, and $\delta T/T = 0.07$ is estimated from the relationship between $V_{\rm pp}^2$ and the temperature of the center of mass of the Brownian particle, as discussed in Section 2.3.2 and in Figures 2.8 and 2.9. For the measurements presented in this section, $T_{\rm c} = 1200 \pm 90$ K and $T_{\rm h} = 2200 \pm 160$ K, in which the sub-index $_{\rm c,h}$ referees to the cold and to the hot temperature used on the heating and cooling processes.

As the procedures for measuring $s(t)$ require repeating the $T(t)$ protocol thousands of times, the total time of the measurements presented here is $\Delta t_{\rm meas} = 6$ min. Over such a big acquisition time, it is very hard to avoid any positional drifts of the different optical beams involved in the experiment. Such drifts generate a difference between *i*) the value of T_i and T_f measured from $V_{\rm pp}^2(t)$ and *ii*) the value $\kappa s_i/k_{\rm B}$ and $\kappa s_f/k_{\rm B}$ measured when the Brownian particle is at equilibrium, before the start of the protocol for $s(t < 0)$, and after the final temperature has been reached for $s(t \gg \tau_x)$. For the heating process, $\kappa s_i/k_{\rm B} = 1290 \pm 50$ K and $\kappa s_f/k_{\rm B} = 2310 \pm 90$ K. In this case, the uncertainties were propagated, with $\kappa s/k_{\rm B}\sqrt{(\delta s/s)^2 + (\delta\kappa/\kappa)^2}$.

As one sees, there is not a sensible difference between such values and those given above based on $V_{\rm pp}^2(t)$ measurements. We consider that measuring the temperature from $\kappa s/k_{\rm B}$ is more accurate than from $V_{\rm pp}^2$, since a change over time in the relationship between $V_{\rm pp}^2(t)$ and the actual effective temperature of the thermal bath is expected to change due to the drift effects, as mentioned above. For these reasons, $T(t)$ used in this section corresponds to the temperatures measured from the initial and final equilibrium position variations, built with the same acquisition frequency $f_{\rm aq} = 2^{16}$ Hz $= 65536$ Hz.

The first entropic observable to be considered is the evolution of the entropy of the medium $\Sigma_{\rm med}(t)$. The evolution of this observable is determined from the cumulative sum, according to Eq. (3.24), and using the "Accumulate[$list(k)$]"[2] function of the software *Mathematica*, with its corresponding uncertainty

[2] Accumulate$[\{a, b, c\}] = \{a, a + b, a + b + c\}$

$$\Sigma_{\rm med}(t) = -\frac{\kappa}{2}\text{Accumulate}\left[\frac{ds(t)}{T(t)}\right], \tag{4.18}$$

$$\delta\Sigma_{\rm med}(t) = \Sigma_{\rm med}(t)\sqrt{\left(\frac{\delta s}{s}\right)^2 + \left(\frac{\delta\kappa}{\kappa}\right)^2 + \left(\frac{\delta T}{T}\right)^2}, \tag{4.19}$$

where in this case $t = k/f_{\rm aq}$, with $\{k\}$ a sequence of integers defined in the interval $k = [-299, 800]$, and $ds(t) = s(t+dt) - s(t)$.

Entropic quantities are show in Figure 4.1. Medium entropy is measured by Eq. (4.18) and shown in panel a) for heating process and in panel c) for cooling, by substituting the measures of κ, $ds(t)$ and $T(t)$ into Eq. (4.18). In order to ensure the initial condition $\Sigma_{\rm med}(t=0) = 0$ an additional procedure is required. The averaged entropy is measured before the beginning of the protocol, and it is subtracted respectively for the heating and cooling cases, $9 \pm 2 \times 10^{-3}/{\rm k_B}$ and $0 \pm 2 \times 10^{-3}/{\rm k_B}$. This procedure was also used for the measurement of $\Delta\Sigma_{\rm sys}(t)$, leading respectively for heating and cooling $2 \pm 2 \times 10^{-3}/{\rm k_B}$ and $3 \pm 3 \times 10^{-3}/{\rm k_B}$. These subtraction then ensures the initial condition that $\Sigma_{\rm med}(t \leq 0)$ and $\Delta\Sigma_{\rm sys}(t \leq 0) = 0$.

In panels 4.1 a) and c), the black curve is obtained by substituting the values T_i, T_f and Eq. (2.8) into Eq. (3.24), giving the plotted curve:

$$\Sigma_{\rm med}(t)/k_{\rm B} = \frac{1}{2}\left(\frac{T_i}{T_f} - 1\right)\left(1 - \exp\left[-2\frac{t}{\tau_x}\right]\right). \tag{4.20}$$

In the limit $t/\tau_x \gg 1$, the dashed lines in a) and c) corresponds to $\Sigma_{\rm med}(t \gg \tau_x)/k_{\rm B} = (1/2)(T_i/T_f - 1)$. In the case of heating, $\Sigma_{\rm med,h}/k_{\rm B}(t \gg \tau_x) = -0.23 \pm 0.02$ and in the case of cooling $\Sigma_{\rm med,c}/k_{\rm B}(t \gg \tau_x) = 0.34 \pm 0.04$.

The other entropic observable corresponds to the system entropy variation $\Delta\Sigma_{\rm sys}(t)$, shown in panels b) and d) respectively for heating and cooling processes, measured from Eq. (3.31). In the case where the initial state of the system is in equilibrium, Eq. (3.31) simplifies to

$$\Delta\Sigma_{\rm sys}(t)/k_{\rm B} = \frac{1}{2}\left(\frac{\kappa s(t)}{k_{\rm B}T(t)} - 1\right) + \frac{1}{2}\ln\frac{T(t)}{T_i}, \tag{4.21}$$

where the uncertainty is determined analogously to $\delta\Sigma_{\rm med}(t)$, from Eq. (4.19).

As discussed in Chapter 3, $\Delta\Sigma_{\rm sys}(t)$ is an instantaneous function of the protocol $T(t)$. Since $T(t)$ corresponds to a discontinuous function, so does $\Delta\Sigma_{\rm sys}(t)$. For $t > 0$, the black curve in these figures corresponds to substituting T_i, T_f and Eq. (2.8) into Eq. (3.31) and leads to the expression

$$\Delta\Sigma_{\rm sys}(t)/k_{\rm B} = \frac{1}{2}\left(\frac{T_i}{T_f} - 1\right)\exp\left[-2\frac{t}{\tau_x}\right] + \frac{1}{2}\ln\frac{T_f}{T_i}. \tag{4.22}$$

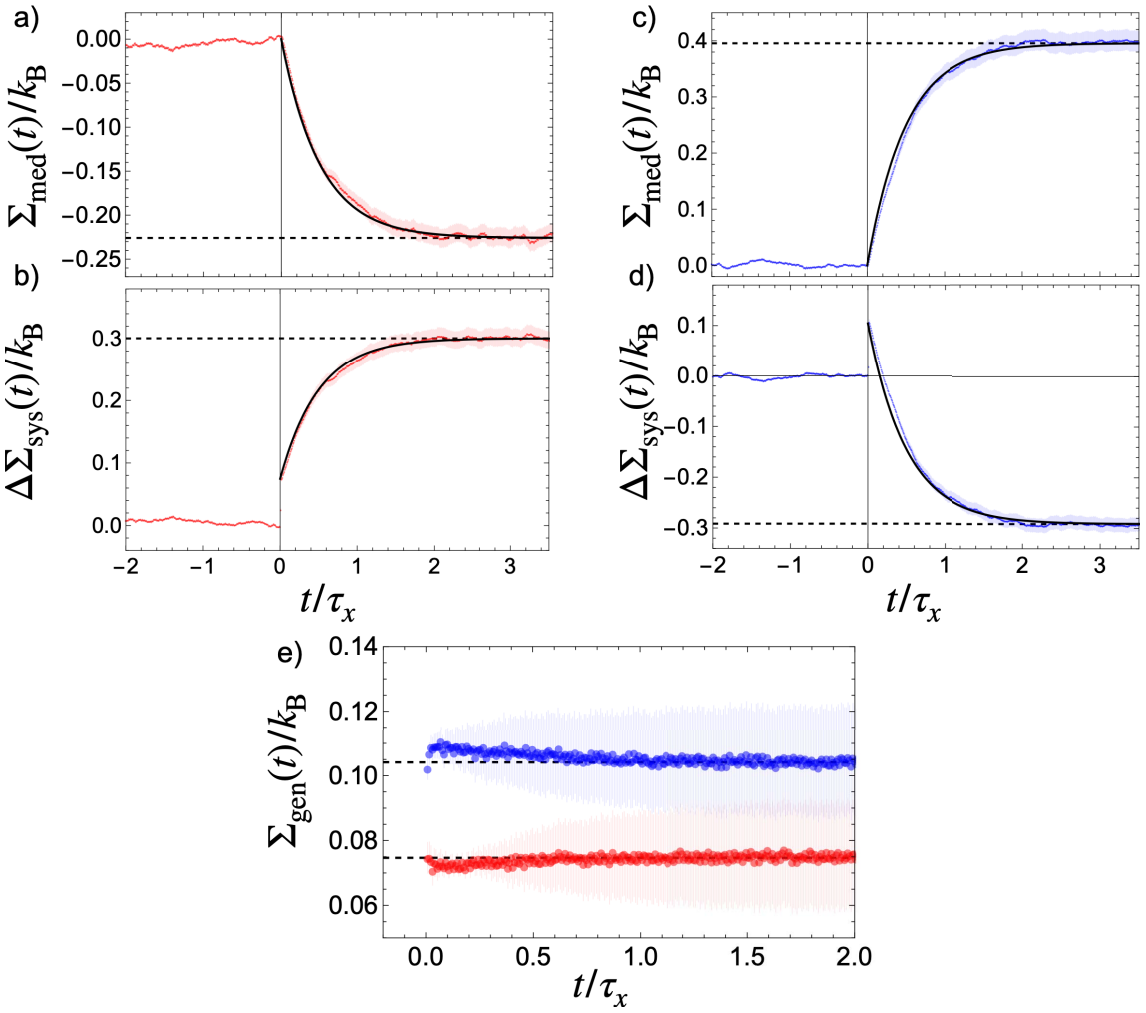

Figure 4.1: Entropic analysis, in units of k_B for time intervals normalized by the position correlation time τ_x, for a STEP-like $T(t)$ protocol. While the measurements in red correspond to heating processes, cooling is represented in blue. The black curves correspond to the theoretical predictions for the entropic observables (medium and system) and dashed lines correspond to the values of those observables after the processes, when the Brownian particle is at equilibrium with the temperature T_f. The uncertainty of these measurements corresponds to the propagation of the errors of the three parameters used to determine those entropic observables, $\delta\kappa/\kappa$, $\delta s/s$ and $\delta T/T$. a) Medium entropy for heating. b) System entropy variation for heating. c) Medium entropy for cooling. d) System entropy variation for cooling. e) Entropy produced for both the heating and cooling processes.

Panels b) and d) show, at the moment of the discontinuity $\Delta\Sigma_{\rm sys}(t=0)>0$, an increase in the entropy of the system for the heating and cooling processes. Through the heating process $\Delta\Sigma_{\rm sys,h}(t)$ continues to increase until the equilibrium value is reached $\Delta\Sigma_{\rm sys,h}/k_{\rm B}(t\gg\tau_x)=(1/2)\ln(T_h/T_c)=0.30\pm0.03$. In the cooling process after an initial increase, $\Delta\Sigma_{\rm sys,c}(t)$ decreases in time until it reaches the equilibrium value $\Delta\Sigma_{\rm sys,c}/k_{\rm B}(t\gg\tau_x)=(1/2)\ln(T_c/T_h)=-0.29\pm0.03$. These values correspond to the dashed lines in panels b) and d). Although the total entropy variation of the system is symmetrical at the end of the processes with, $\Delta\Sigma_{\rm sys,h}(t\gg\tau_x)=-\Delta\Sigma_{\rm sys,c}(t\gg\tau_x)$, throughout the process it is possible to see a clear difference between the heating and cooling processes, since the initial system entropy variation for both processes is positive.

In order to better evaluate the difference between heating and cooling processes, the entropy production $\Sigma_{\rm gen}(t)=\Delta\Sigma_{\rm sys}(t)+\Sigma_{\rm med}(t)$ is plotted in panel e). The equilibrium value corresponding to the dashed line in this panel and it is given by the sum of Eqs. (4.18) and (4.22), and corresponds to Eq. (3.42)

$$\Sigma_{\rm gen}/k_{\rm B}=\frac{1}{2}\ln\frac{T_f}{T_i}-\frac{1}{2}\left(1-\frac{T_i}{T_f}\right). \tag{4.23}$$

It is clear in this figure that the entropic cost of cooling processes is higher than that of heating processes, when the same total temperature variation is considered. The entropy values for $t/\tau_x\gg1$, corresponding to the dashed lines in this figure, are $\Sigma_{\rm gen,h}/k_{\rm B}=0.07\pm0.03$ and $\Sigma_{\rm gen,c}/k_{\rm B}=0.10\pm0.04$, respectively for the heating and cooling processes. Another interesting consequence of this measurement is the decay of $\Sigma_{\rm gen}(t)$ observed within the transient region, in particular in the case of the cooling process.

We note here that the decay on the entropy production after a STEP-like $T(t)$ protocol is not predicted in our model, since Eq. (4.23) is time independent. One possible explanation for this decay can be related to the relaxation of the kinetic energy contribution. Indeed, through a variation of temperature $T_f-T_i=1000$ K is produced, the velocity variance s_v should change accordingly, $m\Delta s_v=k_{\rm B}\Delta T$, in which m is the mass of the Brownian particle. Although this relaxation process occurs on a much shorter time scale than the one we are probing, typically on the μs scale as discussed in Section 2.1.1, the observed decay can be reminiscent of this relaxation process. But, since in our thermodynamic description we consider instantaneous equilibration for the kinetic degree of freedom, such a decay cannot be predicted nor evaluated within this overdamped framework.

An important aspect to consider is the simplicity of the time dependence of the $T(t)$ protocol that generates the decay in the measured $\Sigma_{\rm gen}(t)$. Thus, this decay cannot thus be simply explained by calibration issues generated by the drift of the different

beams. Another interesting feature is the asymmetry of the decay for the heating and cooling processes, while experiments were carried out in a temporal sequence, one repetition after the other. This asymmetry is compatible with the recent observation that the thermalization of a Brownian particle is faster for heating than for cooling processes [37].

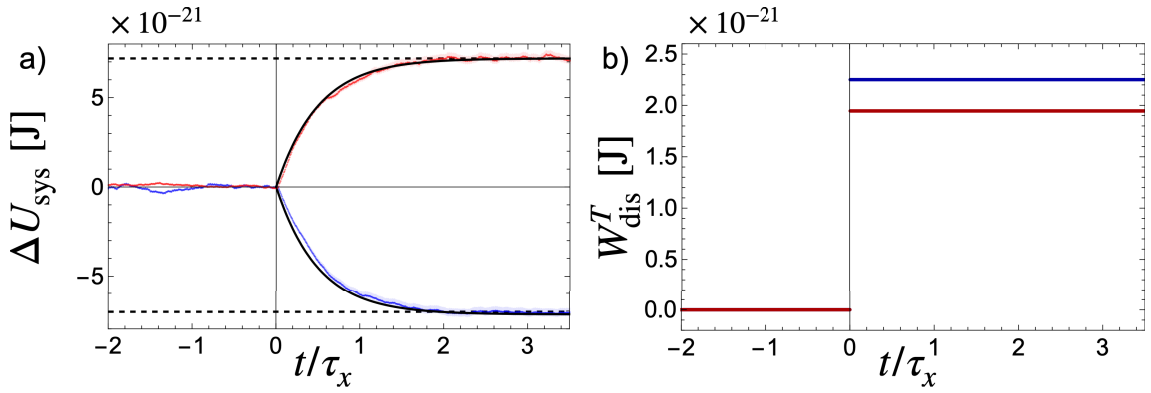

Figure 4.2: Energetic analysis for a STEP-like $T(t)$ protocol, with the same temporal normalization, color coding and propagation of uncertainties used in Figure 4.1. Since temperature is a time dependent parameter, and for reasons explained in details on the main text, we express those quantities in Joules rather than $k_{\mathrm{B}}T_{\mathrm{h}} = 30.4 \times 10^{-21}$ J, $k_{\mathrm{B}}T_{\mathrm{c}} = 16.6 \times 10^{-21}$ J or by the room temperature $k_{\mathrm{B}}T_{\mathrm{RT}} = 4.04 \times 10^{-21}$ J. a) System internal energy variation (negative of heat) for heating and cooling processes. b) Dissipative thermal work for both processes.

The other set of thermodynamic observables that characterize isochoric processes is provided through an energetic analysis. According to the First Law, the variation in the system's internal energy must equal the quantity of heat $\Delta U_{\mathrm{sys}}(t) = -Q(t) = (1/2)\kappa(s(t) - s_i)$, produced along the process. This quantity is shown in Figure 4.2 for heating and cooling processes. From the viewpoint of $\Delta U_{\mathrm{sys}}(t)$ and $Q(t)$, these two processes are completely symmetrical, $\Delta U_{\mathrm{sys,\ h}}(t) = -\Delta U_{\mathrm{sys,\ c}}(t)$, with an absolute value of the total variation given by $|\Delta U_{\mathrm{sys}}| = 7.1 \pm 0.4 \times 10^{-21}$ J.

When isochoric transitions are considered, different energy scales can be used to normalize the data. In relation to the thermal energy given by room temperature, we have $|\Delta U_{\mathrm{sys}}|/k_{\mathrm{B}}T_{\mathrm{RT}} \sim 1.76$. This energy scale defines our precision, as this is the temperature of our photodiode detector. To make it short, one of the factors affecting the precision of a photodiode is thermal noise, also known as Johnson-Nyquist noise. This noise is related to the thermal agitation of the charge carriers in the photodiode, which in turn is proportional to the temperature of the photodiode. As

$k_B(T_h - T_c) > k_B T_{RT}$, the magnitude of the energy change in the isochoric transition we produce is large compared to $k_B T_{RT}$.

Then, based on the precision given by $k_B T_{RT}$, we are able to characterize the different decay time of the forward and backward isochoric process. This characterization is based on two aspects: *i*) by increasing the total variation of the energy in the transition (above $k_B T_{RT}$), and *ii*) using our thermodynamic model to take into account the entropy production along a non-equilibrium potential energy relaxation. This is why we claim that we are able to see the sub-dominant kinetic energy relaxation in the overdamped dynamics, as shown in panel e).

When considering a STEP-like $T(t)$ protocol in the functional expression of the thermal work W_{dis}, given by Eq. (3.45), the energy dissipated is determined as

$$W_{dis} = \frac{k_B(T_f - T_i)}{2} + \frac{k_B T_i}{2} \ln \frac{T_f}{T_i}, \tag{4.24}$$

and shown in Figure 4.2, panel b). In the case of heating, $W_{dis,h} = 1.9 \pm 0.1 \times 10^{-21}$ J and in the case of cooling, $W_{dis,c} = 2.3 \pm 0.2 \times 10^{-21}$ J, where the uncertainty on those quantities are given by $\delta W_{dis} = W_{dis} \delta T / T$. Unlike the case of $\Sigma_{gen}(t)$ measured by the sum of $\Delta\Sigma_{sys}(t)$ and $\Sigma_{med}(t)$, in which it is possible to verify a decay when a STEP-type $T(t)$ protocol is considered, W_{dis} measured from Eq. (4.24) follows the STEP-type evolution.

The thermodynamic analysis of protocols that accelerate isochoric processes will be presented below, in particular the optimal protocols that minimize entropy production for a given transition time Δt.

4.2.2 Thermodynamics of an optimal change

In this section, the measurements associated with optimal isochoric protocols will be presented in detail. While in the previous section the thermodynamic analysis allows to probe some aspects of the asymmetry between heating and cooling processes, the thermodynamic analysis of the measurements presented in this section also consider those asymmetry, but more than that, also consider the relationship between the entropy production Σ_{gen} and the transition time $\Delta t < \tau_x$. To this end, an entropic analysis of optimal processes, derived in the section 4.1, for heating, with $\Delta t = 0.56\tau_x$, and cooling, with $\Delta t = 0.39\tau_x$, will be presented now.

While the drift on the beams cause in the previous protocol only a change in the total temperature variation, as the $T_{opt}(t)$ protocols used in this section have a non-trivial dependence on time, the drift effects on $T_{opt}(t)$ are more significant. It will be first discussed in the case of an optimal heating process illustrated in Figure 4.3. In panel a), the evolution of temperature in terms of "*frames*", or consecutive

measurements spaced by dt, is shown from two different measurement methods. The blue curve corresponds to Eq. (4.12) where $\kappa s_i/k_B = 390 \pm 20$ K, $\kappa s_f/k_B = 1170 \pm 70$ K. Otherwise, the orange curve corresponds to $T_i = 350 \pm 25$ K and $T_f = 1100 \pm 80$ K, measured from V_{pp}^2.

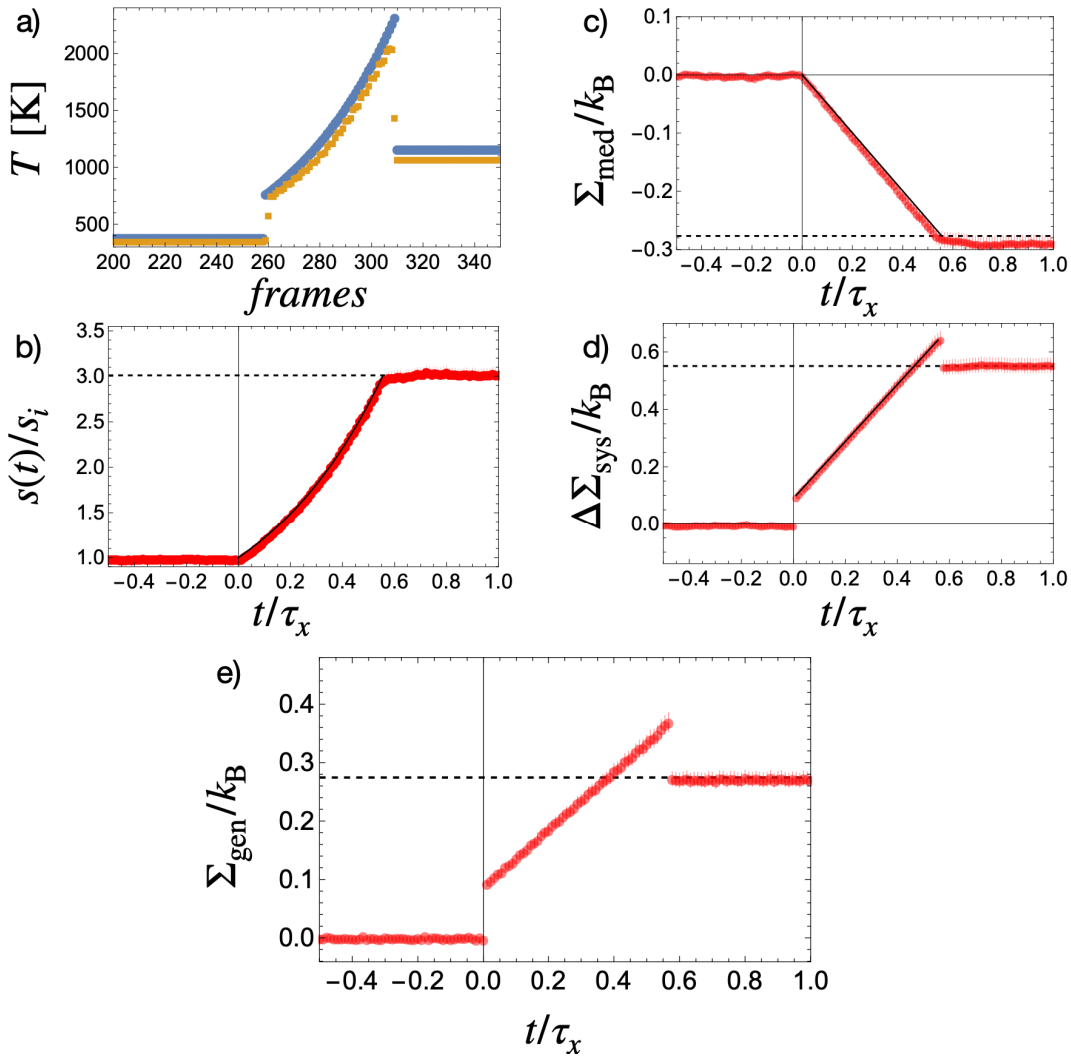

Figure 4.3: Accelerated optimal heating, for $\Delta = 0.56\tau_x$. a) Comparison of two ways of characterizing the $T_{opt}(t)$ protocol, from the measurement of $V_{pp}^2(t)$ in yellow, and from Eq. (4.12) using the measurements of s_i and s_f and Δt, in blue. The $x-$axis corresponds to "$frames$", the index of consecutive measurements time spaced by dt. b) Measurement of the evolution of the position variance. The black line corresponds to Eq. (4.11). c), d) and e) Measurements of entropic quantities – medium, system and generated entropy, respectively – using the methods described in the previous section.

The main consequence of the drift is present on the measurement of $s(t)$, shown in panel b). After $t > \Delta t$, it is possible to see a small decay $s(t > \Delta t) \neq 0$. Furthermore, as larger accelerations are produced, the process $s_{\rm opt}(t)$ becomes even more sensitive to those effects. In this panel, the black curve corresponds to Eq. (4.11).

To illustrate the limitations of the acceleration method, we will now present the highest acceleration measure that we were able to implement for a cooling process in Figure 4.4. In panel a) it is clear that after finalizing the $T_{\rm opt}(t)$ protocol, a significant decay was still observed, $s(t > \Delta t) \neq 0$. In this experiment, the temperatures used were $\kappa s_i/k_{\rm B} = 2210 \pm 180$ K and $\kappa s_f/k_{\rm B} = 1250 \pm 100$ K. This measurement corresponds to the maximum acceleration accessed experimentally since the minimum temperature of this process, the overshooting temperature, was given by $T_{\rm RT} = 293$ K.

In any case, since at the end of the $T_{\rm opt}(t)$ protocol, $\Delta\Sigma_{\rm sys}(t > \Delta t) + \Sigma_{\rm med}(t > \Delta t) = 0$, as can be seen from the total entropy measurement in panel e), we have evidence that the main contribution to the decay observed in $s(t > \Delta t)$ is due to the relaxation of the potential energy. During this time interval, the evolution of the system entropy is such that it is completely counterbalanced by the medium entropy. We do not see any signature of the decay, as observed in Figure 4.1.

Regarding measures of the evolution of entropic quantities, on both Figures 4.3 and 4.4, the same expressions considered in the previous section are used, but considering the optimal process $s_{\rm opt}(t)$, Eq. (4.11), and optimal protocol $T_{\rm opt}(t)$, Eq. (4.12), instead those ones for the STEP-like $T(t)$ protocol. In the case of heating, we verified the linear behavior in time predicted by our model for the optimal protocol for all the measured entropic quantites, Figure 4.3, panels c), d) and e). Another striking feature of this measure is the decrease in entropy produced at the second discontinuity, as discussed at the end of Section 4.1: when transitions involving non-equilibrium states take place, the entropy production associated with these processes can be negative.

The last discussion we present consists of the measure of entropy production compared to different accelerations protocols, the optimal and the ThESE ones, the later derived in section 2.4.3. The discussion of the features when different accelerations are considered for processes of cooling and heating, presented in Figure 4.5, was made in [94].

In Figures 4.5, we first plot Eq. (4.17) for cooling (upper panel) and heating (lower panel) for the optimal protocols (solid black lines). The curves draw exclusion regions for entropy production that correspond to the minimal amount of entropy that can be generated in an isochore for a given Δt.[3] They thus correspond to optimal time-entropy bounds. Our experimental results obtained for different optimal cooling and

[3]In these measurements, Δt corresponds to the nominal value at which the respective protocol $T_{\rm opt}(t)$ is used.

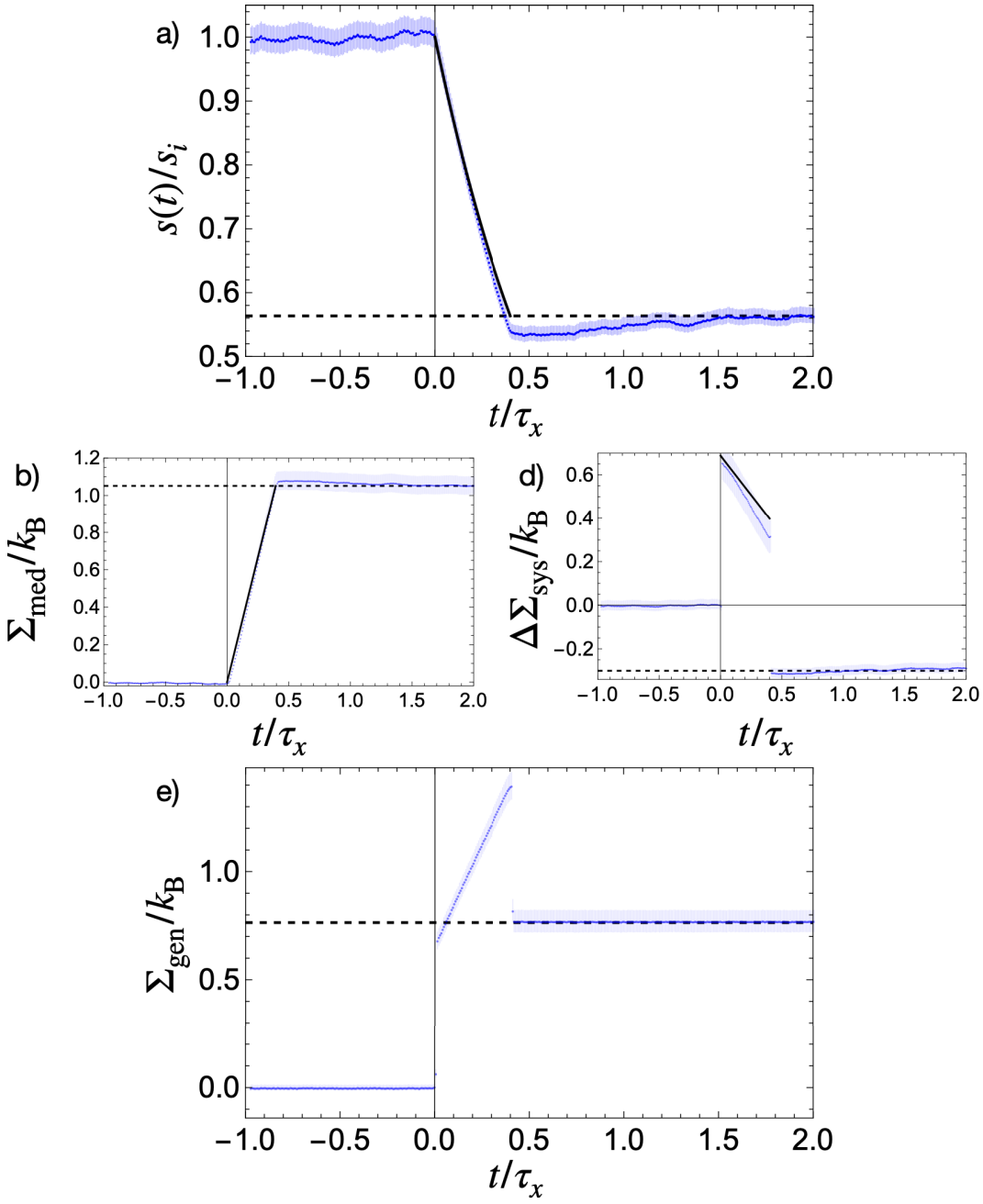

Figure 4.4: Optimal accelerated cooling, designed to have an acceleration rate of $\Delta = 0.39\tau_x$. The quantities presented in this figure correspond to the same methods presented in Figure 4.3

heating protocols $T_{\rm opt}(t)$ injected within our optical trap (same set of temperatures but different transfer durations) all precisely fall on the expected bounds.

In the upper panel of this figure, accelerated cooling processes with $\Delta\Sigma_{\rm sys} < 0$ are shown, while in the lower panel, measurements of accelerated heating processes, $\Delta\Sigma_{\rm sys} > 0$, are shown. In these measurements, Eq. (4.17) corresponds to the transfer

rate limit for a given entropy production. In the case of cooling, this equation puts an asymptotic limit to the transfer rate with a minimal transfer duration of $\Delta t_{\min}/\tau_x = -\Delta\Sigma_{\rm sys}/k_{\rm B} = 0.3$, for the ratio T_f/T_i considered in this experiment. Such a divergence in the entropic cost is clearly seen experimentally in Figure 4.5 for the shortest transfer rate that we probed (vertical gray dashed line).

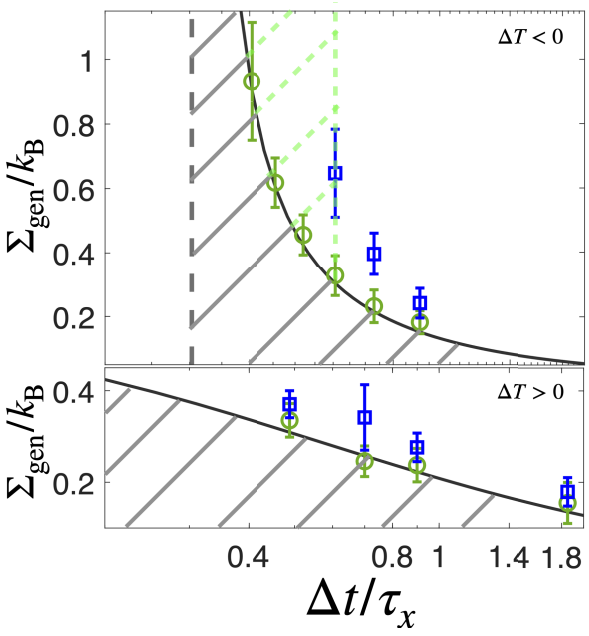

Figure 4.5: Minimal time-entropy bound (solid black lines) corresponding to an optimal $(T_i = 2200, T_f = 1200)$ K cooling process (upper) and heating protocols performed between $T_i = 350$ K to $T_f = 1100$ K (lower). The gray shaded region are forbidden to any acceleration method. Experimental measurements for optimal protocols are shown with green open circles and with blue open squares for ThESE protocols. The error bars correspond to the experimental errors propagated in the same way as in Eq. (4.19). The fundamental limit put on ThESE cooling protocols set at $\Delta t/\tau_x = 0.6$ for the chosen experimental parameters is depicted as a second exclusion region (blue shaded region) for such overshooting temperature protocols.

This divergence corresponds to the fact that for cooling the overshooting temperature $T_{\rm os} = T_{\rm opt}(t_f^-) = T_f(1 + \frac{\tau_x}{k_{\rm B}}\frac{\Delta\Sigma_{\rm sys}}{\Delta t})$ through which the temperature along a protocol passes cannot be less than 0 K. However, experimentally, we necessarily have $T_{\rm os} \geq T_{\rm RT}$ and, for the case shown in Figure 4.5, this implies that the shortest achievable transfer rate for cooling $\Delta t_{\min}/\tau = \frac{\Delta\Sigma_{\rm sys}}{k_{\rm B}(1-T_{\rm RT}/T_f)} \simeq 0.39$, a measurement shown in Figure 4.4.

Room temperature obviously bounds from below all overshoot temperatures that

can be physically hit. This leads to an interesting consequence when comparing optimal and ThESE cooling protocols for identical shortening rates and target temperatures $T_i > T_f$. Because the overshoot temperature for the ThESE protocol is necessarily lower than $T_{\rm os}$ for the optimal protocol for a given Δt, the room temperature bound is reached by the ThESE protocol before the optimal one. More precisely, the ThESE protocol cannot accelerate cooling beyond $\Delta t/\tau_x = 0.6$, while remarkably and as perfectly measured, the optimal protocols can still have access to stronger acceleration rates with ratios between $\Delta t/\tau_x = 0.6$ to 0.4 that remain available experimentally. This important result reveals another, yet unexpected, thermodynamic advantage of optimization giving access to time-entropy regions that are simply forbidden to non-optimized protocols.

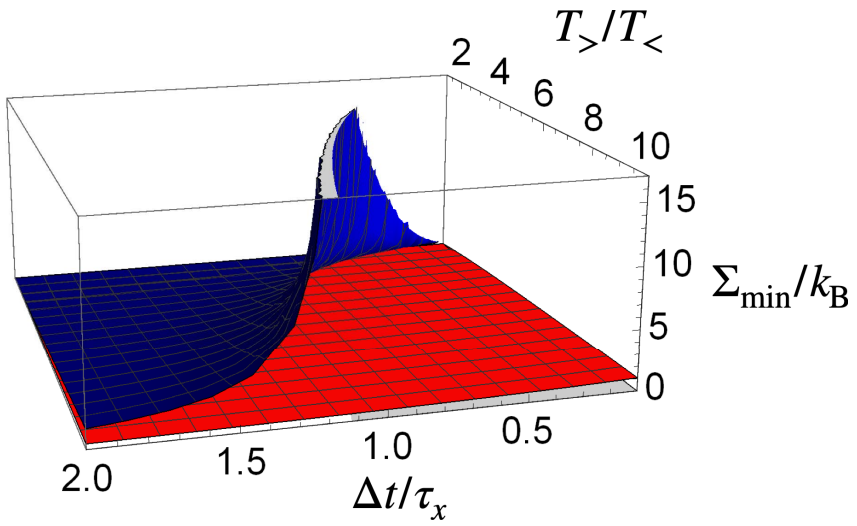

Figure 4.6: 3D plot of Eq. (4.17) considering the optimal heating (red) and cooling (blue) protocols. To combine them, the entropy generated is given as a function of the acceleration rate normalized by the position relaxation time $\Delta\tau/\tau_x$ and the ratio between the highest and lowest temperature $T_>/T_<$.

Contrasting with cooling, optimal heating protocols are not limited by any fundamental limit. With $\Delta\Sigma_{\rm sys} > 0$ in Eq. (4.17), the production of entropy does not diverge and the system can be forced to thermalize arbitrary fast. The optimal time-entropy bound for heating protocols is plotted in the bottom panel in Figure 4.5 together with the experimental measurements obtained when implementing heating ThESE and optimal protocols.

To further quantify the difference between optimal heating and cooling protocols, in Figure 4.6, Eq. (4.17) is plotted on a 3D graph. By exploring the ratio between the highest and lowest temperature $T_>/T_<$, as a function of the acceleration rate Δt,

it is possible to see the striking difference in cost between cooling and heating when the transition time is taken into account in the analyses.

4.3 Conclusion

By identifying the thermodynamic cost associated with an isochoric process as entropy production, we derived a protocol $T_{\text{opt}}(t)$ that minimizes such cost for a given transition time. This theoretical result, deduced in the first section, was followed by the thermodynamic characterization of different isochoric processes. The analysis of these processes is based on the construction of two quantities, the change in entropy of the system $\Delta\Sigma_{\text{sys}}(t)$ and the evolution in entropy of the medium $\Sigma_{\text{med}}(t)$, from the measurements of $s(t)$ and $T(t)$. This analysis allows us to consider the changes in the state of the system due to energy transfer from thermal to potential energy, since it was only this degree of freedom that was considered in the thermodynamic analysis presented in Chapter 3.

The fact that the realizations of the stochastic variable $x_j(t)$ for the heating and cooling processes are probed in temporal sequences when STEP-like $T(t)$ protocols are considered, makes the difference between the measurement of these two processes less impacted by the drift of the different beams. Such a drift generates a modification on the expected temperature over time, but on a scale of minutes, *i.e.* on a scale of hundreds of heating and cooling cycles. We argue that this measurement methodology is an important condition for attributing a physical meaning to the difference in decay between the two processes shown in Figure 4.1, panel e).

We stress that the method presented to characterize STEP-like $T(t)$ protocols relies on the measurements of $\Delta\Sigma_{\text{sys}}(t)$, using Eq. (4.21), and $\Sigma_{\text{med}}(t)$, measured from the difference $s(t+dt) - s(t)$ using Eq. (4.18). This was exactly the discussion presented in Section 3.1.2, when Eq. (3.1) was introduced. In that section, two different ways of measuring infinitesimal quantities were introduced. While in one of the forms, the change of position variance in time dt is measured as $i)$ $ds(t) \equiv 2/\gamma(k_{\text{B}}T(t) - \kappa s(t))dt$, the other form corresponds to $ii)$ $ds(t) \equiv s(t+dt) - s(t)$. While in $i)$, $ds(t)$ corresponds to an instantaneous function, which measures the deviation from a quasi-static process, in $ii)$ $ds(t)$ measures the increase in position variance between two successive measurements.

Next, the thermodynamic analysis for optimal heating and cooling processes was presented. For the heating case, excellent agreement was obtained between the measurements of entropic quantities and the theoretical model presented in Chapter 3. In this case, $\Delta\Sigma_{\text{sys}}(t)$ and $\Sigma_{\text{med}}(t)$ correspond to linear functions in time. As higher acceleration rates are produced, the drift effects of the lasers affect the acceleration

process more significantly, generating a spurious residual decay in the position variance, $s(t > \Delta t) \neq 0$. We claim that this is the most significant source of deviation from our thermodynamic model when optimal cooling processes are probed, Figure 4.4.

Finally, we evaluate the entropy production for different acceleration rates, for two different acceleration protocols. When the transition time is taken into account, the asymmetry between heating and cooling processes is even more striking. While cooling processes have obviously a fundamental limit, since the minimum temperature allowed during cooling acceleration protocols is $T = 0$ K, heating processes have no such limitation.

Chapter 5

Conclusion and perspectives

In this thesis we presented an experimental platform that allows us to measure with high precision the dynamics of a Brownian particle subject to controllable time dependent stochastic forces. We then developed a thermodynamic model to describe isothermal and isochoric processes by considering that the variation of the instantaneous internal energy of such a particle is measured as $\Delta U_{\rm sys}(t) = (1/2)(\kappa(t)s(t) - \kappa_i s_i)$, where κ corresponds to the stiffness of a linear restoring force and s is the position variance of this particle. Finally, we used the thermodynamic model to describe isochoric processes implemented on our platform, in which the temporal evolution of thermodynamic functions became a central ingredient in our discussion.

The possibility of controlling and carrying out experiments with high precision, together with a theoretical model to describe the observed processes, resulted in the two main experimental results of this thesis: *i*) measuring the asymmetry of decay when heating and cooling processes are performed and *ii*) quantifying the relationship between cost and transition time in accelerated isochoric processes. These results were based on the thermodynamic model presented here, in which a new methodology for measuring the entropy of stochastic systems was introduced.

These results open interesting perspectives. We now present a few of these.

Optimal Stirling cycle

From the combination of optimal protocols developed earlier in the group during the PhD thesis of Yoseline Rosales Cabara [95] for the isothermal case [68], and the development presented here for the isochoric one, the ingredients needed to build an optimal Stirling cycle, shown in Figure 5.1, are now gathered. On this optimal cycle, each of the intermediate processes corresponds to an optimal process. The thermodynamic formulation presented in this thesis makes it possible to discuss the maximization of power and efficiency from the construction of an asymmetric cycle as discussed below.

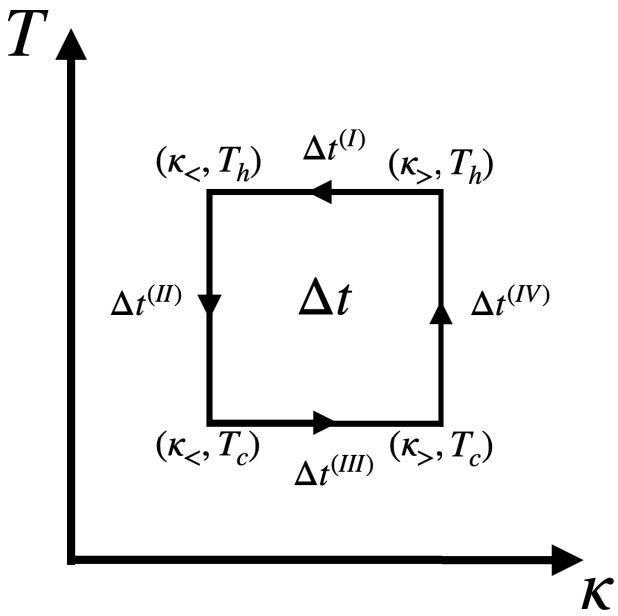

Figure 5.1: State diagram of temperature × stiffness for a Stirling cycle. Such a cycle is composed of 4 intermediate states defined by two values of stiffness $\kappa_>, \kappa_<$ and two values of temperature $T_\mathrm{h}, T_\mathrm{c}$. Each intermediate state is connected by isothermal or isochoric processes of duration $\Delta t^{(i)}$, with $i = I, II, III, IV$. The total time of this cycle, Δt, is given by the sum of these 4 intermediate transition times.

For a given expansion process $\kappa_> \to \kappa_<$ that lasts a time $\Delta t^{(I)}$, and a compression process $\kappa_< \to \kappa_>$ that lasts a time $\Delta t^{(III)}$, it is possible to establish a relationship between the duration of these two processes, given a total time for the two isothermal processes $\Delta t_\kappa = \Delta t^{(I)} + \Delta t^{(III)}$. Next, we can address the question of what the maximum power is when optimal isothermal processes are considered, for a total time duration given by Δt_κ. This question is answered by establishing a relation between $\Delta t^{(I)}$ and $\Delta t^{(III)}$ so that the total energy dissipated on those isothermal processes is minimal, given the temperatures of the hot and cold reservoir, T_h and T_c.

In parallel, using the same formalism, it is possible to establish the relationship between the cooling time $\Delta t^{(II)}$ and the heating one $\Delta t^{(IV)}$, which define the total time of the isochoric processes $\Delta t_T = \Delta t^{(II)} + \Delta t^{(IV)}$. This time relation can also be used to optimize a constraint, for example, the entropic cost of isochoric branches, for a given Δt_T.

Finally, it would be possible to establish a relationship between the time of isothermal and isochoric processes, defining the total cycle time $\Delta t = \Delta t_\kappa + \Delta t_T$, constrained by different criteria, such as the total entropy production associated with this cycle. Such approaches, now reasonably simple to develop, would yield a new type of analysis

regarding power and efficiency for such "fully optimized" type of cycles.

Connecting non-equilibrium states

While the functional formulation presented in Section 3.5 is valid for transitions between non-equilibrium states, this formulation has been explored to only characterize the transition between initial and final states in equilibrium. To illustrate how such an approach can be used to quantify the cost related to connecting non-equilibrium states, we will sketch the lines of an alternative interpretation of the experiment presented in our manuscript on stochastic resetting, put in the arXiv recently [32].

In this experiment, by controlling the stiffness between two values $\kappa_{\max} \gg \kappa_{\min}$, it is possible to implement a stochastic resetting mechanism, when the change from $\kappa_{\min} \to \kappa_{\max}$ happens after a time interval τ, in general shorter than the relaxation time of the Brownian particle $\tau < \tau_x = \gamma/\kappa_{\min}$, drawn from a Poissonnian distribution.

To thermodynamically analyze such a process, it is possible to separate the discussion of the cost into two steps *i*) the cost related to connecting instantaneously two non-equilibrium states and *ii*) the cost induced when considering the specific protocol used in a certain time interval to connect such states. In Figure 5.2 we illustrate these processes, and discuss here how to quantify both costs.

Initially, the position distribution that defines the state of the Brownian particle is given by the position variance $s(t=0) = s_i = k_{\mathrm{B}}T/\kappa_{\max}$, but subject to a confining potential with stiffness $\kappa(t=0) = \kappa_{\min}$. This particle will diffuse towards the distribution defined by the variance $s_{\mathrm{eq}} = k_{\mathrm{B}}T/\kappa_{\min}$. The resetting process then corresponds to interrupting this free diffusion at time $\tau < \tau_x$, causing the position distribution to "return" to the initial distribution, defined by s_i. As $s(\tau) < s_{\mathrm{eq}}$, there is a thermodynamic cost associated with the variation in the entropy of the system associated with this process that can be quantified from Eq. (3.29), applied on the difference between the states at $s(\tau)$ and s_i. This cost then depends only on $\kappa_{\max}, \kappa_{\min}$ and τ.

On the other hand, if the details of the process connecting these states are considered to take place from time τ to time τ_w, it is possible to quantify the cost related to specific protocols. When the protocol corresponds to $\kappa(t)$, as is the case of the experiment presented in this work, it is possible to quantify this cost using Eq. (3.23). The combination of those two costs defines the total entropy produced in a single stochastic resetting event.

The thermodynamic analysis proposed here is therefore directly linked to the problem of quantifying the information contained in non-equilibrium states. Such quantification can be explored in the context of thermal machines that perform useful work from the information content present in non-equilibrium states.

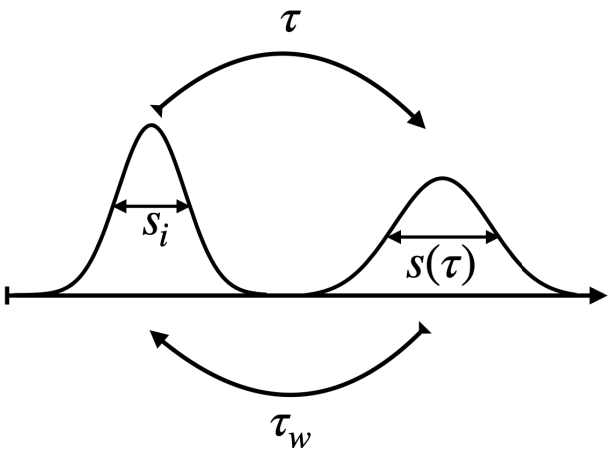

Figure 5.2: Diagram representing the connection of two out of equilibrium states. While the initial state corresponds to a Gaussian distribution of variance s_i, this distribution evolves freely over time τ towards another distribution, also Gaussian, defined by the variance $s(\tau)$. It is then possible to evaluate the change in the system entropy when we consider that the distribution $s(\tau)$ is "transformed" into the initial distribution s_i. If the heat exchanges *during* this transformation are evaluated, it is then possible to measure the change in the entropy of the system that occurs when connecting these non-equilibrium states. The sum of these two quantities corresponds to the total entropy production associated with connecting these two non-equilibrium states.

Combination of $\kappa(t)$ and $T(t)$

When the thermodynamic model presented here is used to quantify the cost of processes, it is based on the assumption that only one control parameter is changed in time. Thus, our method can be applied directly to a process in which $\kappa(t)$ and $T(t)$ are changed sequentially, as illustrated in Figure 5.3. In this type of process, the total transition time between two states Δt is given by the sum of the times in each of the intermediate transformations $\Delta t = \sum_n (\Delta t_T^{(n)} + \Delta t_\kappa^{(n)})$ where $\delta\chi = \delta T, \delta\kappa$ correspond to the increments in the control parameters for each intermediate step.

For this type of process, it would then be necessary to define the protocol $\mu(t)$ that connects each of the intermediate states. In other words, an intermediate change defined as $\chi_n \to \chi_n + \delta\chi$ would be defined from the protocol $\chi(t) = \chi_n + \mu_n(t)\delta\chi$, where at the beginning of this intermediate step $\mu_n(0) = 0$ and at the end of this intermediate step $\mu(t = \Delta t_\chi^{(n)}) = 1$.

We think that this type of approach can be considered for describing infinitesimal

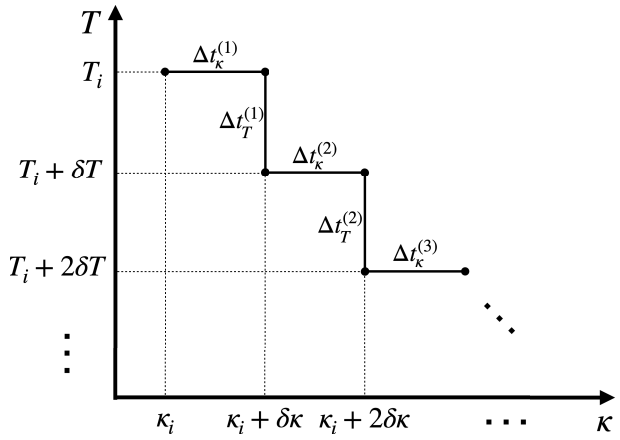

Figure 5.3: State diagram of temperature × stiffness for a sequential change of these two parameters. Each of these changes occurs in a time interval $\Delta t_\chi^{(n)}$, in which an increment $\delta\chi$ is introduced in one of the control parameters. In such a diagram, the intermediate states, defined by the edges between consecutive lines, correspond to equilibrium states.

processes occurring at finite time, establishing a methodology compatible with the geometric formulation of stochastic thermodynamics, when different protocols $\mu(t)$ are considered, in particular the optimal protocols discussed in this thesis.

Asymmetrical decay in isochoric processes

One of the great strengths of our thermodynamic model was that it made it possible to characterize the production of entropy associated with the decay process of the potential energy of a particle confined in a harmonic potential. In our model, we consider that decay processes related to kinetic energy are instantaneous. As such, therefore our model is unable to quantify the energy dissipation processes related to this velocity degree of freedom, as discussed in Figure 4.2.

But since we were able to identify the entropy production related to the potential energy decay process, we can isolate this effect from the one related to the change in the velocity distribution, that in turn is connected with the kinetic energy degree of freedom. This asymmetrical decay is shown in Figure 4.1, panel e).

A natural perspective would then consider a theoretical model in which the exchange of energy between the Brownian particle and the medium is taken into account for the change in the velocity distribution. In such a model, the entropy of the system for a STEP-like $T(t)$ protocol $\Delta\Sigma_{\rm sys}(t)$ would still be measured by Eq. (4.21) and described by Eq. (4.22), while the entropy of the medium $\Sigma_{\rm med}(t)$ would be measured by Eq. (4.18), but the theoretical model that determines $\Sigma_{\rm med}(t)$ would no longer be given by

Eq. (4.20).

When considering the heat involved in a process in which the velocity distribution is altered, an extra term of the type $\propto (T_i/T_f)\exp[-2t\gamma/m]$ should be considered. Such a term would thus explain the asymmetry between the cooling and heating processes since the prefactor T_i/T_f would be greater for cooling processes than for heating ones, thus making such a decay longer.

Experiments with larger temperature variations can be implemented our experimental platform, where this effect involving velocity distributions can be measured more precisely.

Presenting such perspectives draws some of the lines of research that will now be pursued in the laboratory. They will involve the new methods and approaches that are developed in this thesis and by doing so, will refine some of the specific features that still demand to be fully analyzed.

The question of the role of the velocity degrees of freedom in the entropic analysis of state-to-state transformation will play in particular a central role when turning our attention to Brownian systems diffusing in critical and underdamped regimes.

New experiments are currently under way in the laboratory to explore the subtle relations that emerge when looking at the thermodynamic stochastic processes discussed throughout this work.

Chapter 6

Résmé de la thèse

Cette thèse s'intéresse à la dynamique du mouvement brownien [1, 2], un phénomène typique des échelles de temps et de longueur intermédiaires où l'influence dynamique des molécules peut être observée à l'œil nu [3]. Le phénomène correspond au mouvement apparemment erratique de particules en suspension dans un fluide (liquide ou gaz) causé par les collisions aléatoires de ces particules avec les atomes ou les molécules du fluide.

6.1 Température dépendante du temps dans un piège optique

Ce chapitre présente les méthodes expérimentales utilisées pour mettre en œuvre les techniques d'ingénierie des bains. En commençant par une discussion sur les échelles de temps impliquées dans la description d'une microsphère dans une solution aqueuse (régime sur-amorti), confinée par un potentiel harmonique, la plateforme expérimentale pour le piégeage, le contrôle et l'ajout de forces optiques externes est présentée. Un développement important de cette plateforme expérimentale est le contrôle des propriétés statistiques du laser qui exerce une pression de radiation sur la microsphère piégée. Les méthodes d'introduction de telles procédures à l'aide d'un modulateur acousto-optique seront présentées en détail, ainsi que la description de la dynamique de cette microsphère, via l'équation de Langevin. Ce formalisme permet de décrire des processus dans lesquels l'amplitude de la force stochastique additionnelle évolue dans le temps. Le cas des changements discontinus et des protocoles qui accélèrent les transitions d'état à état est présenté.

Le contrôle du mouvement brownien d'une seule particule à l'aide d'une plateforme spécifique correspond au piégeage de la particule, au suivi de sa trajectoire et à l'ajustement de sa dynamique en fonction de la modulation du potentiel de piégeage

et de l'influence d'une force de pression de radiation externe. En contrôlant les caractéristiques statistiques de cette force externe, nous pouvons réaliser des protocoles d'ingénierie des bains thermiques et développer des procédures pour augmenter la température du centre de masse de la particule brownienne de plusieurs milliers de kelvins.

Au cœur de cette technique se trouve la notion de température du centre de masse, mesurée par la densité spectrale de puissance de la position de la particule brownienne lorsqu'elle est en équilibre avec le bain thermique. En s'appuyant sur le lien entre cette température et l'amplitude de la force externe, la température du bain est considérée comme un paramètre de contrôle dépendant du temps $T(t)$.

La caractérisation du mouvement brownien a été entreprise en analysant directement la mesure : l'intensité en fonction du temps d'un laser diffusé par la particule brownienne. En considérant une relation linéaire entre cette intensité et le déplacement instantané de la position de la particule, plusieurs observables sont construits. Il s'agit notamment des trajectoires mesurées en unités de longueur, des distributions de position et de la densité spectrale de puissance de la position.

Une discussion importante du chapitre est la relation entre la nature de la distribution stochastique de la force - qu'elle soit uniforme ou normale - et la fréquence de sa génération. Alors que la température du centre de masse diminue lorsque l'intensité de la pression de radiation est modifiée à des fréquences de génération élevées, à cette limite, une force stochastique avec une distribution initialement uniforme converge vers une distribution normale. Cette interaction devient encore plus pertinente lorsque des forces stochastiques ayant d'autres distributions sont employées pour modifier la dynamique brownienne. Il est essentiel de comprendre que la distribution et la fréquence de génération d'une force stochastique sont étroitement liées et ne peuvent être considérées indépendamment.

Un autre aspect de l'ingénierie des bains correspond à l'introduction d'une corrélation sur le forçage stochastique qui entraîne la particule brownienne, que nous discutons en détail dans le cas de l'ingénierie du "bain actif" dans notre publication [48], et qui est présentée dans la thèse de doctorat de Rémi Goerlich [86].

Nous illustrons ensuite comment la dynamique de Browinan peut être modifiée par l'action de deux protocoles $T(t)$. Alors qu'un changement de température discontinu génère une évolution hors équilibre, où la variance du système $s(t)$ se détend avec une décroissance exponentielle vers un état d'équilibre final, des dépendances temporelles plus complexes sur $T(t)$ peuvent être introduites, conduisant par exemple à une transition accélérée et à une thermalisation. Le concept de *connecting states* guidera la description thermodynamique des processus isothermes et isochoriques que nous proposons dans le chapitre suivant.

6.2 Thermodynamique d'une particule brownienne

la description thermodynamique des processus isothermes et isochores dans lesquels l'énergie interne du système est définie uniquement à partir de l'énergie potentielle est développée dans ce chapitre. La description de ces processus est basée sur l'introduction de fonctions d'état lorsque le système est hors équilibre. Si l'extension de l'énergie interne aux états hors équilibre est simple, ce n'est pas le cas pour l'entropie du système. C'est pourquoi une nouvelle définition de l'entropie associée à une trajectoire stochastique est introduite. Pour quantifier le coût des processus hors d'équilibre, l'énergie dissipative et la production d'entropie sont introduites et discutées en détail lorsque des changements discontinus des paramètres de contrôle sont considérés.

Tant du point de vue stochastique, décrit par la variable stochastique $x_j^2(t)$, que de son comportement moyen, représenté par l'évolution de la variance de position $s(t)$, les fonctions thermodynamiques pour les processus isothermes, décrits par $(\kappa(t), T, s(t))$, ou les processus isochoriques, décrits par $(\kappa, T(t), s(t))$ ont été discutées.

Les relations construites ici sont ancrées dans l'hypothèse initiale selon laquelle l'énergie interne du système est décrite par son énergie potentielle. Par conséquent, les relations fonctionnelles quantifient les coûts énergétiques et entropiques associés aux processus de non-équilibre. Comme nous le verrons dans le chapitre suivant, cette approche de la quantification des coûts, lorsqu'elle est associée à une transition entre des états d'équilibre se produisant sur un intervalle de temps spécifique Δt, permet de déterminer un protocole optimal par la minimisation d'une fonctionnelle définie par le compromis entre ce coût et Δt.

Un aspect essentiel pris en compte est celui des variations infinitésimales des fonctions d'état thermodynamiques, telles que l'énergie interne, l'énergie libre et l'entropie du système, survenant sur une période de temps spécifique, telle que l'intervalle dt entre deux mesures consécutives de $x_j^2(t)$, ou même un instant arbitraire t, où la condition initiale est spécifiée à partir de la distribution gaussienne de la position $p(x, s_i = \langle x_j^2(0) \rangle)$.

Dans ce contexte, alors que les fonctions d'état correspondent à des fonctions instantanées du protocole $\chi(t)$ et du processus $s(t)$, les fonctions dépendant du chemin sont déterminées par les fonctionnelles $J[s_i, s(t); \chi(s)]$. Pour illustrer cette méthodologie, nous avons examiné comment ces fonctions permettent de déterminer l'énergie dissipée et la génération d'entropie, lorsque des changements discontinus des paramètres de contrôle $d\chi = \chi_f - \chi_i$ sont produits sur un intervalle dt.

La différence de nature des fonctions thermodynamiques dépendantes du chemin, si leurs variations infinitésimales dépendent du changement de la variance de position ds, comme la chaleur et l'entropie de l'environnement, ou du changement des

paramètres de contrôle $d\chi$, comme le travail, ses contributions dissipatives et la production d'entropie, est essentielle lorsque l'on considère l'évolution temporelle de ces fonctions. Alors que d'une part le taux d'échange d'énergie entre le système et le réservoir de chaleur correspond à un processus continu, limité par le temps de relaxation de la variance de position $2\tau_x$, qui à son tour contraint la variation ds, d'autre part,

- échanges d'énergie avec le réservoir de chaleur correspondent à un processus continu, limité par le temps de relaxation de la variance de position $2\tau_x$,
- échanges d'énergie avec le réservoir de travail et la variation de l'énergie interne du réservoir de chaleur dépendent respectivement de $d\kappa$ et de dT, quantités dont la variation n'est pas limitée par les processus de relaxation.

Cette nature différente de la manière dont les échanges d'énergie se produisent est fondamentale lorsque l'on considère l'évolution des fonctions thermodynamiques développées ici.

Pour rendre ces définitions cohérentes entre elles, nous avons introduit une nouvelle définition de l'entropie du système. Une propriété essentielle caractérisée par une mesure d'entropie est la relation entre les micro- et macro-états. Dans notre définition, cette relation est mesurée sur une trajectoire stochastique à partir du micro-état $x_j^2(t)$ et de la variance de position correspondante définie à partir des valeurs instantanées du paramètre de contrôle $s_{\rm eq}^{\kappa}(t) = k_{\rm B}T/\kappa(t)$ pour les processus isothermes, et $s_{\rm eq}^{T}(t) = k_{\rm B}T(t)/\kappa$ pour les processus isochoriques. Cette mesure peut être exécutée lorsque l'on peut définir des moyennes dans l'ensemble $\{j\}$ des trajectoires qui partagent la condition initiale $p(x, s_i = \langle x_j^2(0)\rangle)$.

Un aspect intéressant de la discussion dynamique et thermodynamique simultanée du mouvement brownien développée ici est, par exemple, la possibilité de relier l'énergie dissipée dans les processus de non-équilibre à l'équilibre des forces de piégeage, des forces stochastiques et de la force visqueuse : lorsqu'un protocole $\chi(t)$ est suffisamment rapide pour générer une augmentation $ds(t) > 0$ ou une diminution $ds(t) < 0$ de la variance de la position.

Lorsque ces processus se produisent, la force de collision moyenne dans l'intervalle dt n'est pas contrebalancée par la force de piégeage, ce qui fait que la vitesse moyenne dans cet intervalle de temps est différente de zéro. Par conséquent, l'énergie est dissipée par la force visqueuse. Ce système sert de modèle didactique pour discuter des processus thermodynamiques où l'échelle de temps des processus et la limite quasi-statique, qui dans ce cas correspond aux processus où la vitesse moyenne est nulle, peuvent être discutées à partir d'une approche mécanique, de l'analyse de l'équilibre des forces.

6.3 Transformation isochorique

En exploitant l'approche fonctionnelle, nous abordons dans ce dernier chapitre les transitions d'état à état en équilibrant le compromis entre le coût et le temps de transition des processus isochoriques. Cette méthodologie nous permet de dériver des transformations optimales avec des contraintes de temps-entropie associées. En nous appuyant sur le cadre thermodynamique introduit dans le chapitre **??**, nous caractérisons les transformations isochoriques influencées par des modulations temporelles de l'amplitude de la force de pression de radiation stochastique externe. En outre, nous explorons les asymétries entre les processus de chauffage et de refroidissement selon trois aspects différents : pour les changements brusques de température, pour différentes techniques d'accélération, et enfin en comparant le coût des processus de chauffage et de refroidissement en fonction du temps de transition et du changement de température total produit dans le processus isochorique optimal.

En identifiant le coût thermodynamique associé à un processus isochore comme étant la production d'entropie, nous avons dérivé un protocole $T_{\text{opt}}(t)$ qui minimise ce coût pour un temps de transition donné. Ce résultat théorique, déduit dans la première section, a été suivi par la caractérisation thermodynamique de différents processus isochoriques. L'analyse de ces processus est basée sur la construction de deux quantités, le changement d'entropie du système $\Delta\Sigma_{\text{sys}}(t)$ et l'évolution de l'entropie du milieu $\Sigma_{\text{med}}(t)$, à partir des mesures de $s(t)$ et $T(t)$. Cette analyse permet de considérer les changements d'état du système dus au transfert d'énergie de l'énergie thermique à l'énergie potentielle, puisque c'est uniquement ce degré de liberté qui a été considéré dans l'analyse thermodynamique présentée au chapitre 3.

Le fait que les réalisations de la variable stochastique $x_j(t)$ pour les processus de chauffage et de refroidissement soient sondées dans des séquences temporelles lorsque des protocoles $T(t)$ de type STEP sont considérés, rend la différence entre la mesure de ces deux processus moins impactée par la dérive des différents faisceaux. Une telle dérive génère une modification de la température attendue au fil du temps, mais à l'échelle de quelques minutes, c'est-à-dire à l'échelle de centaines de cycles de chauffage et de refroidissement. Nous soutenons que cette méthode de mesure est une condition importante pour attribuer une signification physique à la différence de décroissance entre les deux processus illustrés à la figure 4.1, panneau e).

Nous soulignons que la méthode présentée pour caractériser les protocoles $T(t)$ de type STEP repose sur les mesures de $\Delta\Sigma_{\text{sys}}(t)$, en utilisant l'Eq. (4.21), et $\Sigma_{\text{med}}(t)$, mesuré à partir de la différence $s(t+dt) - s(t)$ en utilisant l'Eq. (4.18). C'est exactement la discussion présentée dans la section 3.1.2, lorsque l'équation (3.1) a été introduite. Dans cette section, deux façons différentes de mesurer des quantités in-

finitésimales ont été présentées. Alors que dans l'une des formes, la variation de la variance de position dans le temps dt est mesurée comme $i)$ $ds(t) \equiv 2/\gamma(k_{\mathrm{B}}T(t) - \kappa s(t))dt$, l'autre forme correspond à $ii)$ $ds(t) \equiv s(t+dt) - s(t)$. Alors que dans $i)$, $ds(t)$ correspond à une fonction instantanée, qui mesure la déviation d'un processus quasi-statique, dans $ii)$ $ds(t)$ mesure l'augmentation de la variance de la position entre deux mesures successives.

Ensuite, l'analyse thermodynamique pour les processus optimaux de chauffage et de refroidissement a été présentée. Dans le cas du chauffage, un excellent accord a été obtenu entre les mesures des quantités entropiques et le modèle théorique présenté au chapitre 3. Dans ce cas, $\Delta\Sigma_{\mathrm{sys}}(t)$ et $\Sigma_{\mathrm{med}}(t)$ correspondent à des fonctions linéaires dans le temps. Lorsque les taux d'accélération sont plus élevés, les effets de dérive des lasers affectent le processus d'accélération de manière plus significative, générant une décroissance résiduelle parasite de la variance de position, $s(t > \Delta t) \neq 0$. Nous affirmons qu'il s'agit de la source la plus importante d'écart par rapport à notre modèle thermodynamique lorsque les processus de refroidissement optimaux sont étudiés, Figure 4.4.

Enfin, nous évaluons la production d'entropie pour différents taux d'accélération, pour deux protocoles d'accélération différents. Lorsque le temps de transition est pris en compte, l'asymétrie entre les processus de chauffage et de refroidissement est encore plus frappante. Alors que les processus de refroidissement ont manifestement une limite fondamentale, puisque la température minimale autorisée pendant les protocoles d'accélération par refroidissement est de $T = 0\mathrm{K}$, les processus de chauffage n'ont pas cette limite.

Bibliography

[1] E. Frey and K. Kroy, "Brownian motion: a paradigm of soft matter and biological physics," *Annalen der Physik*, vol. 517, no. 1-3, pp. 20–50, 2005.

[2] P. Mörters and Y. Peres, *Brownian motion*, vol. 30. Cambridge University Press, 2010.

[3] R. Brown, "Ii. brownian motion," *Reports on Progress in Physics*, vol. 5, no. 1, p. 9, 1938.

[4] K. Sekimoto, *Stochastic energetics*, vol. 799. Springer, 2010.

[5] U. Seifert, "Stochastic thermodynamics, fluctuation theorems and molecular machines," *Reports on progress in physics*, vol. 75, no. 12, p. 126001, 2012.

[6] S. Ciliberto, "Experiments in stochastic thermodynamics: Short history and perspectives," *Physical Review X*, vol. 7, no. 2, p. 021051, 2017.

[7] C. Gonzalez-Ballestero, M. Aspelmeyer, L. Novotny, R. Quidant, and O. Romero-Isart, "Levitodynamics: Levitation and control of microscopic objects in vacuum," *Science*, vol. 374, no. 6564, p. eabg3027, 2021.

[8] Z. Gong, Y.-L. Pan, G. Videen, and C. Wang, "Optical trapping and manipulation of single particles in air: Principles, technical details, and applications," *Journal of Quantitative Spectroscopy and Radiative Transfer*, vol. 214, pp. 94–119, 2018.

[9] N. Li, X.-m. Zhu, W.-q. Li, Z.-h. Fu, M.-z. Hu, and H.-z. Hu, "Review of optical tweezers in vacuum," *Frontiers of information technology & electronic engineering*, vol. 20, no. 5, pp. 655–673, 2019.

[10] F. Ricci, M. T. Cuairan, G. P. Conangla, A. W. Schell, and R. Quidant, "Accurate mass measurement of a levitated nanomechanical resonator for precision force-sensing," *Nano letters*, vol. 19, no. 10, pp. 6711–6715, 2019.

[11] L. E. Hillberry, Y. Xu, S. Miki-Silva, G. H. Alvarez, J. E. Orenstein, L. Ha, D. S. Ether, and M. G. Raizen, "Weighing an optically trapped microsphere in thermal equilibrium with air," *Physical Review Applied*, vol. 14, no. 4, p. 044027, 2020.

[12] M. Frimmer, K. Luszcz, S. Ferreiro, V. Jain, E. Hebestreit, and L. Novotny, "Controlling the net charge on a nanoparticle optically levitated in vacuum," *Physical Review A*, vol. 95, no. 6, p. 061801, 2017.

[13] J. Wang, C. Li, S. Zhu, C. He, Z. Fu, X. Zhu, Z. Chen, and H. HU, "Rapid measurement of the net charge on nanoparticles in optical levitation system," *Applied Physics Express*, 2023.

[14] N. Kiesel, F. Blaser, U. Delić, D. Grass, R. Kaltenbaek, and M. Aspelmeyer, "Cavity cooling of an optically levitated submicron particle," *Proceedings of the National Academy of Sciences*, vol. 110, no. 35, pp. 14180–14185, 2013.

[15] G. P. Conangla, F. Ricci, M. T. Cuairan, A. W. Schell, N. Meyer, and R. Quidant, "Optimal feedback cooling of a charged levitated nanoparticle with adaptive control," *Physical review letters*, vol. 122, no. 22, p. 223602, 2019.

[16] A. Kumar and J. Bechhoefer, "Optical feedback tweezers," in *Optical Trapping and Optical Micromanipulation XV*, vol. 10723, pp. 282–290, SPIE, 2018.

[17] J. Gieseler, B. Deutsch, R. Quidant, and L. Novotny, "Subkelvin parametric feedback cooling of a laser-trapped nanoparticle," *Physical review letters*, vol. 109, no. 10, p. 103603, 2012.

[18] U. Delić, M. Reisenbauer, K. Dare, D. Grass, V. Vuletić, N. Kiesel, and M. Aspelmeyer, "Cooling of a levitated nanoparticle to the motional quantum ground state," *Science*, vol. 367, no. 6480, pp. 892–895, 2020.

[19] M. Kamba, R. Shimizu, and K. Aikawa, "Optical cold damping of neutral nanoparticles near the ground state in an optical lattice," *Optics Express*, vol. 30, no. 15, pp. 26716–26727, 2022.

[20] J. Piotrowski, D. Windey, J. Vijayan, C. Gonzalez-Ballestero, A. de los Ríos Sommer, N. Meyer, R. Quidant, O. Romero-Isart, R. Reimann, and L. Novotny, "Simultaneous ground-state cooling of two mechanical modes of a levitated nanoparticle," *Nature Physics*, pp. 1–5, 2023.

[21] F. J. Cao and M. Feito, "Thermodynamics of feedback controlled systems," *Physical Review E*, vol. 79, no. 4, p. 041118, 2009.

[22] J. M. Horowitz and M. Esposito, "Thermodynamics with continuous information flow," *Physical Review X*, vol. 4, no. 3, p. 031015, 2014.

[23] J. Ehrich, S. Still, and D. A. Sivak, "Energetic cost of feedback control," *Physical Review Research*, vol. 5, no. 2, p. 023080, 2023.

[24] T. Sagawa and M. Ueda, "Nonequilibrium thermodynamics of feedback control," *Physical Review E*, vol. 85, no. 2, p. 021104, 2012.

[25] M. Debiossac, D. Grass, J. J. Alonso, E. Lutz, and N. Kiesel, "Thermodynamics of continuous non-markovian feedback control," *Nature Comm.*, vol. 11, no. 1, pp. 1–6, 2020.

[26] H. S. Leff and A. F. Rex, *Maxwell's demon: entropy, information, computing.* Princeton University Press, 1990.

[27] L. Granger and H. Kantz, "Thermodynamic cost of measurements," *Physical Review E*, vol. 84, no. 6, p. 061110, 2011.

[28] J. M. Parrondo, J. M. Horowitz, and T. Sagawa, "Thermodynamics of information," *Nature physics*, vol. 11, no. 2, pp. 131–139, 2015.

[29] K. Proesmans, J. Ehrich, and J. Bechhoefer, "Finite-time landauer principle," *Physical Review Letters*, vol. 125, no. 10, p. 100602, 2020.

[30] L. T. Giorgini, R. Eichhorn, M. Das, W. Moon, and J. Wettlaufer, "Thermodynamic cost of erasing information in finite time," *Physical Review Research*, vol. 5, no. 2, p. 023084, 2023.

[31] J. Fuchs, S. Goldt, and U. Seifert, "Stochastic thermodynamics of resetting," *Europhysics Letters*, vol. 113, no. 6, p. 60009, 2016.

[32] R. Goerlich, M. Li, L. B. Pires, P.-A. Hervieux, G. Manfredi, and C. Genet, "Experimental test of landauer's principle for stochastic resetting," *arXiv preprint arXiv:2306.09503*, 2023.

[33] I. A. Martinez, E. Roldán, J. M. Parrondo, and D. Petrov, "Effective heating to several thousand kelvins of an optically trapped sphere in a liquid," *Physical Review E*, vol. 87, no. 3, p. 032159, 2013.

[34] V. Blickle and C. Bechinger, "Realization of a micrometre-sized stochastic heat engine," *Nature Physics*, vol. 8, no. 2, pp. 143–146, 2012.

[35] J. A. Albay, Z.-Y. Zhou, C.-H. Chang, and Y. Jun, "Shift a laser beam back and forth to exchange heat and work in thermodynamics," *Scientific reports*, vol. 11, no. 1, pp. 1–10, 2021.

[36] P. Mestres, I. A. Martinez, A. Ortiz-Ambriz, R. A. Rica, and E. Roldan, "Realization of nonequilibrium thermodynamic processes using external colored noise," *Physical Review E*, vol. 90, no. 3, p. 032116, 2014.

[37] M. Ibáñez, C. Dieball, A. Lasanta, A. Godec, and R. A. Rica, "Heating and cooling are fundamentally asymmetric and evolve along distinct pathways," *arXiv preprint arXiv:2302.09061*, 2023.

[38] J. Gieseler, R. Quidant, C. Dellago, and L. Novotny, "Dynamic relaxation of a levitated nanoparticle from a non-equilibrium steady state," *Nature nanotechnology*, vol. 9, no. 5, p. 358, 2014.

[39] A. Militaru, A. Lasanta, M. Frimmer, L. L. Bonilla, L. Novotny, and R. A. Rica, "Kovacs memory effect with an optically levitated nanoparticle," *Physical Review Letters*, vol. 127, no. 13, p. 130603, 2021.

[40] A. Kumar, R. Chétrite, and J. Bechhoefer, "Anomalous heating in a colloidal system," *Proceedings of the National Academy of Sciences*, vol. 119, no. 5, p. e2118484119, 2022.

[41] I. A. Martínez, É. Roldán, L. Dinis, and R. A. Rica, "Colloidal heat engines: a review," *Soft matter*, vol. 13, no. 1, pp. 22–36, 2017.

[42] I. A. Martínez, É. Roldán, L. Dinis, D. Petrov, and R. A. Rica, "Adiabatic processes realized with a trapped brownian particle," *Physical review letters*, vol. 114, no. 12, p. 120601, 2015.

[43] M. Rademacher, M. Konopik, M. Debiossac, D. Grass, E. Lutz, and N. Kiesel, "Nonequilibrium control of thermal and mechanical changes in a levitated system," *Physical Review Letters*, vol. 128, no. 7, p. 070601, 2022.

[44] A. J. Kovacs, J. J. Aklonis, J. M. Hutchinson, and A. R. Ramos, "Isobaric volume and enthalpy recovery of glasses. ii. a transparent multiparameter theory," *Journal of Polymer Science: Polymer Physics Edition*, vol. 17, no. 7, pp. 1097–1162, 1979.

[45] A. Patrón, B. Sánchez-Rey, C. A. Plata, and A. Prados, "Non-equilibrium memory effects: Granular fluids and beyond," *Europhysics Letters*, 2023.

[46] J. T. Park, G. Paneru, C. Kwon, S. Granick, and H. K. Pak, "Rapid-prototyping a brownian particle in an active bath," *Soft Matter*, vol. 16, no. 35, pp. 8122–8127, 2020.

[47] G. Paneru, J. T. Park, and H. K. Pak, "Transport and diffusion enhancement in experimentally realized non-gaussian correlated ratchets," *The Journal of Physical Chemistry Letters*, vol. 12, no. 45, pp. 11078–11084, 2021.

[48] R. Goerlich, L. B. Pires, G. Manfredi, P.-A. Hervieux, and C. Genet, "Harvesting information to control nonequilibrium states of active matter," *Physical Review E*, vol. 106, no. 5, p. 054617, 2022.

[49] S. Joo, X. Durang, O.-c. Lee, and J.-H. Jeon, "Anomalous diffusion of active brownian particles cross-linked to a networked polymer: Langevin dynamics simulation and theory," *Soft Matter*, vol. 16, no. 40, pp. 9188–9201, 2020.

[50] S. M. J. Khadem, R. Klages, and S. H. Klapp, "Stochastic thermodynamics of fractional brownian motion," *Physical Review Research*, vol. 4, no. 4, p. 043186, 2022.

[51] T. Ariga, K. Tateishi, M. Tomishige, and D. Mizuno, "Noise-induced acceleration of single molecule kinesin-1," *Physical review letters*, vol. 127, no. 17, p. 178101, 2021.

[52] D. Guéry-Odelin, A. Ruschhaupt, A. Kiely, E. Torrontegui, S. Martínez-Garaot, and J. G. Muga, "Shortcuts to adiabaticity: Concepts, methods, and applications," *Reviews of Modern Physics*, vol. 91, no. 4, p. 045001, 2019.

[53] D. Guéry-Odelin, C. Jarzynski, C. A. Plata, A. Prados, and E. Trizac, "Driving rapidly while remaining in control: classical shortcuts from hamiltonian to stochastic dynamics," *Reports on Progress in Physics*, 2022.

[54] I. A. Martínez, A. Petrosyan, D. Guéry-Odelin, E. Trizac, and S. Ciliberto, "Engineered swift equilibration of a brownian particle," *Nature physics*, vol. 12, no. 9, pp. 843–846, 2016.

[55] M. Chupeau, B. Besga, D. Guéry-Odelin, E. Trizac, A. Petrosyan, and S. Ciliberto, "Thermal bath engineering for swift equilibration," *Physical Review E*, vol. 98, no. 1, p. 010104, 2018.

[56] D. Raynal, T. de Guillebon, D. Guéry-Odelin, E. Trizac, J.-S. Lauret, and L. Rondin, "Shortcuts to equilibrium with a levitated particle in the underdamped regime," *Phys. Rev. Lett.*, vol. 131, p. 087101, Aug 2023.

[57] M. Chupeau, S. Ciliberto, D. Guéry-Odelin, and E. Trizac, "Engineered swift equilibration for brownian objects: from underdamped to overdamped dynamics," *New Journal of Physics*, vol. 20, no. 7, p. 075003, 2018.

[58] J. A. Albay, S. R. Wulaningrum, C. Kwon, P.-Y. Lai, and Y. Jun, "Thermodynamic cost of a shortcuts-to-isothermal transport of a brownian particle," *Physical Review Research*, vol. 1, no. 3, p. 033122, 2019.

[59] Y. Jun and P.-Y. Lai, "Minimal dissipation protocols of an instantaneous equilibrium brownian particle under time-dependent temperature and potential variations," *Phys. Rev. Res.*, vol. 4, p. 023157, May 2022.

[60] A. Prados, "Optimizing the relaxation route with optimal control," *Physical Review Research*, vol. 3, no. 2, p. 023128, 2021.

[61] A. Patrón, A. Prados, and C. A. Plata, "Thermal brachistochrone for harmonically confined brownian particles," *The European Physical Journal Plus*, vol. 137, no. 9, pp. 1–20, 2022.

[62] Z. Ye, F. Cerisola, P. Abiuso, J. Anders, M. Perarnau-Llobet, and V. Holubec, "Optimal finite-time heat engines under constrained control," *Physical Review Research*, vol. 4, no. 4, p. 043130, 2022.

[63] S. Ito, "Stochastic thermodynamic interpretation of information geometry," *Physical review letters*, vol. 121, no. 3, p. 030605, 2018.

[64] G. Li, J.-F. Chen, C. Sun, and H. Dong, "Geodesic path for the minimal energy cost in shortcuts to isothermality," *Physical Review Letters*, vol. 128, no. 23, p. 230603, 2022.

[65] G. E. Crooks, "Measuring thermodynamic length," *Physical Review Letters*, vol. 99, no. 10, p. 100602, 2007.

[66] T. Schmiedl and U. Seifert, "Optimal finite-time processes in stochastic thermodynamics," *Physical review letters*, vol. 98, no. 10, p. 108301, 2007.

[67] M. V. Bonança and S. Deffner, "Optimal driving of isothermal processes close to equilibrium," *The Journal of chemical physics*, vol. 140, no. 24, p. 244119, 2014.

[68] Y. Rosales-Cabara, G. Manfredi, G. Schnoering, P.-A. Hervieux, L. Mertz, and C. Genet, "Optimal protocols and universal time-energy bound in brownian thermodynamics," *Physical Review Research*, vol. 2, no. 1, p. 012012, 2020.

[69] A. Einstein, "Investigations on the theory of the brownian movement," in *Dover Books on Physics Series*, Dover Publications, 1956.

[70] É. Roldán, I. Neri, R. Chetrite, S. Gupta, S. Pigolotti, F. Jülicher, and K. Sekimoto, "Martingales for physicists," *arXiv preprint arXiv:2210.09983*, 2022.

[71] J. W. Goodman, *Introduction to Fourier optics*. Roberts and Company publishers, 2005.

[72] A. Gennerich, *Optical tweezers*. Springer, 2017.

[73] M. J. Padgett, J. Molloy, and D. McGloin, *Optical Tweezers: methods and applications*. CRC press, 2010.

[74] A. Ashkin, J. M. Dziedzic, J. E. Bjorkholm, and S. Chu, "Observation of a single-beam gradient force optical trap for dielectric particles," *Optics letters*, vol. 11, no. 5, pp. 288–290, 1986.

[75] P. Polimeno, A. Magazzu, M. A. Iati, F. Patti, R. Saija, C. D. E. Boschi, M. G. Donato, P. G. Gucciardi, P. H. Jones, G. Volpe, *et al.*, "Optical tweezers and their applications," *Journal of Quantitative Spectroscopy and Radiative Transfer*, vol. 218, pp. 131–150, 2018.

[76] J. Gieseler, J. R. Gomez-Solano, A. Magazzù, I. P. Castillo, L. P. García, M. Gironella-Torrent, X. Viader-Godoy, F. Ritort, G. Pesce, A. V. Arzola, K. Volke-Sepúlveda, and G. Volpe, "Optical tweezers — from calibration to applications: a tutorial," *Adv. Opt. Photon.*, vol. 13, pp. 74–241, Mar 2021.

[77] G. Volpe, O. M. Maragò, H. Rubinsztein-Dunlop, G. Pesce, A. B. Stilgoe, G. Volpe, G. Tkachenko, V. G. Truong, S. N. Chormaic, F. Kalantarifard, *et al.*, "Roadmap for optical tweezers," *Journal of Physics: Photonics*, vol. 5, no. 2, p. 022501, 2023.

[78] Y. Roichman, B. Sun, A. Stolarski, and D. G. Grier, "Influence of nonconservative optical forces on the dynamics of optically trapped colloidal spheres: the fountain of probability," *Physical review letters*, vol. 101, no. 12, p. 128301, 2008.

[79] Y. Amarouchene, M. Mangeat, B. V. Montes, L. Ondic, T. Guérin, D. S. Dean, and Y. Louyer, "Nonequilibrium dynamics induced by scattering forces for optically trapped nanoparticles in strongly inertial regimes," *Physical Review Letters*, vol. 122, no. 18, p. 183901, 2019.

[80] J. Howard, *Mechanics of motor proteins and the cytoskeleton*. Sinauer Associates, Inc, 2001.

[81] R. Kubo, "The fluctuation-dissipation theorem," *Reports on progress in physics*, vol. 29, no. 1, p. 255, 1966.

[82] K. Berg-Sørensen and H. Flyvbjerg, "Power spectrum analysis for optical tweezers," *Review of Scientific Instruments*, vol. 75, no. 3, pp. 594–612, 2004.

[83] G. Heinzel, A. Rüdiger, and R. Schilling, "Spectrum and spectral density estimation by the discrete fourier transform (dft), including a comprehensive list of window functions and some new at-top windows," 2002.

[84] B. E. Saleh and M. C. Teich, *Fundamentals of photonics*. john Wiley & sons, 2019.

[85] R. E. Walpole, R. H. Myers, S. L. Myers, and K. Ye, *Probability and statistics for engineers and scientists*, vol. 5. Macmillan New York, 1993.

[86] R. Goerlich, *Optical control of Brownian diffusion: from bath engineering to quantum analogues*. PhD thesis, Université de Strasbourg, 2022.

[87] M. Esposito and C. Van den Broeck, "Second law and landauer principle far from equilibrium," *Europhysics Letters*, vol. 95, no. 4, p. 40004, 2011.

[88] U. Seifert, "Entropy production along a stochastic trajectory and an integral fluctuation theorem," *Physical review letters*, vol. 95, no. 4, p. 040602, 2005.

[89] K. Sekimoto, "Langevin equation and thermodynamics," *Progress of Theoretical Physics Supplement*, vol. 130, pp. 17–27, 1998.

[90] É. Roldán, I. A. Martínez, L. Dinis, and R. A. Rica, "Measuring kinetic energy changes in the mesoscale with low acquisition rates," *Applied physics letters*, vol. 104, no. 23, p. 234103, 2014.

[91] D. Arold, A. Dechant, and E. Lutz, "Heat leakage in overdamped harmonic systems," *Physical Review E*, vol. 97, no. 2, p. 022131, 2018.

[92] P. V. Paraguassú, R. Aquino, L. Defaveri, and W. A. M. Morgado, "Effects of the kinetic energy in heat for overdamped systems," *Phys. Rev. E*, vol. 106, p. 044106, Oct 2022.

[93] S. Pigolotti, I. Neri, É. Roldán, and F. Jülicher, "Generic properties of stochastic entropy production," *Physical review letters*, vol. 119, no. 14, p. 140604, 2017.

[94] L. B. Pires, R. Goerlich, A. L. da Fonseca, M. Debiossac, P.-A. Hervieux, G. Manfredi, and C. Genet, "Optimal time-entropy bounds and speed limits for brownian thermal shortcuts," *Phys. Rev. Lett.*, vol. 131, p. 097101, Sep 2023.

[95] Y. Rosales Cabara, *Acting on a brownian probe: from optical forces to optimal thermodynamic protocols*. PhD thesis, Strasbourg, 2020.

Université de Strasbourg

Luís BARBOSA PIRES

Entropic costs for Brownian protocols

École doctorale
Sciences chimiques | ED 222
Université de Strasbourg

Résumé

Cette thèse présente une approche expérimentale pour contrôler le paysage énergétique d'une particule Brownienne piégée par ingénierie du bain thermique par pression de radiation modulée stochastiquement. Cette approche permet la mesure des coûts énergétiques et entropiques impliqués dans les protocoles hors-équilibre dépendant du temps. Ces coûts permettent de définir des protocoles isothermes et isochores (changements de température dans un potentiel constant) optimaux et de révéler des propriétés intéressantes, telles qu'une asymétrie entre processus de chauffe et de refroidissement. Pour obtenir une description thermodynamique cohérente, nous proposons une nouvelle méthode pour mesurer l'entropie du système le long d'une trajectoire stochastique, basée sur la relation entre le micro-état instantané de non-équilibre et le macro-état d'équilibre correspondant. Ce travail étudie la mécanique et de la thermodynamique des processus Browniens isothermes et isochores hors équilibre.

Mots-clés : mouvement brownien confiné, ingénierie des bains thermiques, thermodynamique hors équilibre, coûts thermodynamiques, optimisation.

Résumé en anglais

This thesis presents an experimental approach to control the energetic landscape of a confined Brownian particle through thermal bath engineering using a stochastically modulated radiation pressure force. This approach motivates the quantitative assessment of the energetic and entropic costs involved in time-dependent non-equilibrium protocols. These costs once identified make it possible to design optimal isothermal and isochoric protocols (temperature changes in a constant potential) and to reveal interesting features, such as an asymmetry between heating and cooling processes. To make a consistent thermodynamic description, we propose a new method for measuring the system entropy along a stochastic trajectory based on the relationship between the instantaneous non-equilibrium micro-state and the corresponding equilibrium macro-state. This work provides a comprehensive study of the mechanics and thermodynamics of non-equilibrium isothermal and isochoric Brownian processes.

Keywords: confined Brownian motion, thermal bath engineering, non-equilibrium thermodynamic, thermodynamic costs, optimisation.